**UNIVERSITY OF LIMOGES**

DOCTORAL SCHOOL S2Im

FACULTY OF SCIENCES AND TECHNOLOGIES



Year : 2013 Thesis N°36-2013


# PhD thesis

submitted in partial fulfillment of the requirements for the degree of

**DOCTOR OF PHILOSOPHY IN THE UNIVERSITY OF LIMOGES**

**Mention : Sciences of engineering for information, mathematiques**

Presented and defended by


**Romain DAULIAT**


October $15^{th}$, 2013

# Advanced microstructured fibers design for a robust singlemode high power laser operation

**PhD thesis directed by Philippe ROY and supervised by Raphaël JAMIER, prepared in the Photonics department of Xlim and in the Optical Fiber Technology group of the Institut für Photonische Technologien**

**Jury :**

| | | |
|---|---|---|
| **John BALLATO** | Professor, Clemson University | *Reviewer* |
| **Yves QUIQUEMPOIS** | Professor, Laboratoire de Physique des Lasers, Atomes et Molécules | *Reviewer* |
| **Alain BARTHELEMY** | Directeur de recherche, University of Limoges | *Examiner* |
| **Kay SCHUSTER** | Head of work group, Institut für Photonische Technologien | *Examiner* |
| **François SALIN** | Director of Technology, Eolite Systems | *Guest* |
| **Raphaël JAMIER** | Maître de conférences, University of Limoges | *PhD supervisor* |
| **Philippe ROY** | Chargé de recherche, University of Limoges | *PhD supervisor* |

*"It is easier to split an atom than a prejudice."*

Albert EINSTEIN

*To my brother*

*To my fiancée*

# *Acknowledgements*

During these three marvelous years, i've been glad to exchange with great researchers and learn from them. I would like to compliment all my dear colleagues which have contributed to my growth in this job. I would note that this report is not only my work, but that of a collaboration, between 3 groups who desired to make this work a great success...

First, i want to thanks Philippe, who trusted me after my MSc internship and gave me the privilege to pursue my work within its group. I emphasize its quality as PhD director and greet him to place me in the forefront of his project. It was a real pleasure for me to be part of it. I'm also particularly grateful to him for providing such favourable work place and allow me to spend time with our partners: IPHT and Eolite Systems.

Moreover, it was also pleasant to collaborate with Raphaël, to share intense discussions about our researches, to benefit from his critical and wise regard about our work. He never forgets to bring the worst gift from his trip, as the "awesome" snow globe from Santander. I will wish him a great and happy future for his young children: Louis and the twin Arthur/Margaux! I also thank Jean-Louis for his enthusiasm and his sympathy.

I can't continue this section without showing me grateful to Dmitry. Our numerous discussions have been really useful to improve my background knowledges on the optics research field, and our friendly competition to develop the most robust fibers laser has been a pleasure to live. Furthemore, i will keep some imperishable memories of our collaboration.

I also want to present my sincere acknowledgement to our german colleagues for the warm welcome they gave me. Notably, i felt glad to work in the group headed by Kay Schuster, whose the human qualities have no longer to be demonstrated. I take this opportunity to greet all the researchers from this group: Stephan Grimm, Doris Litzkendorf and Anne Ludwig with which i have exchanged about the manufacturing processes, Jens Kobelke and Joerg Bierlich for interesting discussions about the fiber drawing and the german culture, Claudia Aichele for discussion about the MCVD and tubes preparation for the air-clad fabrication, Anka Schwuchow for giving me access to their equipment, Sylvia Jetschke and Martin Leich for useful talk about photodarkening, just to name a few. Otherwise, i address a special comment to Kay Schuster and Hardy Baierl for their presence by my side during my 3-months stay, i am deeply grateful to you. Finally, i pay attention on the involvement of Hartmut Bartelt on the organisation of my coming in the IPHT.

My work has also been achieved in narrow collaboration with Eolite Systems, who believed in our scientific proposal and contributed to the advance of this project, mainly thanks to François Salin. His scientific advices were of great interest to develop the innovative fibers described on this report. Moreover, i thanks Pierre Deslandes for supporting us on the realization of Q-switch lasers. This collaboration has resulted in another PhD thesis, achieved by Aurélien Benoit. The latter has strongly contributed on the characterization of fiber laser discussed in the last chapter of this report.

In this dynamic, I want to greatly thank Dr John Ballato and Dr Yves Quiquempois to accept the review of my work and provide wise comments on it.

Moreover, a PhD thesis represents also a group of friends and mine have been perfect. First, i thank Emilien to be there along all these years, for all the chicha we've shared and the parts of Shogi we tried to play. Moreover, i think to my everlasting roommate Ricky, for these 3 years we shared, the wonderful Mauritian meal, your Guitar Hero part in easy mode, your kindness even when i decided to buy a bar for our flat. Then, don't be afraid Tonton, i won't forget the "Trouspinette", i'm just going to find new customers. Dears "doudous" (Yannick and Barbara), take care of Louka and the expected second baby! I also think to my long-term friends Flo, Julie and Antho, strewed all around France. Geoffroy, P'tit Ben and Franҫis, i've enjoyed all the time we spend together during these three years. I hope the best for you and to see you soon. I also have a thought for Denis, working in the University of Cambridge since one year and get a 3-years position in EPFL.

I am glad to note that i have found persons of confidence, helping me to manage the PhD association during this two years: John and Geoffroy for Adelcom (2011/2012), and then a larger group composed of Richard, Guillaume, Emilien and John again. This group achieved a good work, inviting researchers for lectures, presenting their work to young visitors (students notably), creating a directory listing the PhD graduated recently in our laboratory, ...

Finally, i thank my beloved fiancee to support me all this time and to be such a fantastic (sometimes crazy) girl. I'm proud of her and wish us the best for the future. I greet my step family for welcoming me so well. And, obviously, i finish my acknowledgement by my own family. I have to be very grateful to my parents which has been perfect all along these years, letting me grow by myself but being present when it was needed. For sure, i can't forgot some astonishing women, my grandma' Marinette and her daughter Clémence, always ready for laughing or telling funny stories. My last words in this section goes to my dear young brother, i am proud of you more than everything and wish you to shape your dream!

# Contents

# List of Figures

# List of Tables

# List of Abbreviations

| | |
|---|---|
| $\Delta$n | Refractive index contrast |
| $\Delta\Gamma$ | Modal discrimination |
| $\Gamma$ | Overlap Factor |
| $\Lambda$ | Pitch |
| AC | Angle-Cleaved |
| Al | Aluminium |
| AP | Angle-Polished |
| Ar | Argon |
| ARROW | Anti-Resonant Reflecting Optical Waveguides |
| ASE | Amplification of Spontaneous Emission |
| BPP | Beam Parameters Product |
| CCC | Chirally Coupled Core fiber |
| $CO_2$ | Carbon Dioxide |
| DMF | Distributed Mode Filtering fiber |
| dn | Refractive index mismatching |
| DND | Direct Nano-particle Deposition |
| DPSS | Diode Pumped Solid State laser |
| EM | Electro-Magnetic |
| ESM | Endlessly Single-Mode |
| F | Fluorine |
| FCVD | Furnace Chemical Vapor Deposition |
| FEM | Finite-Element Method |
| FM | Fundamental Mode |
| He-Ne | Helium- Neon |
| HOM | High-Order Mode |
| LCF | Leakage Channel Fiber |
| LMA | Large Mode Area |
| LP | Linearly Polarized |
| LPF | Large Pitch Fiber |
| LPG | Long Period Grating |
| MCVD | Modified Chemical Vapor Deposition |
| MFD | Mode Field Diameter |
| MOF | Microstructured Optical Fiber |
| MTIR | Modified Total Internal Reflection |
| NA | Numerical Aperture |
| Nd | Neodymium |
| OVD | Outside Vapor Deposition |
| PB | Photo-Bleaching |
| PBG | Photonic BandGap |
| PCF | Photonic Crystal Fiber |
| PCVD | Plasma Chemical Vapor Deposition |
| PD | PhotoDarkening |
| PDE | Partial Differential Equation |
| PP | Perpendicularly Polished |
| RI | Refractive Index |
| SBS | Stimulated Brillouin Scattering |
| SPM | Self-Phase Modulation |
| SRS | Stimulated Raman Scattering |
| SSL | Solid-State Laser |

TEM Transverse ElectroMagnetic modes

Ti-Sa Titanium-Sapphire

TIR Total Internal Reflection

TSHB Transverse Spatial Hole Burning

UV Ultraviolet

VAP Vapor Axial Deposition

VCSEL Vertical Cavity Surface Emitting Laser

VLMA Very Large Mode Area

XPM Cross-Phase Modulation

Yb Ytterbium

# General introduction

Although lasers are ubiquitous in our life (CD-ROM, printer...) and play a major role in industry or medicine nowadays, its history is not so former and has begun during the twentieth century. This one was rich in understanding of physical phenomena and inventions, notably concerning the electromagnetic waves (microwaves and light). Starting from the pioneer researches of Albert Eintein on the stimulated emission of radiation published in 1917 [Einstein17], a large interest has been initiated on this topic. By a theoretical analysis of the Planck radiation formula, A. Einstein understood that the well-known process of absorption can be accompanied by a complementary process. Indeed, an incident wave can stimulate atoms to emit the same kind of radiation (wavelength, direction, polarization,...). Seven years later, Richard Tolman introduced the notion of gain or "negative absorption": 'The possibility arises that molecules in the upper quantum state may return to the lower quantum state in such way as to reinforce the primary beam by "negative absorption"' [Tolman24]. Then, it took years before observing a new scientific breakthrough in this field of research with the description of the optical pumping by Alfred Kastler [Kastler50], providing the inversion of population required for an efficient stimulated emission.

At the end of the first half of $20^{th}$ century, researchers had all the ingredients to create a source of coherent radiation as Charles Fabry and Alfred Pérot explained in 1896 the conditions to get constructive or destructive interference, enabling to build resonant cavities. Thus, in 1954, the concept of Microwave Amplification of Stimulated Emission of Radiation (MASER) was reported [Gordon54, Gordon55]. It was demonstrated the amplification of coherent microwaves using ammoniac molecules embedded in a cavity and excited by a radiation at 23.793 GHz. This invention has allowed the $1^{st}$ trans-atlantic transmission of televisual images from Andover (Maine, USA) to Pleumeur-Bodou (Finistère, France) on July, $10^{th}$ 1962.

In 1958, Arthur Schawlow (Nobel Price in 1981) and Charles Townes published their theoretical investigation on "Extension of maser techniques to optical radiation" [Schawlow58]. Although the Bell Labs did not judge that this idea deserves the deposit of a patent, it has been done due to the insistence of C.H. Townes. At this moment, they named this system "optical maser". In fact, this is Gordon Gould which defined first the acronym of 'Laser': Light Amplification of Stimulated Emission of Radiation and proposed a schematic representation in November 1957 but he did not published this work. He was finally recognized as inventor of the laser in 1977.

In 1960, Theodore Maiman achieved in the Hughes Research Laboratories the first demonstration of a laser using a small pink ruby crystal [Maiman60b]. Initially, Maiman observed the fluorescence of $Cr^{3+}$ ions in $Al_2O_3$ and published this results in *Physical review Letters* [Maiman60a]. Few month later, he submits a second paper to this review, which was refused because it was judged as "just another maser paper". So, Maiman chose to submit it in *Nature*. This publication is now recognized historically as the first article noticing an observation of a pulse laser emission (May, 16th of 1960).

Following this demonstration, intensive researches have been realized and the laser effect was obtained in different gain mediums:

- 1960 : $1^{st}$ solid state laser doped with Uranium [Sorokin60]
- 1961 : Invention of He-Ne [Javan61]
- 1962 : $1^{st}$ $Nd^{3+}$ doped fiber laser, demonstration in amplification [Koester64]
  First fabrication of the semiconductor laser [Hall62]
- 1964 : Invention of Nd:YAG laser [Geusic64]
  Invention of $CO_2$ laser [Patel64]
  Invention of Argon laser [Bridges64]

In the end of the 60's, another primary technological bolt was relieved by Charles Kao through the development of a low loss silica waveguide (optical fiber). This

invention enabled a long distance transmission of an optical signal with losses in the range of 20dB/km [Kao86]. Charles Kao received the Nobel Price of Physics in 2009 "for groundbreaking achievements concerning the transmission of light in fibers for optical communication". During the same period, Elias Snitzer described the potential of optical fibers for the modes selection and discussed the condition governing the laser cavity [Snitzer61].

Hence, the intense development of lasers and amplifiers until today was also induced by the fabrication of quantum well semiconductors which have drastically improved the efficiency of laser diodes and are nowadays indispensable for the pumping of lasers and amplifiers. Thanks in part to these pumping sources, David Payne [Payne87] and Emmanuel Desurvire [Desurvire87] have demonstrated simultaneously the realization of Erbium doped fiber amplifiers. This technological breakthrough, associated with the use of wavelength division multiplexor, has revolutionized the worldwide optical fiber network, increasing significantly the optical bits rate and becoming the main solution for data delivery. The fabrication of optical fibers has then known a very fast growth, reinforcing the interest of research groups for rare-earth (RE) doped fiber lasers/amplifiers. In particular, intensive researches have been led on Yb-doped fiber due to their high quantum efficiency ($\approx$ 82%), making them really useful in the high power regime. Moreover, the variety of RE ions available give access to several spectral bands, enlarging their potential: Er-doped fiber for telecommunications, Yb-doped fiber for industrial applications (cutting, drilling...) and Tm-doped fiber for medicine, just to name a few.

From now on, lasers are widespread used in a broad range of applications, spanning from industries (cutting, drilling,...) to military activities (LIDAR for instance), medicine (endoscopy...), or astronomy. As a proof, the research work done during the past few years is rewarded by global revenues of the laser market approaching \$8 billions at the end of the year 2012. Telecommunications and industrial applications represent respectively a half and a third of the global revenues of the laser

sources [Overton13, Belforte13]. Obviously, this technology is in constant evolution due to the tremendous potential of laser sources to fulfil the expectations of various applications. To support this statement, one can note that the industrial market is dominated by several laser sources depending on their specific use (see Fig. 1). $CO_2$ lasers provide an energetic beam mainly used for metal processing whereas fiber lasers are rather used in marking and engraving as they emit a relatively small beam (hundreds to thousands $\mu m^2$).

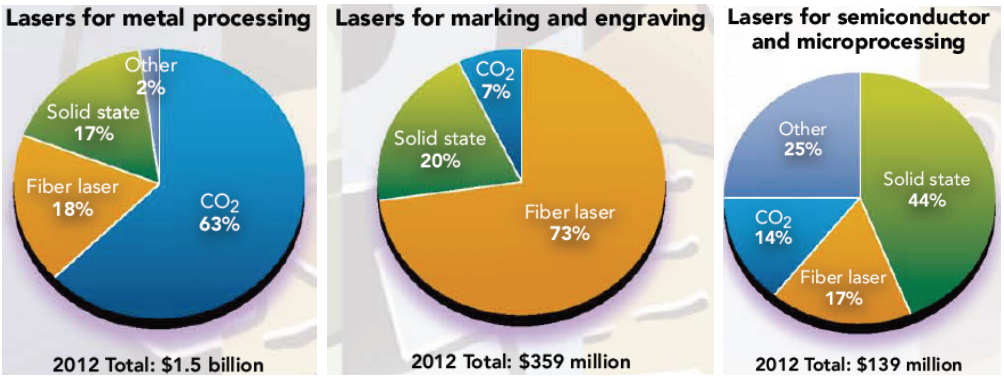


**Figure 1:** Repartition of laser sources revenues related to industrial applications [Belforte13].

The infatuation for such sources relies also on their outstanding versatility to emit a spatially and spectrally coherent beam over a wide power range. For instance, the association of a semiconductor diode laser and a robust optical fiber enables to transmit informations with a high fidelity of the data transfer. In medicine, this interest is undoubtedly linked to the specific characteristics of laser sources, i.e. the creation of a light beam composed of discrete wavelengths (which can be adapted to the absorption frequency of the cells under treatment) and the emission of a near diffraction-limited beam (irradiation of a small area with high precision without damaging surrounding tissues). Femtosecond lasers are notably employed for eye surgery. Moreover, laser sources can be also used for security, or civilian applications (sensors or Lidar for atmospheric detection of pollutants).

In this context, researches conducted during the last twenty years on the development of fiber laser sources have sky-rocketed and the latter appears now as

a viable alternative for conversion and propagation of strong light intensity, making them a serious candidate for high power applications. Contrary to other lasers sources, optical fibers exhibit an impressive transverse signal confinement (squared micro-meter scale effective area) over long lengths of interaction with the gain region. This small beam size is beneficial for accurate operation of micro-machining (marking and etching for instance). Moreover, optical fiber laser sources present other assets: their compactness, a long term reliability (no optics), the beam delivery, a high efficiency and beam quality, a low maintenance ...

However, the dramatic increase of average optical power (in continuous wave) and energy (in pulsed regime) delivered by fiber lasers systems remains a key issue. It is well-known that two major physical phenomena limit the increase of the power transported or generated in such optical waveguide: non-linear processes, disturbing the temporal, spectral and spatial properties of the emitted beam, and a dielectric breakdown. The thresholds of appearance for these harmful effects are proportional to the power density and conversely proportional to the fiber length. Thus, these barriers can be raised by increasing the fiber core size. This objective has led to the development of Large Mode Area fibers (LMA) whose the Mode Field Diameter (MFD) exceeds 50 $\mu$m. In addition, an essential criterion for the development of fiber lasers/amplifiers concerns the robustness of the singlemode emission. Unfortunately, very large mode area fibers sustain undoubtedly a larger mode content as a core enlargement contribute to make more and more modes able to be propagated. This statement implies that efforts have to be done in order to devise LMA fibers exhibiting an efficient discrimination of the High-Order Modes (HOM) in the fiber core, favouring thus the selective amplification and emission of the fundamental Gaussian mode.

The work describes in this manuscript is anchored on this topic and is relative to the development of a novel kind microstructured optical fiber exhibiting a incomparable low core modes content. To introduce the interest of this work, the Chap. 1

provides an overview on the evolutions and limitations of laser gain mediums, allowing to emphasize their potential for operation in high power regime. Then, their manufacturing processes will be address and the optical phenomena limiting the power scaling in such optical waveguides discuss. Hence, the main optical fibers operating in the high power regime will be presented and strategies employed to get a robust singlemode emission will be evidence. Then, I will describe the numerical approach I have used to investigate the modal content in microstructured optical fibers (see Chap.2). This *modus operandi* will be applied to a state-of-the-art very large mode area fiber to validate the procedure and provide a reference to my further study. A complete study of this structure will be done in order to highlight their performances in term of sensitivity to mode coupling, modal discrimination, resistance to the curvature... Hence, a strategy to devise all-solid microstructured fibers exhibiting a robust singlemode emission will be reported in Chap. 3. In order to release some constraints due to the CVD techniques, we resorted to an alternative manufacturing process based on the powder sintering and vitrification. Thus, a collaboration with the "Institute for Photonic Technology" in Jena was undertaken. Fiber structures exhibiting a large modal discrimination and an endlessly singlemodeness over a broad spectral range will be presented. Their tolerance to an index mismatch of the gain medium will be study with care. Solutions proposed in this report rely mainly on the understanding of the modal discrimination regarding the leakage channels and the fiber symmetry, and the behaviour of modes couplings occurring on HOMs. Finally, the fabrication of all-solid microstructured fibers will be show in Chap. 4 and the performances achieved with these innovative structures reported. The characterization of these fibers was achieved in collaboration with the company "Eolite lasers".

Chapter 1

# Evolution of the laser gain medium for emitting a bright single-mode beam

---

Contents

Since its first demonstration by T. Maiman [Maiman60a], the laser was subject to intensive researches aiming to broadened the potential of this coherent light source for applications ranging from industrial application, so requiring high power singlemode beam, to medicine for instance, on which the laser beam should be able to analyse microscopic human cells. Due to the strong interest of scientists for this versatile light source, the laser has known a lot of evolutions over the years, particularly concerning its gain medium, leading notably to the development of rare-earth (RE) doped bulk and fiber laser sources. Fiber lasers, in particular, exhibit numerous advantages such as high efficiencies (up to 80% for Yb-doped fiber laser), compactness, long-term reliability or also a strong signal confinement (hundreds to thousands micrometers squared), just to name a few. However, the latter can be detrimental when the emitted or delivered average power is increased. In this case, harmful phenomena occur (non-linear effects, optical damages ...) and degrade spatially, temporally and spectrally the beam quality. So as to push away the appearance threshold of these disruptive effects, the fiber core size shall be enlarged and the fiber length reduced. Thus, the development of Very Large Mode Area fibers (VLMA) whose the Mode Field Diameter (MFD) exceeds 50 $\mu$m has been initiated and different approaches have been followed to maintain a singlemode emission.

In this chapter, a brief review of the light-matter interactions is achieved, introducing the principles of absorption, spontaneous emission and stimulated emission. Then, assets and weaknesses of the main gain mediums used for operation in the high power regime are discussed and the emphasis is placed on the fiber laser. Optical fibers manufacturing processes are also addressed, evidencing their accuracy on the control of the Refractive Index (RI) profile. The talk will be focus on the power scaling in fiber lasers by first summarizing the restrictive phenomena (non-linear processes, optical damages and thermal effects) and then reviewing fiber evolutions which has led to the emission of a robust singlemode beam in the high power regime.

## 1.1 Light-matter interaction

Basically, the amplification of electromagnetic (EM) waves relies on the interaction between radiation and matter (seen as a set of atoms). As defined by the Bohr model, atoms can be schematically represented as a positively charged nucleus surrounded by electrons on circular orbits around the nucleus (Fig. 1.1(a)). These orbits refers to discrete energy levels: one can note $E_i$ their energy, $g_i$ their degeneracy level and $N_i$ the number of electrons having this energy (also called "population density"). At the thermodynamic equilibrium, the electrons distribution is described by the Boltzmann's law, where $k_B$ is the Boltzmann's constant and T the absolute temperature:

$$\frac{N_2}{N_1} = \frac{g_2}{g_1} e^{-(E_1 - E_2)/k_B T} \tag{1.1}$$

Hence, three quantum-mechanical processes govern the electrons behaviour: the absorption, the spontaneous emission and the stimulated emission (Fig. 1.1(b)). For each of them, the atom energy undergoes a variation equal to $\Delta E = E_2$ - $E_1$, either as a gain, or as a loss. The gap between two energy levels defines the frequency of the particles involved in these processes (h is the Planck's constant):

$$\nu = -\frac{(E_1 - E_2)}{h} \tag{1.2}$$

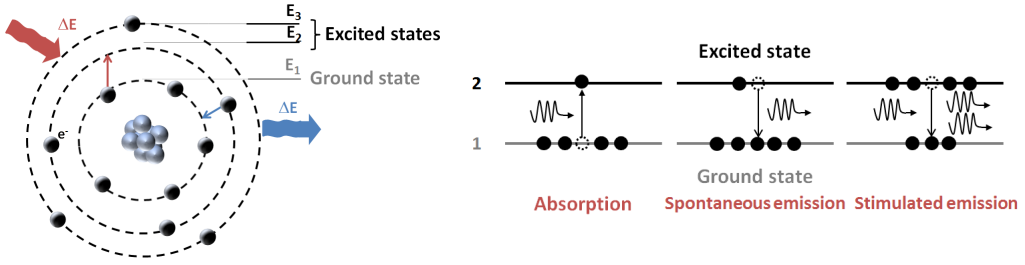


(a) (b)

**Figure 1.1:** (a) Schematic representation of an atom with its different energy levels (b) Simplified energy diagram aiming to describe the light-matter interaction. Wavy arrows represent photons and dot (filled) circles are the initial (final) position of electrons.

The description of the radiation-matter interaction can be led through a simple model based on two energy levels:

- *Absorption*: an electron on the ground state can catch the energy of a travelling photon, promoting it to an upper energy level whose the gap with the ground state coincides with the photon energy. The temporal evolution of the population in each level impacted by the absorption process ($dN_{2abs}$, $dN_{1abs}$) is defined by:

$$\frac{dN_{1abs}}{dt} = -\frac{dN_{2abs}}{dt} = -B_{12} * \rho_\nu * N_1 \tag{1.3}$$

  where $B_{12}$ is the Einstein coefficient for this particular transition and $\rho_\nu$ the radiation density of the incident field at the frequency $\nu$, and $N_1$ the number of atoms in the lower state.

- *Stimulated emission*: the photons emission can also be induced by an incoming photon travelling through the gain medium and having a suitable energy/wavelength [Einstein17]. In this case, if there is more electrons in the excited energy level than the ground state, the condition of population inversion is satisfied and the stimulated emission becomes more probable than absorption, leading to a net optical amplification. The temporal evolution of

the population $N_1$ and $N_2$ is given by:

$$\frac{dN_{1,sti}}{dt} = -\frac{dN_{2,sti}}{dt} = -B_{21} * \rho_\nu * N_2 \tag{1.4}$$

where $B_{21}$ is the Einstein coefficient relative to this transition.

- *Spontaneous emission*: following the absorption process, electrons filling the excited states can also spontaneously return to the ground state, releasing their energy through the generation of a photon. Note that the phase as well as the direction of the generated photons is random.

Hence, several operating regimes exist. Each of them requires a "pump" radiation to supply energy to the gain medium, promoting electrons from the ground state to the excited one. Thus, photons are emitted spontaneously and can be amplified, generating an "Amplification of Spontaneous Emission" (ASE) . This phenomenon is an unwanted process limiting the maximum gain achievable in the laser cavity. The population of each level implied in this mechanism evolves as follows:

$$\frac{dN_{1,sp}}{dt} = -\frac{dN_{2,sp}}{dt} = \frac{N_2}{\tau_2} \tag{1.5}$$

with $\tau_2$ is the electron lifetime on the excited state. From there, two strategies can be used to emit a coherent light. In the two cases, the pump power has to be sufficient to provide a population inversion of the gain medium (the excited state has a higher population density than the ground state). In this situation, an incoming 'signal' radiation travelling through the gain medium can be efficiently amplified by a single-pass in the gain medium. In this way, the stimulated emission strengthens the incident signal radiation all along the gain medium length by strongly increasing the number of signal photons. Otherwise, if the gain medium is embedded in an optical resonator, the ASE achieves multiple round-trips in this cavity, favouring the amplification of this recirculating radiation whose the power can rise exponentially. The small amount of power emitted spontaneously is amplified due to the stimulated

process, leading to the emission of a coherent laser beam.

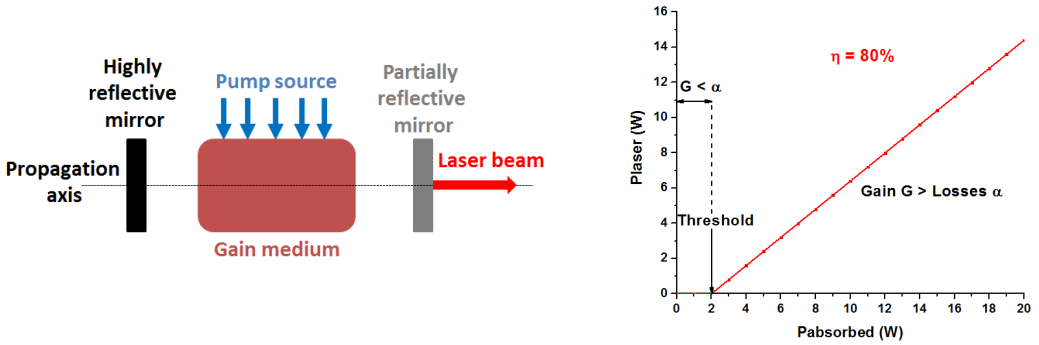


**Figure 1.2:** (a) Schematic representation of an optical oscillator comprising a gain medium, an optical pump source and two mirrors. (b) Example of efficiency slope with $\alpha$ the resonator losses and G the gain of the active medium.

For a better understanding of the laser dynamic, three parameters have to be described. Foremost, the gain represents the potential of an active medium to amplify a radiation. Moreover, the laser threshold is defined by the lowest absorbed power enabling to get a population inversion, and so a laser effect. It can only be overcome if the gain exceeds the losses (Fig. 1.2(b)), therefore a sufficient pump power is required to favour the population inversion. Hence, the output power increases linearly as a function of the absorbed power and is quantify by the "efficiency slope $\eta$", describing the efficiency of the system to convert the pump energy into laser radiation. This parameter is intrinsic to the gain medium. Thereby, different gain mediums have been notably developed in order to maximize this efficiency or to provide a large gain. In the following, the major gain mediums used in the high power regime are presented, evidencing the interest of optical fibers.

## 1.2 Gain medium

A wide variety of gain medium have been studied since the first experiments done on lasers: crystals, glasses, semiconductors, gases, or liquids. Among them, some

are relevant for high power operation as they can sustain strong power densities without damages and propagate/generate energetic pulses. Throughout this section, the most appropriate gain medium for operation in this regime are presented and the interest of RE-doped optical fiber lasers evidenced.

### 1.2.1 Gas lasers

The genesis of the lasers has been marked from the beginning by the development of gas lasers which are still widespread used. A gas, ionized by an electric current discharge, acts as optical amplifier (Fig. 1.3). The first one was the Helium-Neon (HeNe) laser, invented and built by Ali Javan and William R. Bennett in 1961 [Javan61]. Historically, this is the first laser working in CW regime. It produces a low power continuous light beam exhibiting a very thin bandwidth of 2 pm around 632.8 nm and 1.15 $\mu$m notably. Later, different gases have been chosen as gain medium: Argon (Ar) and Carbon Dioxide ($CO_2$) for instance. For a long time, Ar lasers were the main source in the visible (514.5 nm) and UV (351 nm) ranges, providing a good beam quality up to few tens of watts. Now, Ar lasers are supplanted by laser diodes or DPSS lasers due to their better efficiency and beam quality. On the other hand, $CO_2$ lasers got an undeniable place on the market of metal processing [Overton13]. The interest in carbon dioxide lasers stems from their continuous power capability, specific emitted wavelength and ease of construction. Their emission

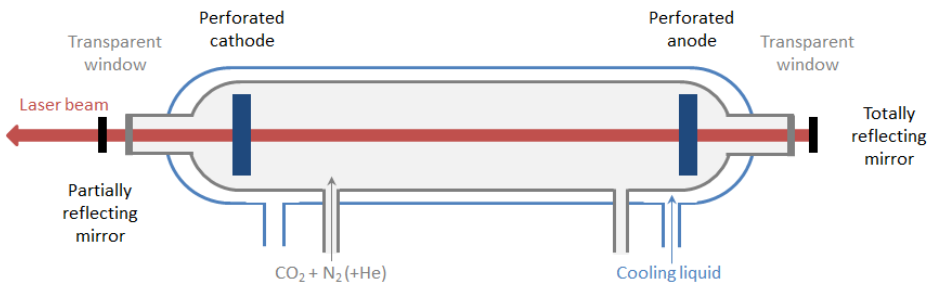


**Figure 1.3:** Schematic representation of a $CO_2$ laser.

wavelengths are centered around 9.4 and 10.6 $\mu$m and their average output powers reaches up to the kilowatt level (8kW are commercially available from Rofin). $CO_2$ laser can also be used in pulsed regime, by means of a rotating mirror or an electro-optic switch, giving rise to a Q-switched pulse emission of peak power up to GW. However, their wallplug efficiency reaches only 20% to the best, which is lower than for DPSS or thin disk lasers and are bulky. Moreover, the beam quality is quite poor compared to other laser sources (BPP ten times larger than thin disk laser).

### 1.2.2 Laser diodes

Laser diodes are today the main source used for the pumping of laser mediums such as crystals or fiber lasers. They are composed of a semiconductor diode which is electrically pumped, leaving electrons be promoted from the valence band to the conduction one and allowing by the way, a light emission by spontaneous and stimulated transitions. Conventional laser diodes are built as edge-emitting lasers, where the light beam is emitted from the edge (Fig. 1.4a). The optical properties of such lasers are determined by the geometry of their optical cavity. The emitted beam has frequently an elliptical shape and is generally very divergent notably for high power emission. However, their thin emission spectrum makes them particularly interesting for an efficient pumping of rare-earth (RE) doped fiber lasers: GaAlAs semiconductors for pumping of Tm-doped fiber laser at 792 nm or InGaAs ones for pumping of Yb and Er doped fiber laser at 975 nm (see Fig. 1.5). Moreover, laser diodes have also demonstrated their potential for other applications such as telecommunications (InGaAsP at 1310 nm or AlGaAs at 1064 nm), gas sensing (GaInAsSb in the near infrared) or optical storage (InGaN at 405 nm).

In order to improve the beam quality and consequently the power coupling efficiency into fiber lasers, VCSEL (Vertical Cavity Surface Emitting Laser) have been developed. They are composed of an active medium placed between two semiconductor distributed Bragg reflectors. Such semiconductors presents some advantages

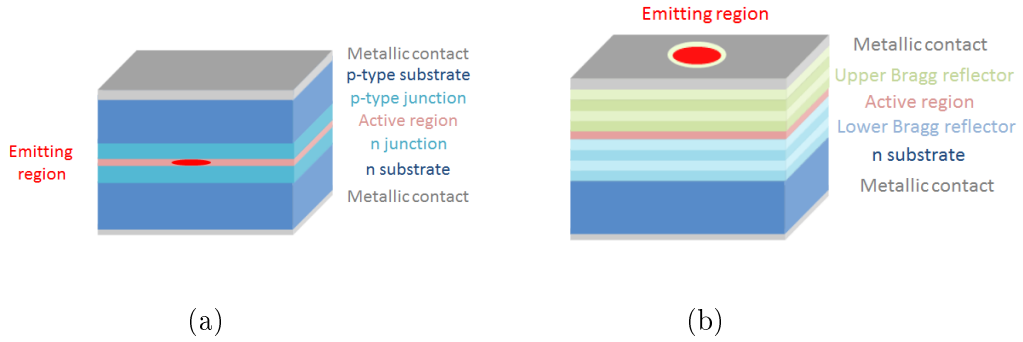


(a) (b)

**Figure 1.4:** Schematic representation of (a) an edge-emitting and (b) surface-emitting semiconductor laser.

compared to edge-emitting laser diodes: their larger output aperture limits the divergence angle of the output beam and makes possible high coupling efficiency with optical fibers (Fig. 1.4b). For pumping, the realization of 2D VCSEL made of several thousands of emitters has lead to the emission of hundreds watts of laser radiation with a high wall-plug efficiency and compete with diode stack based on edge-emitting semiconductors.

The electric to optic conversion efficiency of diode lasers typically reaches 50%. At low power level, single transverse mode emission can be achieved but for the optical pumping and emission of very high power, the emitted beam remains very divergent. These systems require additional optical elements as collimating lenses or apertures to shape the beam and optimize the coupling to laser cavities and/or optical fibers.

### 1.2.3 Bulk lasers

Historically, the first lasers have been achieved using a crystal: Ruby [Maiman60b], Uranium [Sorokin60], or the well-known Nd:YAG [Geusic64]. Subsequently, a strong interest was focused on these bulk lasers know also as "Solid-State Lasers" (SSL). However, this appellation gathers now several kind of lasers:

- bulk lasers such as the Nd:YAG or TiSa based on the use of a doped crystal

as gain medium. Generally, they exhibit narrow linewidth spectra (except for TiSa and Alexandrite) and their cavity is made of free space propagation.

- bulk lasers using a doped glass with rare-earth ions (Neodymium (Nd) or Ytterbium (Yb)), most of time associated with Aluminium (Al) or Fluorine (F) to modify their fluorescence properties. They also emit a broadband spectra and are usually used in pulsed lasers.

- semiconductor lasers discussed above. These laser sources are set nowadays as a standard for the pumping of other gain medium (notably RE doped fiber lasers), so much that SSL are generalized to Diode-Pumped SSL (DPSS lasers)

- RE doped fiber laser which will be discussed later.

This diversity of gain medium allows to access a numerous wavelength of operation (see Fig. 1.5). Here, the emphasis is on the bulk laser (crystals and lasers).

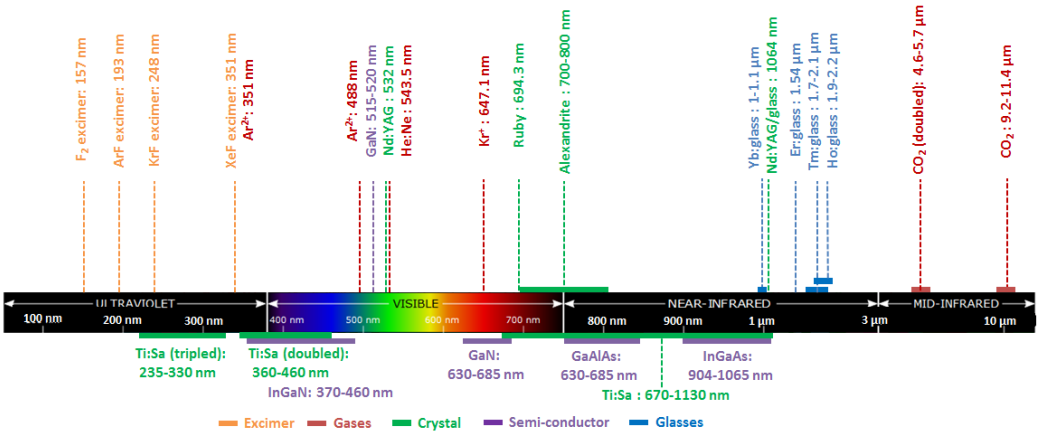


**Figure 1.5:** Frieze reporting the emission wavelengths or bands of the main laser sources.

Nowadays, the most widespread DPSS bulk lasers are the Nd:YAG (Neodymium:Yttrium-Aluminum-Garnet) and the Ti-Sa (Titanium-Sapphire), emitting very high peak power levels (PeraWatts: [Lureau12]) and high energy (MegaJoules: http://www-lmj.cea.fr/). Such lasers are versatile sources in term of output power level, pulse width, pulse repetition rate or wavelength. Depending

on the targeted applications, laser sources have to possess particular characteristics that DPSS can widely fulfill, notably a strong efficiency and a good beam quality (near diffraction-limited) compared to laser diodes. Moreover, some crystals provide tunable emission wavelength such as the Ti:Sa (from 660 to 1130 nm) or the Alexandrite crystal (from 700 to 800 nm). Owing to the large size of the crystal, bulk lasers present a strong capacity for the energy storage, making possible the emission of energetic pulses (at least on the mJ-ns range for a Q-switch configuration). Recently, a DPSS bulk laser characterized by a pulse duration of 40fs, a peak power of 400TW and a repetition rate of one shot per minute, leading to a pulse energy of 15J has been developed (http://hedp.osu.edu/facilities/scarlet). The above-mentioned advantages make such lasers useful in industry as tools for material processing (cutting, drilling, welding or etching), semiconductor fabrication (wafer cutting) or in medicine as sources for therapeutic, cosmetic or surgical procedures. Nevertheless, crystals suffer from several shortcomings. First, as they are used in a bulk cavity, their sensitivity to vibrations is not negligible. Moreover, their inherent large dimensions restrict the temperature dissipation, leading to disruptive thermal effects as the "thermal lensing", significantly altering the beam quality. This disturbance arises from the unconverted absorbed power which contribute to heat the crystal. In this way, a gradient temperature profile appears across the crystal and the refractive index (RI) of the medium is influenced through a thermo-optic effect (quantified by the coefficient dn/dT), favoring the self-focusing of the beam and potentially leading to the destruction of the crystal. Furthermore, the Kerr non-linear effect can also induce an increase of the RI for strong optical intensities, acting then as a focusing lens. These observations demonstrate the strong requirement on the cooling of laser devices. To struggle against these thermal issues, alternatives DPSS lasers have been designed.

### 1.2.4 Thin disk lasers

In order to improve the heat dissipation of the gain medium and thus lower the temperature rise, the area to volume ratio has to be increased either by enlarging the surface of interaction with the cooling area or by reducing the gain volume. In this purpose, crystals have been reshaped. Initially called "active mirrors" as the gain medium is a slice of glass coated on one side to totally reflect the incident light, thin disk lasers were developed for the first time in 1981 [Abate81] and then more widely investigated by Giesen *et al.* [Giesen94]. The latter has contributes to evidence the potential of thin-disk for scaling their output power. Such lasers are a special kind of DPSS lasers. They are commonly composed of a gain medium of 100-200$\mu$m in thickness fixed on a cooled heat sink (Fig. 1.6a).

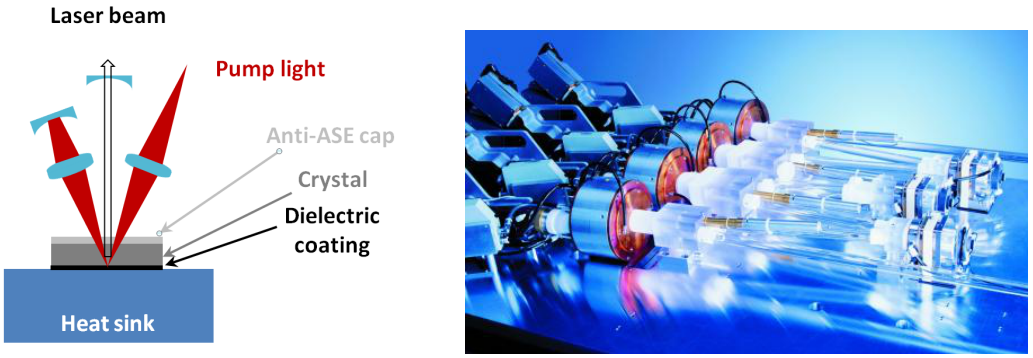


(a) (b)

**Figure 1.6:** (a) Schematic representation of a thin disk laser system. (b) Illustration of thin disk lasers device from TRUMPF.

In this case, the heat is dominantly extracted through the cooled end facet, which acts also as reflector for the laser and the pump light. An aspherical lens is used to focus the pump radiation on the disk. Due to the small thickness of the gain medium, a double pass of the pump light is not enough for a total pump absorption. Therefore, a multipass pumping scheme is usually implemented using a spherical lens and a highly reflecting mirror. For signal emission, an additional spherical mirror is used to provide an efficient optical feedback. Finally, an undoped

layer is commonly placed on the top of the thin-disk to reduce the impact of the ASE by allowing spontaneously emitted photons to escape from the resonant cavity [Furuse13]. In such a device, the heat sink efficiently cools the disk and thermal issues are mitigated compared to crystals, improving by the way the beam quality. Regarding the Beam Parameters Product (BPP), which is the product of the beam radius at the waist (longitudinal position where the beam is the smallest) and the half-angle of divergence (evolution of the beam diameter expanding far from the waist), a 6 times improvement has been achieved to bulk DPSS lasers based on a bulk crystal. So, this laser medium yields a beam of high quality even at high power levels. Otherwise, Yb:YAG thin-disk lasers has demonstrated optical-to-optical efficiencies reaching approximately 65%, enabling an overall "wallplug" efficiency of about 30%. Due to these advantages (efficiency, temperature management...), thin-disk lasers exhibiting diffraction-limited beam quality have been built with output powers up to several kilowatts [Tang03], essentially by adjusting the diameter of the pumped spot. For instance, Trumpf propose a 16 kW laser based on the use of, at least, four thin disks (see Trumpf website).

### 1.2.5 Fiber lasers

Thanks to the technical breakthroughs achieved by C.J. Koestler in 1961 (first optical fiber amplifier [Koester64]) and C. Kao in 1970 (fabrication of low-loss optical fiber [Kao86]), fiber lasers have been perceived as an interesting medium for light propagation and amplification. In the middle of the 80's, D. Payne [Payne87] and E. Desurvire [Desurvire87] simultaneously developed an efficient Erbium-doped fiber amplifiers having low optical loss (less than 0.2 dB/km) and providing gain in a broadband fitting the third telecommunication window (1530-1605 nm). This was one of the major breakthrough in the range of telecommunications (phone and internet), increasing the capacity for data transmission compared to electric cable as it allows the parallel amplification of numerous multiplexed channels in all optical

long-haul transmission lines. Then, optical fiber lasers have been intensively investigated and numerous outstanding properties have been evidenced: management of propagating modes, broad amplification bandwidth, wavelength tunability, compactness due to their flexibility, reliability, management of dispersion and birefringence,... Moreover, recent developments have highlighted their ability to withstand high CW powers (few kW) or energetic pulses (up to mJ), positioning them as a serious alternative to bulk lasers for material processing or medicine.

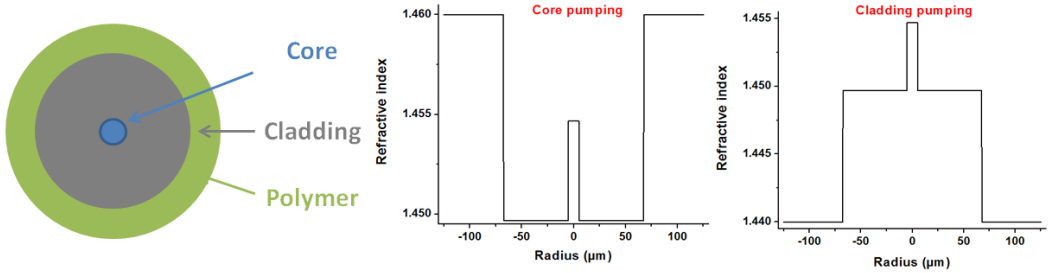


(a) (b) (c)

**Figure 1.7:** (a) Schematic representation of an optical fiber and refractive index profiles of a (b) single and (c) double-clad fiber.

In their simplest form, optical fibers are circular waveguides composed of 3 different materials (Fig. 1.7(a)). The light is confined into a small core whose the refractive index is larger than that of the surrounding "cladding", commonly made of pure silica. This refractive index contrast allows the light propagation by Total Internal Reflection in the fiber core. Moreover, a coating surrounds these two silica based media and protect them against mechanical constraints (fiber bending) and its environment (particles, moisture). Initially, the high-index coating also contributed to clean the cladding from parasitic light. The propagated light was thus only located into the fiber core (Fig. 1.7(b)) and consequently, the signal (and eventually pump) laser diodes had to exhibit a beam whose the properties (its size for instance) match that of the fiber core, which was singlemode in most systems.

However, for the power scaling, fiber lasers and amplifiers have faced the limita-

tion of the transverse singlemode pump laser diodes, so optical fibers had to mutate in order to allow the use of multimode laser diodes for pumping. Thus, low-index polymers have replaced high-index ones to provide an efficient coupling for the pump light emitted by high power, low brightness pump laser diodes into the fiber cladding (Fig. 1.7(c)). These fibers are called "double clad fibers" as the polymer acts as a cladding for the pump radiation. Moreover, some investigations have been led on the cladding shape, highlighting that an hexagonal or D-shape double clad enhances the absorption of the pump light [Leproux01]. Double-clad fibers acts as brightness and wavelength converters as the multimodal pump power is efficiently changed into a singlemode signal propagating in the central core. As depicted in Fig. 1.8(a), a lot of radiative transitions can be observed when rare-earth ions are incorporated into various glass host matrices. Nevertheless, for high power delivery, mainly the silica oxide glasses are recognized for their mechanical properties and the most efficient transitions are obtained with the erbium (Er), ytterbium (Yb) and thulium (Tm).

First, Er-doped fiber lasers/amplifiers has known a real infatuation due to their emission wavelength making them useful for telecommunications. These fiber laser sources are now widespread used and has allowed to drastically increase the bit rate, in combination with wavelength division multiplexors. Their quantum efficiency is relatively low (do not exceed 40% [Kotov13]), implying a strong conversion of the absorbed pump power into heat through non radiative processes, and has unfortunately been an obstacle to their use in high power applications. On the contrary, Yb-doped fiber lasers exhibit an efficiency two times higher. They present also the advantage to possess a large gain spectrum, allowing emission from 1030 to 1100 nm, which is particularly interesting for emission of short pulses (fs range). Thanks to their low quantum defect, Yb-doped fiber lasers have initiated the power scaling into fiber lasers, combining today ten kilowatts of output power with a near diffraction-limited beam (see IPG photonics website). More recently, Tm-doped fiber lasers have sparked the interest of the scientific community owing to their ability to emit

an eye-safe radiation around 2 $\mu$m and the use of this radiation in optical parametric oscillator to reach the mid-infrared range. Moreover, although the quantum efficiency is limited to 41% under pumping at 792 nm, it has been evidenced during the last decade that this threshold can be overcome up to 82% theoretically [Jackson03] by means of an energy transfer process called "cross relaxation". Up to date, several experimental demonstrations have reported a laser efficiency exceeding 55% [Frith07, Jackson07] and the maximum output power noticed reaches the kW level [Moulton10].

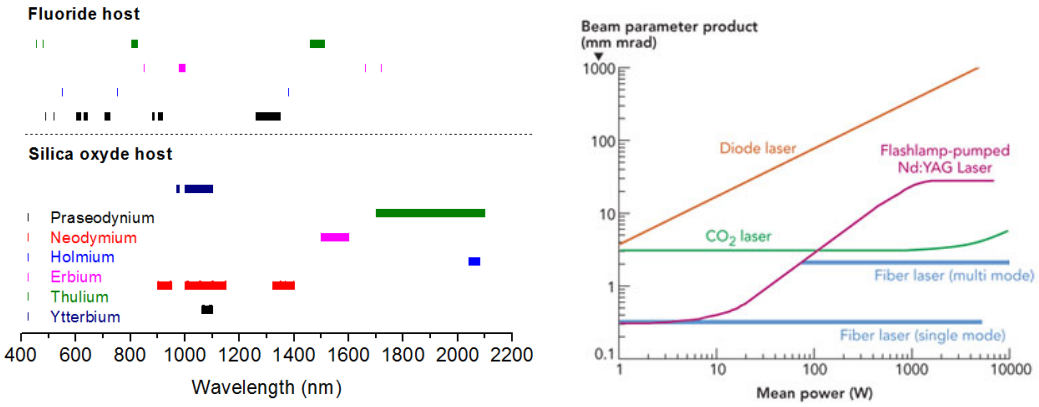


(a) (b)

**Figure 1.8:** (a) Emission spectral band for the main rare-earth into silica oxide and fluoride host. (b) Evolution of the beam quality for different gain medium depending on the power.

An important point to underline is that active optical fiber lasers are not only used as light amplifiers but their waveguide properties are also exploited: the light confinement along the fiber strengthens the gain efficiency, their flexibility facilitates the beam delivery and the chromatic dispersion can be managed. Moreover, they exhibit the advantage to supply a really small spot size at least ten times lower than competitive laser sources (5 to 100 $\mu$m in diameter). Their high surface-to-volume ratio contributes to an efficient cooling (large surface of interaction with the air), so the heat can be easily dissipated. However, the amount of RE contributing to the amplification is limited by the core diameter so as to maintain a singlemode

emission. Owing to their small spot size and potentially long length, fiber lasers are subject to non-linear effects, modifying the spectral, spatial and temporal properties of the emitted beam (see Subsection 1.4.1).

To summarize, the Table 1.1 compares the laser sources presented above, regarding the level of emitted power/energy, the beam quality, the spot size and the wall-plug efficiency. Moreover, the Fig. 1.8(b) presents the beam parameter product (BPP) evolution with the power increase. It is worth to note that fiber lasers present undeniable advantages compared to other competitive sources, notably the delivery of a high average power micrometer scale beam exhibiting a low divergence ($M^2 \approx 1$). They have already demonstrated their potential for high power emission in the continuous wave regime (kW range) as well as in pulsed regime(down to fs pulses duration, up to mJ energy level). Thus, fiber lasers sources are particularly convenient for micro-machining applications. Moreover, their compactness and maintenance-free positioned them as the major solution for on-board applications.

**Table 1.1:** Comparison of the optical properties for different laser gain medium in term of power/energy levels, beam quality, beam size at the waist and wallplug (electro-optical) efficiency.

| Gain medium | Performances | Beam quality | Spot size | Wallplug efficiency |
|---|---|---|---|---|
| Solid state lasers | TW peak, MJ | Limited by thermal effects | $\approx 800\mu$m | <35% |
| Thin disk lasers | kW / 1J | $M^2 \approx 1$ | $\approx$ 1mm | <35% |
| $CO_2$ lasers | kW/$100^{th}$ kJ | $M^2 \approx 1$ | Few mm | 20% |
| Diode lasers | Up to $10^{th}$ kW | $M^2 >> 1$ | Few mm | 60-70% |
| Fiber lasers | 10kW, mJ | $M^2 \approx 1$ | 1-100$\mu$m | <50% |

Nevertheless, the power scaling in such laser medium increases drastically the constraint regarding the requirement for a singlemode emission, the fiber manufacturing and their sensitivity to non-linear effects. Thus, it will be evidenced later that it is necessary to enlarge the fiber core size and its RE concentration in order to reduce the impact of the non-linear phenomena. However, this suggests to be able to produce large volume of material, which is not so trivial with current man-

ufacturing processes. Moreover, the increase of RE concentration implies a rise of the RI, leading to guide more and more modes and enabling no longer to provide a singlemode emission. Thus, novel kind of optical fiber designs shall be devised to allow a singlemode emission from a LMA fiber. This chapter is pursued by the description of the current fiber manufacturing processes, which is one of the most important step on the development of optical fibers.

## 1.3 Standard optical fiber manufacturing processes

Fiber manufacturing is investigated since at least fifty years. The technology has mainly been driven by the telecommunication and the first real technological bolt has been released by C. Kao. With the assistance of Georges Hockman, he demonstrated for the first time the potential of optical fibers for long haul optical communication (losses as low as 20 dB/km) and by showing that optical fiber attenuation was not a basic property of the material but was due to the presence of impurities like metallic ions and OH groups [Kao86]. Today conventional optical fibers exhibit losses on the range of 0.2 dB/km at 1550 nm. Thanks to these progress, they have replaced the simple copper coaxial wires for telecommunication operation, multiplying by 65 000 times the quantity of delivered informations. In the following, the discussion is focused on silica based optical fibers due to their ability to withstand high power operation. Moreover, some manufacturing methods like the extrusion or moulding are not addressed here.

For conventional optical fibers, the manufacturing starts from the preparation of a preform (silica rod), the central part of which is doped with one or several chemical species (Germanium for instance), in order to increase its RI, constituting the future fiber core. Initially, the preform has a diameter of up to 15 cm for industrial production and a length going from 30 cm to few meters. The main challenge is to obtain low scattering losses and a low impurities content in the final fiber. Nowadays, few manufacturing processes are performing for the fabrication of low

loss optical fiber with a relative control of the transverse RI, mainly based on two approaches: internal deposition processes such as the conventional Modified Chemical Vapor Deposition (MCVD), the Furnace Chemical Vapor Deposition (FCVD) and the Plasma Chemical Vapor Deposition (PCVD) or, on the other hand, the external deposition techniques: the Outside Vapor Deposition (OVD), the Vapor Axial Deposition (VAP) [Nagel82]...

### 1.3.1 Preform fabrication

Among the CVD methods used to produce really pure glasses (very low impurities content), the most common one is called MCVD. In this case, dopants are incorporated on a gaseous state (chloride) to limit the formation of OH content during the deposition. They are flown through a tube, together with an oxidizing-inert mixture of gases ($0_2$, Ar, He) to mitigate the formation of impurities, and then oxidized by an external burner mounted on a glass working lathe. The gas is evacuated at the other extremity of the tube. A homogeneous gas phase reaction occurs wherever the gas temperature reaches at least 1200 °C. Oxide solid particles are deposited in a fine soot on the inner part of the glass tube due to the flame heating. At higher temperature, the soot is sintered into a glass layer of 10 to 150 $\mu$m. For the most conventional fibers, this layer is made of pure silica and will constitute the optical cladding. The dopant mixture is then modified to form the fiber core with higher RI. Previous sintering and vitrification steps are then repeated. The rotating tube is progressively collapsed by successive burner passes around 2000 °C. Finally, the last passage of the burner at low speed is carefully controlled to avoid creation of bubbles, totally collapsing the tube. To reduce scattering losses due to the insertion of index raising dopant in the fiber core, the step index can be obtained using a low index cladding (fluorine doped layer for instance) surrounding a pure silica core. The main advantage of fibers made by CVD is their natural low propagation losses down to 0.2 dB/km (even when they are doped with RE) [Poole86], due to very low

impurities content. Unfortunately, some shortcomings persist: a small batch size, a potential variation of fiber properties from batch to batch and a low homogeneity for large core material (control of the refractive index in the vicinity of $5 \cdot 10^{-4}$ to $1 \cdot 10^{-3}$).

For the fabrication of RE doped fibers, two methods are used. Rare-earths can be evaporated from a crucible, flown into the tube and directly deposited as soots (Vapor phase deposition). A most efficient way is the solution doping [Townsend87]. The preform is filled with an alcoholic or aqueous solution containing the RE dopant when the core material is porous. Then, the preform is dried, vitrified and collapsed as for a standard method. Moreover, the introduction of rare-earth cations in a silica glass induces additional Rayleigh scattering, although generally negligible compare to the gain enhancement.

Hence, different alternative CVD processes have been developed:

- to reduce the impurities content (mettalic ions) and increase the volume deposited, Draka or Samsung resort to the Furnace-CVD process. In this case, the burner is replaced by a microwave furnace.

- moreover, the Plasma-CVD process can also be employed to lowered the impurities content and manufactured 15 $\mu$m core gradient index multimode fibers. Microwaves are used instead of a burner to heat the deposition region, so the deposition is slow but very accurate.

Otherwise, others techniques are based on the outside deposition of soots:

- the Outside Vapor Deposition (OVD) relies on the flame hydrolysis, creating a soot deposited layer by layer along a mandrel which is removed before sintering. Then the preform has to be consolidated and collapsed in a furnace. This approach is really convenient for the fabrication of large volume of material and is notably used by Corning. The RE doping using this process is under investigations.

- this procedure can also be realised using a plasma torch. The Plasma Outside Deposition (POD) enables, for instance, the deposition of a fluorine doped layer forming the fiber cladding.

- on the other hand, the Vapor Axial Deposition (VAD) follows the same chemical principle than the OVD but the deposition is achieved axially on a rod end facet. An important difference between the OVD and CVD processes is that the doping profile is determined only by the burner geometry, rather than a variation of the gas mixture over time.

- finally, Liekki Corporation has developed recently a new fiber manufacturing technology called "Direct Nano-particles Deposition" (DND). The deposition of doped silica nanosize particles is achieved on a rod. This method offers a high control of the refractive index homogeneity, a potential for high RE concentrations (low clustering tendency) and to produce large core preform with a good homogeneity [Tammela06]. Now, these preforms are drawn to get standard step-index or gradient fibers.

### 1.3.2 Alternative process: powder sintering and vitrification

Alternatives manufacturing processes relying on the use of powder vitrification have in particular demonstrated their strong interest for the fabrication of large volume of doped material (10 to 25 larger than with MCVD). First, the company Silitec has developed a powder techniques based on the direct vitrification of powder [Devautour09b]. This method allows notably to get a homogeneous refractive index profile whose irregularities does not exceed few $3.10^{-3}$. Furthermore, a similar procedure, called "Repusil", has been devised by Heraeus and the Institute for Photonic Technology (IPHT, Jena) [Langner08] for the fabrication of RE doped silica preforms. The procedure is initiated with synthetic porous $SiO_2$ nano-particles dissolve in a liquid to form a suspension. Then, a solution composed of rare-earth and other dopants (e.g. Yb, Tm, Al, Ce ...) is added to the suspension (Fig. 1.9(1)). There-

after, this suspension is stirred and dehydrated to get RE-doped granulates, which are then dried to evaporate all the water residues (Fig. 1.9(2)). In the third step, dried granulates are consolidated in a rod called "green body" (Fig. 1.9(3)) and then placed in a pure silica tube. A chemical purification with chlorine is performed to remove the organic impurities and $OH^-$ residues (Fig. 1.9(4)). Hence, the green bodies are sintered (Fig. 1.9(5)) and vitrified (Fig. 1.9(6)) by a burner or in a furnace on a MCVD lathe to achieve a bubble-free homogeneous RE-doped preform.

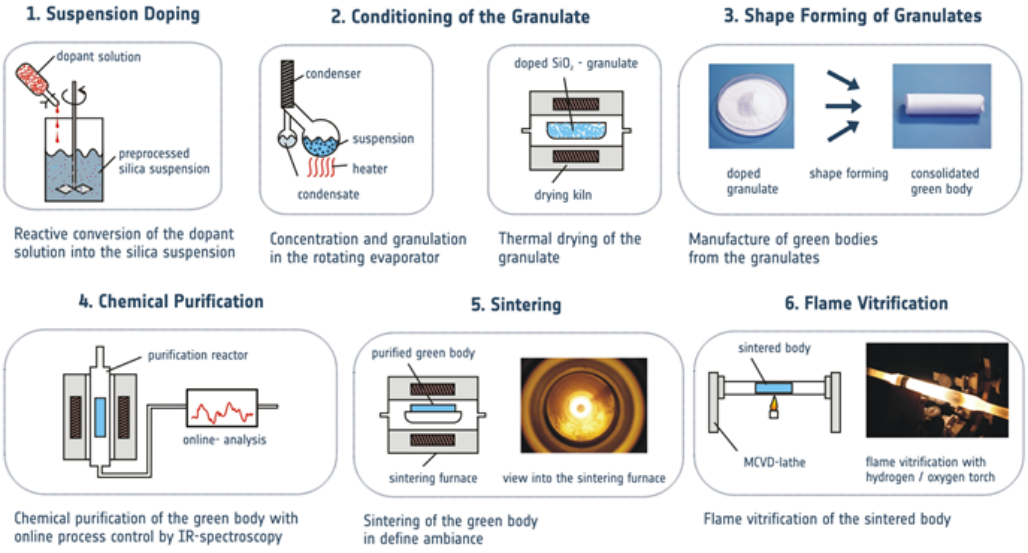


**Figure 1.9:** Schematic description of the 6 steps on which is based the Repusil process.

This manufacturing process presents the advantage to make possible the production of large rod size (up to 15 mm in diameter and 150 mm in length) with an excellent homogeneity on the refractive index profile (few $10^{-4}$ axially and longitudinally). Using this technology, the fabrication of a 100 $\mu$m core Yb-doped fiber has been reported [Langner12]. This fiber exhibits relatively low background losses: 20 dB/km at 1200 nm, a high efficiency ($\approx$ 80% [Leich11]) and has been able to withstand a high emitted power reaching 4 kW. All these performances place this manufacturing process as a serious and relevant alternative to standard CVD techniques. In the frame of the work reported in this manuscript, we resorted to the experience of our partner (IPHT) on this technology for the realization of

microstrutured optical fibers.

### 1.3.3 Stack and draw

In the middle of the $90^{'s}$, a new family of optical fibers, called "microstructured optical fibers" and discussed in detailed in Section.1.5, have emerged. Their unprecedented structure is a pure silica glass with tens of tiny air holes running along their length. Their fabrication method called "Stack and draw" starts by the fabrication of pure silica rods and tubes (raw materials). These preforms (length $\approx$ 1 m, outer diameter from 10 to 40 mm) are then drawn into several rods/capillaries of about 1-2 mm in diameter and up to 1 m in length (Fig. 1.10). All these rods/capillaries are then stacked following the fiber refractive index repartition and placed into a silica tube to maintain the stack. Finally, this stack is "drawn" into a fiber or an intermediate canes. Indeed, the drawing being a homothetic process, depending on the size of the expected pattern, an intermediate cane can be inserted in a silica tube with tailored dimensions and drawn to reduce the size of elementary pattern to submicronic dimensions.

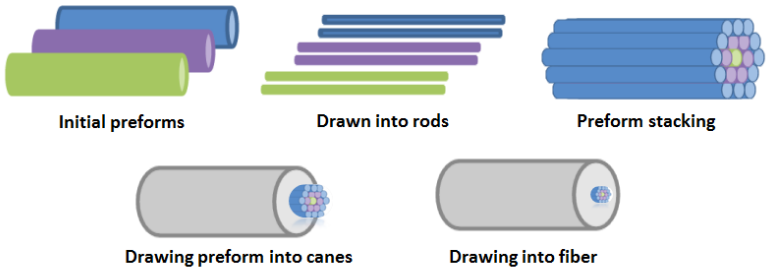


**Figure 1.10:** Schematic description of the "stack and draw" process: the initial preform is drawn into rods, which are then stacked in accordance to the final refractive index repartition. The stacked preform is drawn into canes and then into fiber.

More recently, this method demonstrated very good capabilities for multi-material optical fabrication [Markos12]. Furthermore, this "Stack and draw" method has also been used to increase to control of the refractive index profile of MCVD

made preform. With a multiple steps procedure, each initial canes are stacked and drawn until the size of the pattern reaches sub-wavelength dimensions. In this way, the refractive index is perceived as a flat average profile. This method allows the development of complex structures from rods/tubes of different shapes. This process is highly versatile and makes easier the fabrication of fiber with various materials and complex designs (undoped, doped one or "air hole").

### 1.3.4 Fiber drawing

Once the final preform is ready, the optical fiber manufacturing consists in its drawing at high temperature ($\approx 2000°C$). First, the preform is hold on a feeder on the top of a vertical drawing tower and introduced into an in-line furnace. The latter will be heat up to slightly overcome the melting point of the glass. In this way, the glass becomes soft and a thin fiber can be drawn from the bottom of the preform thanks to a capstan and winding mechanism. The capstan pulls the fiber with a well-controlled speed and tension, reducing the constrains on the fiber and redirecting it to the winding mechanism on which the fiber is wound. During the drawing, the fiber diameter is measured and held constant by adjusting automatically or manually the feed rate of the preform, the furnace temperature and the drawing speed. Before the fiber is wound, one or two stages of coating can be applied on the fiber. For a double coating, the central one is soft enough to minimize mechanical stresses on the fiber whereas the second provide a mechanical and chemical protection (avoiding micro-bending disturbance and moisture). Acrylate and silicone are typically used. After application of the coating, the fiber goes through a UV furnace in order to dry or polymerize the coating.

### 1.3.5 Composition

Depending on the targeted performances (wavelength, refractive index...), the host matrix has to be chosen to fulfil this objective. For this, different host matrix

are available: silica, chalcogenide, telluride or fluoride glasses, plastic... The most common is the silica glass. Indeed, it presents notably a relatively low thermal expansion coefficient (good thermal dissipation), a low non-linear coefficient and a relative high threshold of dielectric breakdown. For high power delivery, these properties are essential and justify the choice of the silica matrix in our work. Then, the glass composition will determine the fluorescence properties of the optical fiber. Silica host matrix leads to efficient emission on different spectral band: from 1$\mu$m to 1.1$\mu$m with Yb, 1.53$\mu$m to 1.56$\mu$m with Er, 1.9$\mu$m to 2.1$\mu$m with Tm... Afterwards, the co-doping with passive ions plays an important role, modifying energy levels and cross sections (absorption and emission), increasing of the maximum doping in active ions (avoid quenching), acting on energy transfer between several actives ions and changing the refractive index (see Fig. 1.11).

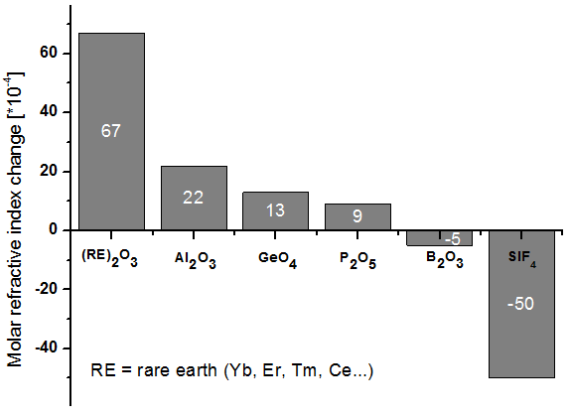


**Figure 1.11:** RI change per unit of concentration (mol%) of different dopants: rare-earth (RE), aluminium ($Al_2O_3$), germanium ($GeO_4$), phosphorus ($P_2O_5$), boron ($B_2O_3$) and fluorine ($SiF_4$).

Several compounds are usually employed as co-dopant:

Aluminium: This is an index raising dopant enhancing the solubility of the rare-earth ions ($Yb^{3+}$, $Er^{3+}$) in silica matrix and restricting the evaporation of $RE_2O_3$, resulting in an uniform radial distribution of rare-earth. It also limits the formation of aggregates and flatten the gain spectrum.

Germanium: This is an index raising dopant commonly used to promote the

photo-inscription of Bragg gratings or for the fabrication of graded-index passive optical fibers.

Phosphorus: It slightly increases the refractive index and facilitates the introduction of dopants by improving the solubility. It also reduces the melting point of the glass and favours the energy transfer occurring between $Yb^{3+}$ and $Er^{3+}$ ions.

Boron: This is an index-depressing dopant, mainly used to produce birefringent fibers (induced stress).

Fluorine: Index-depressing dopant contributing to get a good material homogeneity. It lowers the melting point.

Lanthanum: A rare-earth that is not optically active and can be used to reduce the formation of aggregates.

These dopants are the most widely used for the optical fiber manufacturing. Modifying the host matrix, they also influence its optical properties. Now that the optical fiber manufacturing has been discussed and the influence of the co-dopants addressed, we will focus on the limitation for a power scaling. Indeed, single mode fiber lasers are impacted by a lot of physical phenomena depending on the host matrix or the waveguide properties. In the next part, the main limitation in term of optical characteristic, material damages, thermal induced disturbances and long term reliability will be described.

## 1.4 Power scaling of fiber lasers and limitations

During the last decades, the output power of fiber lasers has grown quickly, reaching today the multi-kW level in CW [Gapontsev08] and the GW peak power/mJ energy in pulse regime [Eidam11a]. To access such outstanding performances, some works have been done around detrimental effects stemming from the power rise. These disruptive phenomena are of different natures: onset of non-linearities, optical damages, thermal effects [Dawson08] and photo-darkening [Koponen05]. Each of them influences the spectral, temporal or/and spatial characteristic of the laser beam and

sometimes provoke irreversible fiber damage.

### 1.4.1 Non-linearities

The power scaling in fiber lasers/amplifiers is an inevitable evolution and is subject to strong interests. However, either in broad band sources or in narrow linewidth lasers, the rise in average power is limited by an inelastic scattering effect, respectively the stimulated Raman scattering (SRS) and the stimulated Brillouin scattering (SBS), which distort the optical properties of the emitted beam.

#### 1.4.1.1 Stimulated Raman Scattering

The stimulated Raman scattering is a phonon assisted process. The energy brought by the pump photons is partially scattered to a lower frequency photon (lower energy), generating a red-shift radiation called "Stokes wave" which propagates forward. The Raman shift of the Stokes wave is close to 13 THz in silica at 1 $\mu$m but depends on the fiber material. The residual energy is then carried away by some optical phonons. Moreover, this process is reversible: an existing optical phonon can bring energy to a photon, generating a photon of higher energy, belonging to an anti-Stokes wave of shorter wavelength. In optical fiber amplifiers aiming to deliver intense pulses, SRS grows quickly and may transfer part of the pulse energy out of the wavelength band of interest, resulting in a pulse peak power limitation. The critical pump power before significant Stokes lines appear is driven by:

$$P_{out}^{SRS} = \frac{16 * \pi * r_{mf}^2}{g_r * L_{eff}}; \tag{1.6}$$

where $r_{mf}$ is the mode field radius, $g_r$ is the Raman gain (around $10^{-13}$m/W at 1$\mu$m for silica and divided by two for unpolarized amplifiers) and $L_{eff}$ is the effective fiber length. The definition of this equation is established for low pump power. To scale this formula to the kW range, an increase of the constant from 16 to 25 seems to be more appropriated. Anyway, the SRS threshold can be pushed

away by shortening the fiber length and by enlarging the mode field area. Various innovative proposals were done to struggle against this issue, such as chirped-pulse amplification [Eidam11a] spreading the pulse duration to reduce the peak power and/or the design of special fiber [Fini06b], filtering the Raman wavelength.

#### 1.4.1.2 Stimulated Brillouin Scattering

Stimulated Brillouin scattering (SBS) is also a phonon-assisted process. The pump power induces the generation of acoustic phonons through a process of electrostriction, which longitudinally modulates the fiber refractive index. Then, this induced index grating scatters the pump photons via Bragg reflections, downshifting the light. The frequency shifted backward-propagating Stokes wave creates by this way is three orders of magnitude smaller than for SRS: 10 GHz into silica at 1 $\mu$m. As for SRS, this effect is reversible. Moreover, and contrary to the SRS, the critical pump power is dependent of the spectral width:

$$P_{out}^{SBS} = \frac{17 * \pi * r_{mf}^2}{g_b(\Delta\nu) * L_{eff}}; \tag{1.7}$$

Here, $g_b$ is the Brillouin gain coefficient, depending of the spectral width $\Delta_\nu$ (about $5.10^{-11}$ m/W at 1 $\mu$m in silica with $\Delta\nu \approx$ 20MHz). This formula is established for low pump power, a scaling from 17 to 26 seems more appropriate on the kW range. As for SBS, the critical pump power depends on the fiber length and the core size. In addition, the pump and signal width has to managed to be mitigate the SBS. Once again, the deleterious phenomena can be pushed away by shortening the fiber length and enlarging the mode field.

#### 1.4.1.3 Kerr effect

Otherwise, the Kerr effect induces disturbing non-linear processes such as the self-focusing, the self-phase (SPM) or cross-phase (XPM) modulation and the Four-Wave Mixing (FWM). The Kerr effect occurs when intense light beam travels through a

non-linear medium (silica for instance), modifying its refractive index proportionally to the light intensity:

$$\Delta n = n_2 * I \qquad n_2 = \frac{3}{8 * n} * \chi^3; \tag{1.8}$$

with $n_2$ being the non-linear index ($\approx 3.10^{-16}$ cm$^2$/W for standard silica fibers), depending of the third order of the molecular susceptibility, and 'I' the optical intensity. Moreover, the Kerr effect also induces a non-linear phase shift, provoking a pulse chirp: the instantaneous frequency becomes time-dependent and distorts the initial pulse. This phenomenon is the source of the SPM, impacting the temporal laser properties and broadening the spectrum. Furthermore, the pump radiation can also affect the phase of the signal one by this way. In this case, one talks about cross-phase modulation. These non-linear processes are notably useful for the realization of very broad band laser called super-continuum but must be fought for the development of high power laser sources. Moreover, as the beam is commonly more intense on the fiber axis, it implies a larger increase of the refractive index on it. Hence, it acts like a focusing lens, and can led to the destruction of the optical medium. This disturbance has been noticed in bulk laser but is commonly negligible in fiber lasers. However, this phenomenon could appear in VLMA fibers. The Kerr lens occurs in silica fibers around 4 MW of peak power around 1 $\mu$m, so far above the 2 previous mentioned phenomenon.

### 1.4.2 Thermal issues

On the other hand, the power scaling in optical fibers is also limited by the temperature deposition in the gain medium due to the quantum defect. This implies a modification of the material refractive index and consequently impacts on the guidance properties. Thermal fracture, core melting, thermal lensing, or modal instabilities can thus occurred. A detailed investigation of the thermal induced damages in optical fibers was achieved by Brown *et al.* [Brown01]. They have established

that the maximum extractable power per unit length is directly proportional to the heat deposition on the fiber: (1-$\eta_{heat}$)/$\eta_{heat}$, with $\eta_{heat}$ standing for the amount of absorbed pump power converted into heat through non-radiative transitions and the quantum defect (relative difference between the laser energy and the pump one). In fact, all the absorbed energy which does not contribute to the emission is converted into heat ($\eta_{laser}$+$\eta_{heat}$ = 1, where $\eta_{laser}$ is the optical efficiency of the laser system). In the high power regime, the amount of heat becomes significant and can have some deleterious impacts on the fiber laser properties.

***Thermal lens***

Initially, the absorbed pump radiation heats up the gain medium through a thermo-optic effect, which is quantified by the thermo-optic coefficient dn/dT (11.8*$10^{-6}$ .$K^{-1}$ for silica), and a thermal induced stress. The refractive index profile of the fiber is thus influenced and shows a quadratic shape on the gain region and logarithmic outside [Hädrich06]. Hence, this thermal induced refractive index change induces the self-focusing of the beam. The threshold for which the thermal lens competes with the index guiding is:

$$P_{out}^{lens} = \frac{\eta_{laser}}{\eta_{heat}} * \frac{\pi * k * \lambda^2}{2 * \frac{dn}{dT} * a^2} * L \tag{1.9}$$

where $\lambda$ represents the signal wavelength, k is the thermal conductivity of the medium (1.38 W/(m.K) for pure silica), a is the core radius. However, optical fibers are usually immune to thermal lensing because the induced refractive index change is too weak to substantially influence the guidance properties of the fiber ($\Delta n \approx 8 \cdot 10^{-6}$ in a 10 $\mu$m core step-index fiber pumped with 180W [Brown01]). However, for a fiber exhibiting a large core and so a very high thermal load, this can result in a significant disturbance and a decrease of the beam quality/stability.

***Thermal fracture***

Furthermore, a large heat deposition can also lead to a partial destruction of the material. Each material presents an inherent resistance to constraints quantified by

their rupture modulus Rm, which is around 2460 W/m for pure silica. In order to avoid fractures, the maximum extractable power per units length has to be maintain lower than:

$$P_{out}^{rupture} = \frac{\eta_{laser}}{\eta_{heat}} * \frac{4 * \pi * R_m}{1 - \frac{a^2}{2*b^2}} * L \tag{1.10}$$

where Rm is the rupture modulus of the glass, L the fiber length, a is the core radius and b, the cladding radius. Nevertheless, the rupture modulus decreases when dopants are introduced in the silica matrix.

***Core melting***

Finally, an excessive heat load into the fiber core can melt it. This occurs for an output power of about:

$$P_{out}^{melting} = \frac{\eta_{laser}}{\eta_{heat}} * \frac{4 * k * (T_m - T_c)}{1 + \frac{2*\kappa}{b*h} + 2 * \ln(\frac{b}{a})} * L \tag{1.11}$$

where $T_m$ is the melting temperature (1700°C for silica), $T_c$ is the cooling temperature, and h is the convective coefficient depending on the cooling method: 5 to 50 W/(m$^2$.K) for natural air convection and 100 to 15 000 W/(m$^2$.K) for forced water cooling. In many cases, strategies like polymer suppression and thermal cooling are used. An efficient cooling can be achieved by embedding the fiber into a flowing water bath.

### 1.4.3 Modal instabilities

Recently, a strongly disruptive effect called "modal instabilities" has been evidenced in Large Mode Area (LMA) fibers supporting the propagation of few modes [Eidam10]. This severally degrades the laser beam quality by disturbing the single-mode behavior. Intense investigations tending to describe the behaviour of these instabilities have been already conducted [Smith11, Ward12, Hansen13]. A thorough explanation was provided in [Jauregui12] but the origin of this phenomenon is not totally clear. Modal instabilities occur since the pump power exceeds a threshold

value (se Fig. 1.12) depending on the operating conditions (absorbed power, laser efficiency...) and the fiber structure.

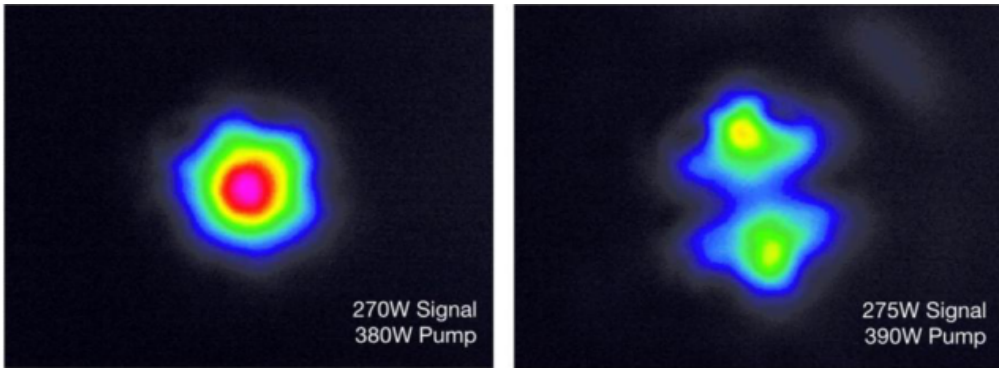


**Figure 1.12:** Near-field images of 63 $\mu$m core Large Pitch Fiber below (left) and above (right) the modal-instability threshold. The signal output power at 1040 nm and the pump power at 976 nm wavelength are depicted. The temporal dynamics can be seen in [Eidam11b].

This effect originates from the fact that double clad LMA fibers inherently support the propagation of a lot of modes. As the fundamental mode presents the largest overlap with the gain medium, it benefits more gain and is mainly amplified. Nevertheless, when at least two modes are sustained by the fiber core, they interfere, creating a periodically oscillating intensity pattern all along the fiber length. The periodicity of the pattern is driven by the beat length $L_b$ between this two modes: $L_b = \frac{\lambda}{\Delta n_{eff}}$. Then, the population inversion is impacted and exhibits by the way a longitudinal oscillating distribution. This involves consequently that the standard exponentially decreasing pump absorption is modulated mimicking the population inversion evolution. In turn, this longitudinally varying absorption generates an oscillating heat load, which after a certain time, will modify the temperature profile. Moreover, as the refractive index is temperature dependent, the oscillating longitudinal temperature profile gives birth to a so-called "Long-Period Grating" (LPG). When the temperature gradient is strong enough, the beam can not evolved as fast as these rapidly varying waveguide conditions, delaying the beam with respect to the index profile, and making the energy transfer possible between the two modes implies in the process. In conclusion, a fast temporal fluctuations of the mode

intensity (kHz frequency) are experimentally observed [Eidam11b].

Hence, to pushed away this disturbance, the core modal content should be reduced further by delocalizing the High-Order Modes (HOMs) out of the gain region. So, novel fiber designs exhibiting an efficiently discrimination of the HOMs must be devised. Moreover, although optical fibers have a natural tendency for temperature dissipation because of their inherent large surface to volume ratio, the use of flowing water cooling is beneficial for extremely high power higher than hundred watts/meter, notably to struggle against modal instabilities. The rise in temperature can also be compensate by embedding slightly the core RI for instance.

### 1.4.4 Photodarkening

To conclude this section concerning the limit of the power scaling on the optical fibers, it is important to evoke the "darkening", acting on the long term reliability of amplifiers and lasers. It can be induced by different radiations. Photodarkening (PD) is related to the irradiation of gain medium by light (UV, visible and IR) [Koponen06] whereas radiodarkening concerns effect induced by X-rays [Mady10] or Γ-rays [Deschamps13]. We will focus on the PD, most likely for standard applications [Koponen05]. The photodarkening induces a large increase of losses from the UV to near IR range (see Fig. 1.13). This provokes a gradual decrease of the output power and a decrease of lifetime. This behaviour has been observed for different rare-earths: $Tm^{3+}$ [Broer91],$Ce^{3+}$ [Broer93], $Pr^{3+}$ and $Eu^{2+}$ [Behrens90], $Tb^{3+}$ [Atkins06] and also $Yb^{3+}$ [Paschotta97]. During the laser/amplifier operation, it has been highlighted that the efficiency can drastically felt down. In [Jetschke09], they show that photo-induced losses follow an exponential evolution over the time before reaching an equilibrium state [Jetschke07]. These losses stem from the generation of "color centers" due to the trapping of electrons or holes into the glass/crystal lattice defects notably, causing clustering, charge transfer process [Engholm07], capture of electrons on $Yb^{3+}$ pairs, photo-ionization... It has been reported that the

formation of $Yb^{2+}$ ions plays also an important role on the onset of photo-induced losses [Rydberg13]. Furthermore, a recent work demonstrates that the fluorescence properties of the gain medium are also impacted [Jetschke13].

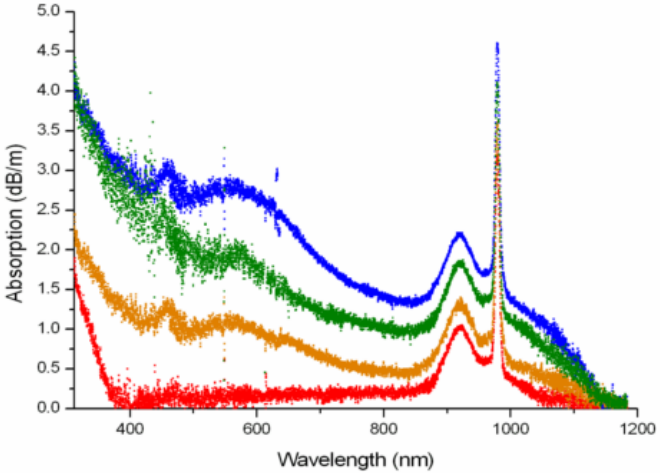


**Figure 1.13:** Example of photodarkening induced losses in an Yb-doped fiber versus the exposure time: pristine fiber (red), 7 min (orange), 15 min (green) and 100 min (blue). Picture extracted from [Manek - Hönninger07].

Investigation on the optical properties of fiber lasers and their material composition has allowed to improve the resistance to this phenomenon. Although it is not trivial to provide a brief overview of the photodarkening mitigation due to the wide variety of host matrices and laser configurations, several relevant examples are summarized. First of all, Koponen *et al.* has demonstrated the dependence of the PD excess losses to the density of excited ions, and therefore, the population inversion [Koponen08]. In parallel, different research teams have studied the influence of the material composition to fight against this mischief. The strategy to catch the free holes/electrons has been to co-doped the silica lattice to reduce the formation of color centers. The impact of several chemical species having an electronic composition close to that of the silica (Aluminium, Phosphorus) or that of rare-earths: Cerium has been investigated. Initially, Yb-Al codoped silica fibers have been studied as they present a high absorption and emission cross sections, flat gain, high efficiency but also good mechanical and thermal properties. Moreover, Aluminium

contributes to reduce the clustering, which is a source of darkening. With this composition, the resistance of Yb doped fiber laser has been significantly enhance compare to a codoping with germanium [Morasse07]. Later, the use of Phosphorus in Yb or Yb-Al doped silica fibers has provided an efficient route to struggle the photo-induced losses, limiting by the way the risk of clustering [Engholm08, Jetschke08]. Moreover, the introduction of large content of aluminium (5 mol%) in a phosphosilicate fiber (6 to 12 mol%) has enabled the fabrication of degradation free fibers based on Yb-doped phosphate glass [Lee08]. Unfortunately, phosphosilicate fibers exhibit some drawbacks: reduction of cross-sections, lower efficiency, central refractive index dip during the preform collapsing due to diffusion and higher background losses. To push further this investigation, Engholm *et al.* suggested to incorporate $Ce^{+2}$ ions on Yb-Al matrix to trap free electrons. Thus, the interesting optical properties stemming from the Al doping are maintained [Engholm09, Jelger10]. Finally, an alternative fabrication process: the direct nanoparticle deposition(DND) has demonstrated a PD mitigation, for which the photo-induced attenuation was less than half that of the conventional fibers [Koponen05].

In the other hand, partially or fully reversed photodarkening process has been noticed and called photobleaching (PB). It is making possible through a temperature treatment [Leich09] or an exposure to specific light: 355nm [Manek - Hönninger07, Söderlund09], 543nm [Guzman-Chavez07], 633nm [Gebavi12, Gebavi13] to annihilate the defect generated by the PD process. Moreover, it has been demonstrated that an oxygen [Yoo07] and hydrogen loading [Jasapara06] limits the creation of defects.

This overview of power scaling limitations has underlined that progress can still be done on this topic by enlarging fiber cores to push away the non-linearity, by managing the thermal load, and by optimizing the material composition. Moreover, an improvement of the singlemodeness should be beneficial to fight against modal instabilities. In the next section, a summary of the different available solutions to

increase the singlemode robustness of fiber lasers will be discussed.

## 1.5 Fiber design evolution for singlemode operation in high power regime

From the first core pumped fiber lasers, the power scaling has been governed by several major evolutions in fiber structures. The launched pump power was drastically enhanced (5 orders of magnitude) thanks to the development of double clad fibers. Moreover, to fight against non-linear processes disturbing the temporal, spectral and spatial properties of the laser beam, the fiber core and laser cavities have also evolved. Non-linear processes being proportional to the fiber length and conversely proportional to the mode field area, the first challenge is the reduction of the required fiber length by increasing the pump absorption through a strong rare-earth ions concentration or a modification of the cladding shape. On the other hand, the power density of the emitted beam shall be lowered by enlarging the fiber core, although the waveguide tends to support more and more guided modes for very large core diameters. Several innovative fiber designs have been thus developed to keep a singlemode behavior.

### 1.5.1 Double clad fibers

To skirt the power limitations of singlemode pump laser diodes, the structure of optical fibers has evolved and a second cladding has been implemented, allowing the efficient coupling of very high power, low brightness multimode diodes into the fiber (Fig. 1.14(a)-(b)). Thus, the fiber becomes a brightness converter as the multimodal pump is changed into a singlemode signal with a lower spot size. Initially, a low index polymer has simply replaced the high index one previously used in order to provide a large surface and large angle of acceptance/numerical aperture (NA) for an efficient coupling of the pump radiation. The pump light being propagate into a strongly multimode cladding, the overlap of the pump radiation with the active

core is relatively low compared to that of standard core-pumped optical amplifiers. Thus, a longer fiber length is required in double clad optical fiber to absorbed a sufficient amount of pump power. The absorbed pump power can be maximized by increasing the RE concentration, increasing by the way the core refractive index, or by optimizing the double clad shape. For instance, the pump light can propagate in a caustic way for a circular cladding (related to helical rays), so part of the pump power travel through the fiber without crossing the fiber core. Since 1988 [Snitzer88], alternative cladding shapes have been used to improve the core absorption: D-shape, double D-shape, rectangular, elliptical or hexagonal [Leproux01]. It was also shown that coiling a long length of fiber in a kidney shape contributes to the improvement of the pump absorption and the suppression of HOMs [Tünnermann10]. This method is today employed in commercially available multi-kW fiber laser sources but, owing to the long fiber length, the non-linear effects strongly disturb the emitted spectra. This solution is not convenient for application requiring a narrow linewidth or short pulses.

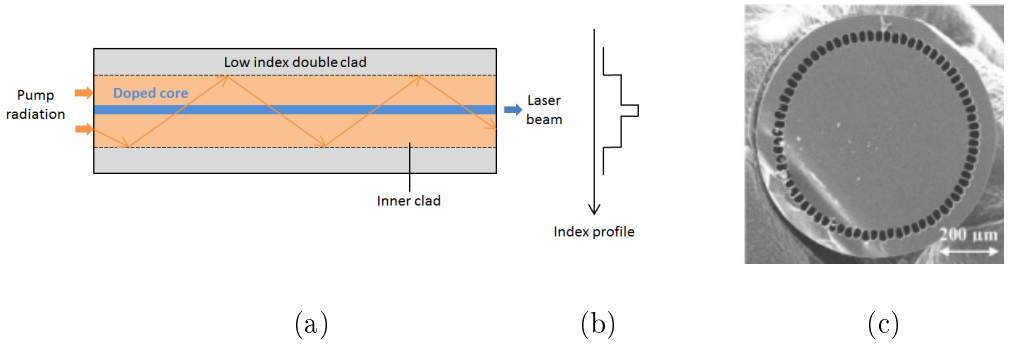


**Figure 1.14:** (a) Schematic double clad fiber side view and (b) RI profile. (c) Microscope picture of an "air clad".

Under strong pumping, low index polymers quickly reach their limit as a direct interaction with the pump radiation provoke their burning. The standard epoxy acrylate low index coating is usually unusable for pump powers exceeding few tens of watts in a 125 $\mu$m silica fiber. Moreover, Teflon based coatings can provide an enhancement of one order of magnitude and a high NA ($\approx$0.6) but their application

along the fiber length is not so simple. In order to avoid the interaction of the pump radiation with the polymer, alternative double clads have been developed. A fluorine doped silica layer can be used as pump cladding, providing a NA of about 0.22. Up to date, the major solution is the use of an "air-clad", consisting in a ring of air holes surrounding the inner cladding and running along the fiber length (Fig. 1.14(c)). This allows to reach very high NA (up to 0.8 [Wadsworth03]). Investigations on such double clad was done, demonstrating that the thickness of the silica bridges separating each air hole has to be thin enough ($\lambda/2$) and their length sufficiently long (at least 2 times $\lambda$) to provide a NA exceeding 0.5 [Issa04]. Today, the use of air-clad is widespread into high power fiber lasers, allowing to pump fiber lasers with a power reaching the kW range.

### 1.5.2 Optical fiber singlemodeness

Following the pumping of the gain medium, a laser emission can occurred from an optical cavity (under conditions of population inversion). In order to maximize its amplification, the emitted beam strongly interacts with the gain medium and is efficiently amplified. Hence, the second requirement on fiber laser concerns their beam quality. Especially for the marking and engraving, a Gaussian beam contributes to obtain an accurate and clean material processing whose the borders are sharp and not rough. However, the pump power scaling has led to the increase of the emitted power, and so the power density on the gain medium. As mentioned in the previous section, large power densities imply the appearance of non-linear processes disturbing the spatial, spectral and temporal properties of the emitted beam. To reduce the impact of these unwanted phenomena, it is necessary to enlarge the fiber core size and to shorten the fiber length. Nevertheless, the singlemodeness of fiber lasers is bound to the mitigation of the waveguide's tendency to support more and more guided modes when the core size rose. In conventional optical fibers composed of two media: a high index core propagating the emitted signal and a cladding of lower

index, this tendency is strictly related to the refractive index contrast between the core and the cladding, and the core radius. This ability is transcribed through the spatial frequency parameter V:

$$V = \frac{2 * \pi}{\lambda} * a * NA \qquad NA = \sqrt{n_{core}^2 - n_{cladd}^2} \tag{1.12}$$

where $\lambda$ is the operating wavelength, a is the core radius. $n_{core}$ and $n_{cladd}$ are respectively the core and cladding RI, defining the angle of acceptance/numerical aperture (NA) of the fiber. Through this equation, it appears clearly that to maintain a singlemode operation (V <2.405), a core enlargement has to be compensated by a lowering of the refractive index contrast, in such way that for a 20 $\mu$m core Yb-doped fiber ($\lambda$ = 1.06 $\mu$m), a contrast as low as $5 \cdot 6.10^{-4}$ is required. Unfortunately, this level of accuracy is not achievable with current manufacturing processes. In this context, novel kinds of fiber designs have been developed since two decades to provide a large mode field area (MFA) singlemode emission by delocalizing HOMs out of the fiber core. These proposals rely on two guidance mechanisms.

### 1.5.3 Guidance principles

Nowadays, a wide variety of optical fibers have been devised to reach outstanding optical performances such as: dispersion management, polarization control, singlemodeness at high power, ... All these optical waveguides are based on two different guidance mechanisms: the Total Internal Reflection (TIR) , or further the Modified Total Internal Reflection (MTIR) , on which the light is totally reflected in the dioptre between the core and the clad as the fiber core has a higher index than the cladding; and the Photonic BandGap (PBG), guiding the light through a resonant effect.

#### 1.5.3.1 Total Internal Reflection

This light guidance mechanism has been initially demonstrated by D. Colladon and J. Babinet in 1840 [Colladon42] by propagating the light through a thin and curved water stream. In the same way, the light is guided in flexible step-index optical fiber (Fig. 1.15(a)). In facts, a ray of light travelling through a high index medium (the fiber core) and facing the interface with a surrounding low index material (its inner cladding) may be trapped into the high index region by total reflection on the dioptre while the angle of incidence $\Theta_1$ is larger than the critical angle (Fig. 1.15(b)). In the opposite, the ray of light is refracted and leaks in the low index region. These behaviours are governed by the Snell-Descartes law:

$$n_1 * sin(\Theta_1) = n_2 * sin(\Theta_2) \tag{1.13}$$

where $n_1$ and $n_2$ represent the refractive indices of the two media and $\Theta_1$, $\Theta_2$ the incident and refracted angles. So, as illustrated in Fig. 1.15(b), when $\Theta_1$ overcomes the critical angle $\Theta_c = \sin^{-1}(n_2/n_1)$, the light can be propagated along the high-index medium by total internal reflections. Commonly, standard optical waveguides

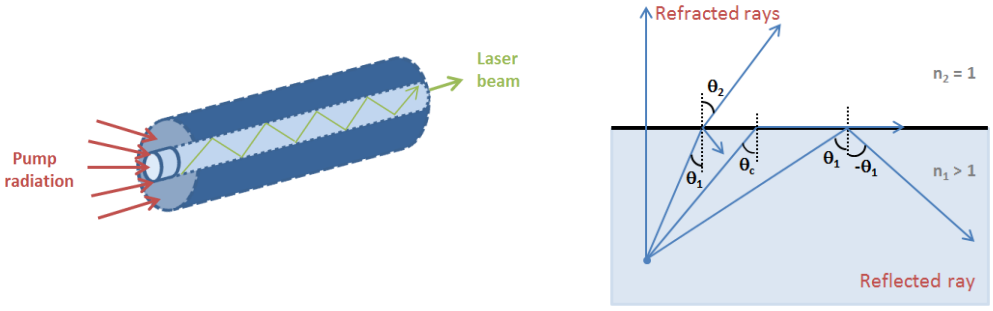


(a) (b)

**Figure 1.15:** (a) Schematic representation of a double clad fiber on which the pump light is launched in the double clad and the laser radiation is confined into the fiber core. To simplify the representation, the low-index polymer is not reported. (b) Principle of the Total Internal Reflection for 3 different angles of incidence: 1- Refraction, 2- Critical angle and 3- Total internal reflection. Dotted lines represent the normal axis to the interface.

(slab, optical fibers...) rely on this principle. Moreover, since the 90's, microstructured optical waveguides are appeared on which the high-index medium is no longer azimuthally surrounding by a low index interface, but rather by discrete low-index inclusions. In this situation, one talk about "Modified Total Internal Reflection". Several examples of optical fibers based on this principle will be reported later.

#### 1.5.3.2 Photonic Band Gap effect

In 1912, W. L. Bragg found that incident waves, the wavelength of which is $\lambda$, striking a periodic structure defined by a lattice pitch noted 'd', can be reflected if the following condition is fulfilled (Bragg law):

$$2d * sin(\Theta) = m * \lambda \tag{1.14}$$

where $\Theta$ stands for the incident angle of the waves and m is an integer. This relation displays that waves can be reflected by the crystal only for specific wavelengths and angles of incidence, giving it properties of spectral filtering. Later, W.L. Bragg achieved the first unidimensional photonic crystal waveguide (Fig. 1.16(a)). The latter, called Bragg mirror, is composed of a periodic superposition of alternate low and high-index layers whose thickness defines the wavelength which is reflected at 99.9%

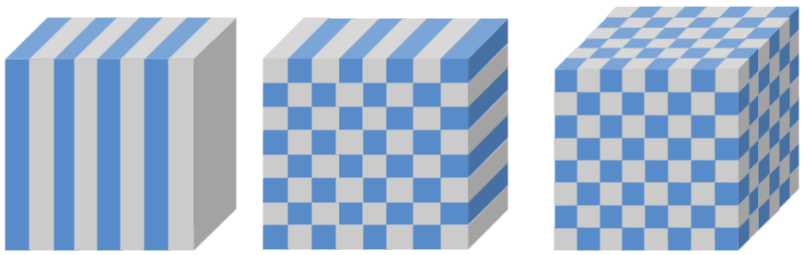

(a) (b) (c)

**Figure 1.16:** Examples of (a) unidimensional, (b) bidimensional and (c) tridimensional photonic crystal.

if a sufficient number of layers are piled, leaving the other wavelengths cross through it. In a larger scale, a photonic crystal is an optical microstructure whose dielectric properties are varying periodically. Yablonovitch and John [Yablonovitch93] have described in details the light propagation in such waveguide. Nowadays, different classes of photonic crystal arrangements exists and are reported in Fig. 1.16.

Thus, for optical structures, the periodic variation of the refractive index gives particular properties to the medium, periodically authorizing (or not) the propagation of light, giving birth to the concept of photonic bandgap: PBG. By adding a defect on the lattice periodicity, the light reflected by the photonic crystal is trapped and can be propagated along this defect. In this way, the waveguide transports light on a core having a lower refractive index than the surrounding medium. By opposition to the TIR process, this guiding mechanism based on the PBG effect relies on the resonances and anti-resonances of the photonic crystal.

At the resonance, the light can cross the photonic crystal (bottom of the Fig. 1.17(a)). This event is governed by:

$$\lambda_m = \frac{2n_1 d}{m}\left[\left(\frac{n_2}{n_1} - 1\right)^{1/2}\right] \tag{1.15}$$

where $n_1$ is the refractive index of the low-index layers, $n_2$ is that of the high-index layers, 'd' is their thickness, and m is an integer. Otherwise, when the anti-resonant condition is fulfilled, waves are reflected by the crystal (top of the Fig. 1.17(a)) and light is guided in the defect. Thus, such structures exhibit a spectral filtering, as depicted in Fig. 1.17(b) for a 2D PBG fiber. For instance, the light confinement by PBG effects allows the development of silica waveguide with an air/gas filling core, called hollow core fibers [Ouzounov03].

Using these two guidance mechanisms, fiber designers were ingenious and have devised LMA fiber whose the fiber core can reach up to 135 $\mu$m while a singlemode operation is maintained [Limpert12b]. For this, different approaches have been followed to efficiently discriminate the HOMs and favour the amplification/emission

of the sole fundamental mode.

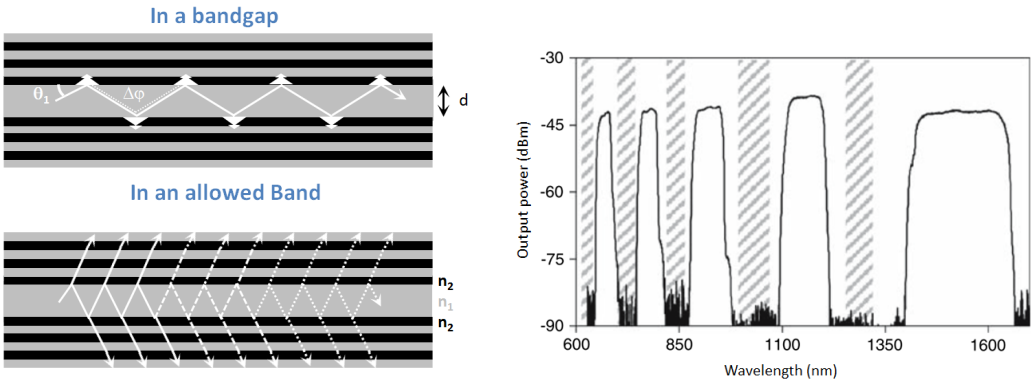


(a) (b)

**Figure 1.17:** (a) Behaviour of light into a photonic crystal. (b) Example of spectrum after propagation on a photonic bandgap structure [Bouwmans07]. Hatched regions refer to the allowed bands of the photonic crystal.

### 1.5.4 Method for HOM discrimination

In this section, methods enabling to reduce the modal content in the fiber core are discussed. Among them, the selective amplification, the controlled bending for HOMs suppression, the resonant coupling to delocalize high-order modes (HOM) out of the core or the development of complex microstructured optical fibers (MOF) have been used.

#### 1.5.4.1 Selective amplification

It is well-known that on LMA fibers exhibiting a relatively low NA, a partial active doping of the fiber core (50 to 60% of the core diameter) contribute to an efficient selective amplification of the fundamental mode. This principle has been theoretically demonstrated for the first time by Marciante *et al.* on a 50 and 100 $\mu$m core step index fibers having a NA of 0.5. In this situation, a singlemode emission has been evidenced in these slightly multimode fibers thanks to the gain competition between all modes [Marciante07]. Indeed, each guided modes present its own field

distribution and only the $LP_{0m}$ modes exhibit a maximum of their electric field on the center of the fiber core. Therefore, by carefully designing the dimension of the doped region, these modes can be preferentially amplified. Moreover, as high-order $LP_{0m}$ modes spread more than the $LP_{01}$, the latter should be preferentially amplified.

Furthermore, the influence of the transverse profile of active ions (step-index or gradient) was also checked, showing that a graded index gain profile mainly amplified narrow peaked $LP_{0m}$ modes and makes more difficult the filtering of HOMs [Marciante09]. To the contrary, it provides a stronger resistance against bend induced mode deformations. Thanks to this selective doping, the fundamental mode is preferentially amplified and the beam quality can be improved [Marciante10].

#### 1.5.4.2 Bending losses

On the other hand, the confinement conditions of optical fibers are influenced when the latter is subjected to curvatures. All modes are concerned but HOMs suffer larger losses due to their lower effective indices and confinement. By this way, light is slowly shifted out of the core and the mode field diameter (MFD) is lowered when the bending radius is reduced. This behavior can be modelled as a modification of the refractive index profile. Although the definition of the equivalent refractive index profile is still debated, its common expression is:

$$n(\theta,r) = n_{mat}(\theta,r) * \sqrt{1 + \frac{2r}{R_b}} \tag{1.16}$$

where $n_{mat}(\theta,r)$ stands for the refractive index profile of the straight fiber, $R_b$ is the bending radius and r is the radial position [Fini06a, Schermer07]. The bending influence can be seen as a tilt of the refractive index profile (Fig. 1.18(a)). Thus, modes can escape from the fiber core and HOMs experience significant induced bending losses whereas the fundamental mode is maintained quite well confined, allowing a singlemode emission. For a slightly multimode 25 $\mu$m core (V≈7.4) with

a bending radius of about 1.5 cm, no deterioration of the laser efficiency was noticed and a good beam quality obtained: $M^2 \approx 1.09$ [Koplow00] [1]. Furthermore, Jeong *et al.* have obtained a 900 $\mu m^2$ singlemode beam ($M^2$=1.4) with 1.36 kW of output power [Jeong04]. Unfortunately, this method requires long fiber length, contributing to enhance the non-linear processes and the discrimination is not sufficient for core diameters larger than 25 $\mu$m at 1 $\mu$m, that is to say when the mode density increases. Moreover, this method is no longer relevant for larger core size as a reduction of the refractive index contrast is necessary, requiring larger control of the refractive index profile, which is not achievable with CVD techniques, notably with RE solution doping. An alternative strategy was to realize a triple clad fiber whose the index of the inner cladding can be adjusted with a strongest accuracy thanks to Ge doping for instance.

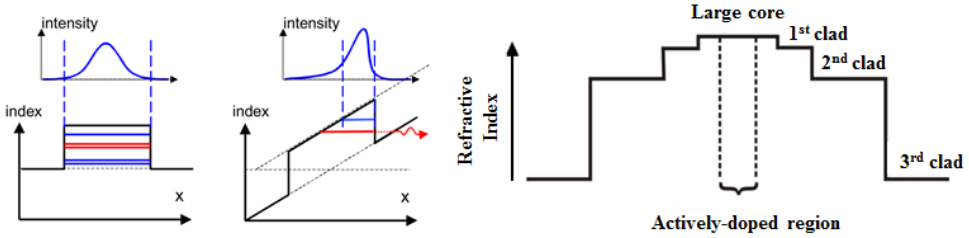


(a) (b)

**Figure 1.18:** (a) Influence of the fiber bending on the intensity profile of the fundamental mode (on the top) and the RI profile [Fini06a]. Effective indices of the guided modes are also depicted on the RI profile (top blue line: fundamental modes, other lines: HOMs). (b) Transverse RI profile of a triple-clad fiber.

Triple clad fibers take benefit from the combination of a selective doping of the fiber core and a significant rise of the HOMs losses induced by the fiber coiling. These fibers are composed of a partially doped core, a slightly depressed inner clad aiming to limit the number of guided modes in the rare-earth doped region

[1] Although a $M^2$ value approaching 1 is commonly considered to describe a singlemode operation, the reliability of this parameter is still under debate [Wielandy07] and alternative methods have been proposed to characterize the beam quality: $C^2$ [Schimpf11], $S^2$ [Nicholson08].

of the central core (NA≈0.06) and a second clad made of pure silica. A third one confining the pump radiation is used (Fig. 1.18(b)). By this way, strong RE ions concentrations over a large core, together with a singlemode emission, are made achievable by adjusting the refractive index of the first clad. The fiber can thus be shorted and mitigates the impact of non-linearities. Laperle *et al.* has reported the fabrication of a 33 $\mu$m core Yb-doped triple clad fiber laser, made by MCVD and solution doping [Laperle06]. They demonstrated an efficient nearly diffraction-limited emitted beam (efficiency: 84%, $M^2$ = 1.1) having a mode field diameter of about 18 $\mu$m at 26 W of emitted power and a relatively low bending sensitivity (down to 5 cm). Unfortunately, no larger core have been reported on triple clad structure due to the intrinsic limits on the refractive index control stemming from the use of CVD methods.

#### 1.5.4.3 Resonant coupling of HOM

Otherwise, HOMs can be discriminated by a selective coupling and so delocalized out of the core. Chirally Coupled Core fibers (CCC) fulfill this function. In this structure, HOMs guided in a slightly multimode core can be resonantly coupled out to a helical guide wrapped around it, where they are strongly attenuated, leaving only the fundamental mode being located and propagated in the central core (Fig. 1.19). However, the helix period and radius have to be choose with care to allow the suitable coupling of the HOMs into this helical guide. An experimental demonstration was done with a 34 $\mu$m core CCC fiber, the beam quality of which tending to the diffraction-limited condition ($M^2 \approx 1$) [Liu07]. CCC fibers have also been used in pulsed regime. The emission of 80 fs duration, 25 nJ energy pulses at a repetition rate of 39 MHz [Chen10] was reported. Moreover, in the similariton regime, a 86 fs, 61 nJ pulse was obtained [Lefrancois13]. Nevertheless, for fiber core larger than 35 $\mu$m, it is more difficult to ensure a resonant condition for all the HOMs localized into the core. The mode overlap with the helical guide is reduced

and leads to a weaker mode coupling. For these two reasons, this approach cannot be used for core diameters above 40 $\mu$m. In a similar way, a resonant ring surrounding the core or an array of high index inclusions can selectively coupled HOMs, as it has been reported [Fini05,Lavoute06].

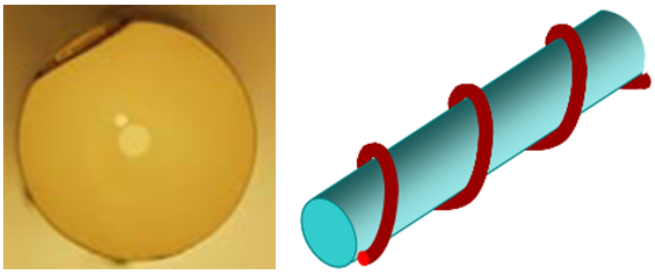

(a) (b)

**Figure 1.19:** (a) Microscope picture and (b) schematic representation of a chirally coupled core fiber [Liu07].

As mentioned above, the control of the refractive index is a restrictive issue to enlarged the active core diameters while keeping a singlemode emission. Taking into account the limits of the CVD processes, the material structuration appears relevant. Indeed, the major breakthrough for the development of singlemode LMA fibers was the cladding microstructuration achieved with the stack-and-draw technique [Yan05]. This allows to manage the optical properties (average cladding refractive index, material and waveguide dispersion, polarization, birefringence...) and to control the number of guided modes sustained by the core. Thus, the fiber laser community has demonstrated a large interest for microstructured optical fibers (MOF) and several performing solutions have been proposed. One strategy to reach the wanted singlemode emission is to reduce the core NA.

#### 1.5.4.4 Low core NA microstructured optical fibers

Initially, the first MOFs were called Photonic Crystal Fibers (PCF) and were based on a periodic arrangement of tiny air holes embedded on a silica undoped media

and running along the fiber length [Knight96]. The objective was to demontrate the photonic bandgap effect in such "photonic crystal" but the real PBG was evidenced later [Cregan99]. Nevertheless, this new family of fiber exhibits outstanding capabilities and has been intensively studied. For such PCF structures, the guiding is called Modified Total Internal Reflection (MTIR) as the core to clad interface is no longer azimuthally continuous. To form the fiber core, the central air hole is removed, creating a channel for propagation of the laser radiation (Fig. 1.20(a)). The size of the tiny air holes constituting the inner clad can be accurately controlled, offering low core NA as well as larger depending on the final application. The potential of PCF was studied and their endlessly singlemode behaviour (ESM) has been quickly evidenced [Birks97]. It was shown that over the entire spectral range, a singlemode operation occurs if the holes diameter 'd' does not exceed 0.406 times the pitch $\Lambda$ (distance between the center of neighbour holes) [Kuhlmey02, Mortensen03]. Besides, only few works have been reported on the fabrication of all-solid PCF [Feng03, Chen06, Zhang12], despite their endlessly singlemodeness was also highlighted [Chen06, Dong08]. In this case, the boundary between the singlemode and multimode operation is close to $d/\Lambda = 0.42$, underlining that the inclusions index are not so influential.

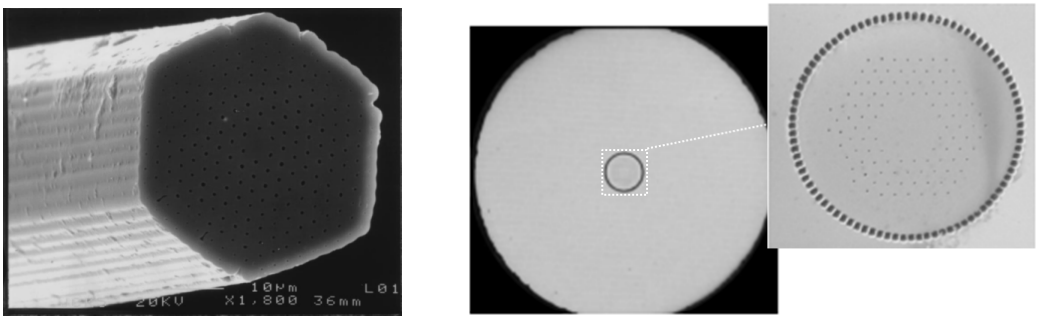

(a) (b)

**Figure 1.20:** (a) Scanning electron microscope image of the first fabricated air-silica PCF from [Knight96]. (b) Cross sections of a rod-type PCF composed of a 60 $\mu$m core and air air-clad. Extracted from [Limpert06].

Furthermore, it has been highlighted that the ESM ability is conversely proportional to the number of missing holes. For instance, air-silica PCF having 3 and 7 missing holes exhibit this potential respectively for holes diameter lower than 0.165 and 0.046 times the pitch $\Lambda$. From a practical point of view, the control of tiny air holes diameter is very challenging but was nevertheless made, even for industrial products. Thanks to their inner cladding microstructuration, the core of PCFs can be enlarged up to 100 $\mu$m while maintaining a singlemode emission [Brooks06], enabling a high pump absorption and pushing away the appearance of non-linear phenomena. To efficiently coupled in the pump radiation and get a strong pump density, an air-clad is commonly used (Fig. 1.20(b)).

Otherwise, in order to get an efficient leakage of the HOMs, PCFs have to exhibit a perfect index matching between the rare-earth doped core and the surrounding silica. In this aim, their core is achieved by multiple steps of "stack and draw" in which a set of low-index fluorine doped rods are stacked together with the RE doped core rods and drawn down to sub-micrometric dimensions. Thus, the refractive index profile is seen as a homogeneous average index and its control is facilitated. Nevertheless, this procedure is time and money-consuming. Furthermore, as modes are inherently leaky in such weakly guiding structures, the sensitivity of microstructured fibers to bending is quiet high and is a real hindrance when the core diameter exceeds 40 $\mu$m. To solve this problem, the drawing of rod-type PCF is commonly achieved by adding a thick layer of silica around the fiber. The outer diameter reaches 1 mm or more, keeping the fiber straight and free of macro-bending. Such MOFs, illustrated in Fig. 1.20, has demonstrated very interesting performance in high power regime, delivering 320W from a 60 $\mu$m exhibiting an efficiency of 78% in continuous wave regime [Limpert06] or a 1ns pulse bringing 4.3mJ of energy and 100MW of peak power from a 100 $\mu$m core [Brooks06].

#### 1.5.4.5 Differential mode losses - Leaky fibers

**Large Pitch Fibers**

As mentioned above, PCFs show the most robust singlemode emission when only one element of the infinite periodic cladding is missing. In order to go further in the mitigation of the non-linear processes, it has been envisaged to enlarge the core size while using only one missing hole, contrary to VLMA PCF. In this way, Limpert *et al.* have developed Large Pitch Fibers (LPF) (Fig. 1.21(a)). By definition, a LPF is a microstructured fiber exhibiting a pitch larger than 10 times the wavelength [Jansen10]. Due to the large fiber dimensions compared to the wavelength (core size and pitch), the microstructured cladding can be seen a "modal sieve". Moreover, as the spatial mode intensity profile expands with the order of the modes, HOMs leak more out the core than the fundamental mode, allowing an efficient modal discrimination. Therefore, the gain will preferentially benefit to the "Gaussian shaped" mode as its overlap with the actively doped core region is significantly largest. So, those optical waveguides are inherently multimode but a singlemode emission can be obtained thanks to gain selection.

A prominent property of LPF is their scalability. The ESM behavior is still valid when the core diameter is increased as long as the ratio d/Λ stay lower than

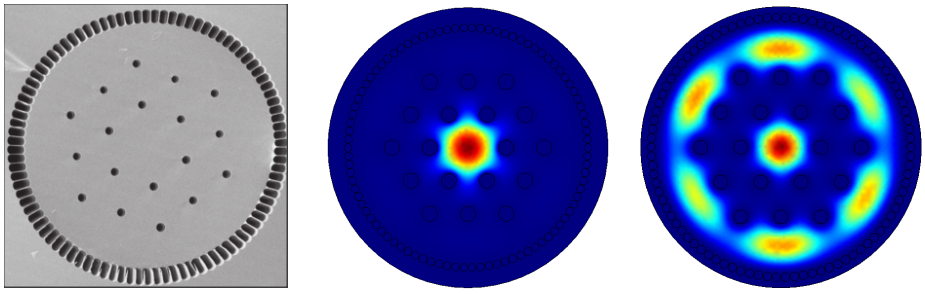

(a) (b) (c)

**Figure 1.21:** (a) Scanning electron microscope image of a rod-type large pitch fiber (LPF) with 135 $\mu$m core from [Limpert12b]. (b) Mode field repartition of the fundamental mode. (c) Mode field distribution of the fundamental mode influenced by the anti-crossing process.

0.406. This allows the fabrication of several LPFs with different pitches from only one preform. This ability was observed for fiber core ranging from 50 to 135 $\mu$m [Baumgartl11, Stutzki12]. Nevertheless, the refractive index matching between the actively doped region and the silica has to be lower than $5.10^{-5}$ [Jansen10]. This issue limits the concentration in rare-earth ions, the linear gain and drastically increase the complexity of the manufacturing process (as for rod-type PCF evoked previously). Moreover, multiples stack and draw steps are used to produced the core material, making these fiber really expensive (in the range of 10 000 dollars per meter).

Yb doped LPFs have been characterized in different configurations and have demonstrated their impressive potential. The emission of 534 nJ-98 fs pulses from a mode-locked laser [Baumgartl11] and 2.2 mJ/482 fs pulses showing up to 3.8 GW of peak power on a chirped pulse amplifier [Eidam11a] have been reported. Moreover, a multi-stage Q-switch fiber laser was realized, emitting 26 mJ-sub 60 ns pulses exhibiting the larger MFD reported to date (90 $\mu$m). Unfortunately, degradations of the beam quality has been noticed into LPF due to modal instabilities (Subsection 1.4.3) or anti-crossing, as depicted in Fig. 1.21(b-c) and [Jansen11]. While the first is a thermal induced process implying the energy transfer between two guided modes, the second stems from a coupling between the fundamental and a cladding mode. Thus, a special care has to be carried during the fiber development in order to set us free of modes couplings, in particular by judiciously defining the air clad diameter, and reducing the modal content into the fiber core to push away the threshold of appearance of the modal instabilities.

### Leakage Channel Fibers

Another concept of leaky structures, known as Leakage Channel Fibers (LCF), was proposed in 2005. They are composed of an array (one or two rings) of large air holes/low index inclusions spaced by thin silica bridges, acting as "leakage channels".

Contrary to PCF/LPF, inclusions are larger than interstitial silica bridges. Once again, the actively doped core has to exhibit a refractive index matching with the silica, limiting the rare earth ions concentration. The design of LCFs consists to appropriately define the leakage channels width (that is to say the thickness of the silica bridge separating to neighbour inclusions) in order to confine the fundamental mode into the gain area whereas HOMs leak through the channels. By using large inclusions, it was expected to provide a better resistance to bending compared to others leaky structures. Since the first report discussing the fabrication of a passive air-silica LCF (1 ring of air holes), a bending resistance down to 7.5 cm has been reported while maintaining a robust singlemode operation [Wong05]. Then, this concept has been manufactured with an actively doped core (Fig. 1.22(a)). A singlemode beam having a MFA of 3160 $\mu m^2$ was reported despite a small curvature radius of 15 cm [Dong06].

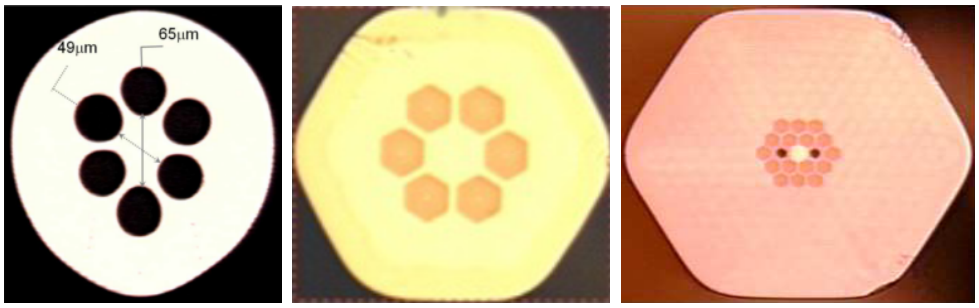


(a) (b) (c)

**Figure 1.22:** Microscope pictures of three leakage channel fiber: (a) air silica, (b) all glass and (c) all glass polarization maintain design [Dong09a].

An intensive work was also achieved on all-glass LCFs as air holes structures require a delicate balance between each drawing parameters (pressure, furnace temperature, feed rate...) to improve the repeatability of the fabrication. Moreover, all-glass fiber facilitate the fiber integration (splicing, cleaving...). A detailed investigation on the influence of the silica bridges width and the refractive index contrast was led [Dong09d]. This study highlights a smooth influence of the refractive in-

dex on the modal discrimination and a reduction the optimum ratio d/Λ when the fiber core is enlarged. Hence, only the propagation of the fundamental mode was noticed from a passive LCF having core diameters up to 152 $\mu$m. A first example of all-glass LCF exhibits a 52.7 $\mu$m core and a normalized holes diameter d/Λ of 0.8 (Fig. 1.22(b)). The effective area of its emitted beam at 1.05 $\mu$m was 1548 $\mu m^2$. Then, to improve the differential loss, a two rings LCF was proposed, demonstrating a 20 times improvement of the loss ratio between the fundamental and the first HOM [Dong09a], allowing by the way to decrease the critical bending radius down to 13 cm. Polarization maintaining LCF was also proposed [Dong09c] (Fig. 1.22(c)). Nevertheless, the outstanding performances of LCF are tainted of a shortcoming, relying on the leaky behavior of the core modes. As for LPF, the fundamental mode can experience efficient coupling with cladding modes, drastically impacting the beam quality.

#### 1.5.4.6 Spectral filtering

In 1976, Yeh and Yariv theoretically described new optical waveguides based on the principle of Bragg reflections. They initially applied this proposal to slab [Yeh76] and then to optical fibers, giving birth to the Bragg fibers [Yeh78]. These waveguides are composed of an alternate succession of high and low-index layers surrounding a depressed-index core (Fig. 1.23(a)). Through an anti-resonant effect (PBG guidance), the light can be trapped into the core by Bragg reflection. Conversely, under resonant conditions, light spread out the core. The light propagation is only allowed into the core for specific wavelengths, offering the ability to spectrally tailor the emitted beam. Then, researches on Bragg fibers had to wait for a technological breakthrough. The first experimental demonstration was done in the beginning of the years 2000. Their potential has been studied in details to evidence the influence of each opto-geometric parameters (dimensions and refractive index contrast) [Argyros02, Litchinitser02]. Then, a singlemode emission was

clearly demonstrated experimentally: $M^2 \approx 1.17$ [Février08] and RE-doped Bragg fibers have reached a MFD as large as 870 $\mu m^2$ [Aleshkina11] up to now. Moreover, it has been highlighted in [Gaponov10] that a selective doping is required to get a singlemode emission (less than 70% of the core diameter). They also noticed an outstanding low critical bending radius: down to 7.5 cm while maintaining a good beam quality ($M^2 \approx 1.12$).

Shortly later, all-solid two dimensions (2D) photonic crystal lattice were studied and have provided a robust singlemode emission. Together with the Bragg fibers, they are identified as Anti-Resonant Reflecting Optical Waveguides (ARROW) [Duguay86]. Their main characteristic is to authorize the light propagation only on specific spectral bands, matching the photonic bandgap of the lattice. A wide variety of 2D ARROW have been investigated and they are currently investigated for high power delivery or generation. These fibers can be classified in two categories: solid core and hollow core PBG fibers [Cregan99]. The second one presents the outstanding ability to guide light in an air core surrounded by an array of tailored silica resonators (Fig. 1.23(b)). In this case, the air core can be replaced by different gases offering a large potential for gas-light interaction [Benabid06]. Moreover, hollow core fibers are able to withstand and deliver high power/energy pulses [Wang12, Beaudou12], can exhibit a large birefringence [Chen04], present a

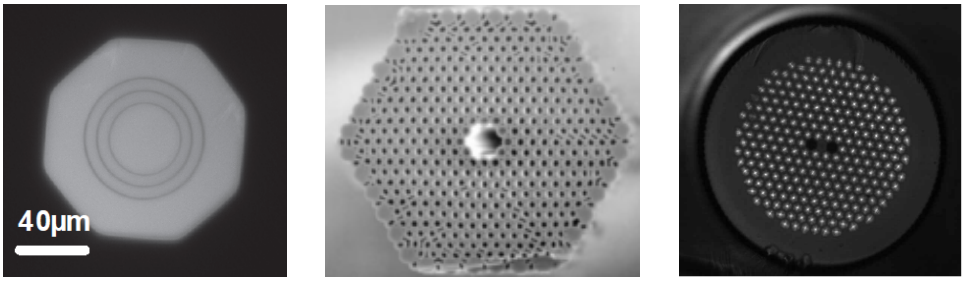


(a) (b) (c)

**Figure 1.23:** Microscope pictures of (a) a Bragg fiber, (b) hollow core fiber from [Cregan99] and (c) an all solid 2D PBG with two borons rods surrounding the core [Olausson08].

reduction of non-linearities by a ratio 1000 compared to silica fibers [Ouzounov03] and tailor the emitted wavelength [Litchinitser04]. In counterpart, the drawing conditions are more drastic than for all solid fibers. Nevertheless, despite being challenging, their integration is upcoming (splicing, cleaving).

Otherwise, all solid 2D PBG fibers are composed of a solid low-index core, whose the background losses can be as low as 20 dB/km [Bouwmans05], surrounded by a periodic array of high-index doped silica rods (Fig 1.23b). The first experimental demonstration was done on a small fiber core [Luan04]. Then, their spectral filtering properties have been beneficial to force Yb-doped fiber laser to emit on unusual transitions, allowing emission at 976 nm [Pureur08] or 1178 nm [Olausson10]. Their relevance for LMA fibers and high power delivery has also been established. For instance, Kashiwagi *et al.* report a singlemode propagation from a 48 $\mu$m core fiber (MFA = 712 $\mu m^2$) composed of seven core cells surrounded by five rings of high index rods. Low bending losses were also demonstrated (0.1 dB/m for a bending radius 10 cm) [Kashiwagi12]. Moreover, acting on the inner cladding structuration, Baz *et al.* have obtained robust singlemode emission from both passive and active fibers. The MFD of the emitted radiations measures respectively 44 $\mu$m (MFA $\approx$ 1520 $\mu m^2$) and 36 $\mu$m. In these fibers, the inner cladding microstructuration has contributed to maximize the propagation losses of HOMs while maintaining convenient ones for the fundamental mode. However, the current limitation for an additional power scaling of the core diameter remains the increase of confinement losses for the fundamental mode and the bending induced losses.

#### 1.5.4.7 Distributed Mode Filtering fibers

Finally, interest was brought on fibers combining the two guiding principles in order to take benefit from each of them: the spectral filtering offered by the photonic bandgap and the modal discrimination stemming from the mode leakage in fiber based on the modified total internal reflection. Distributed Mode Filtering (DMF)

fibers exhibit a cladding microstructuration identical to that of rod-type PCF, but some air holes are jacketed with a thin high index layer, playing the role of resonant elements (Fig. 1.24(a)). In this way, the confinement by MTIR is assisted by the resonant process, leading to a singlemode operation on a narrow spectral band, as depicted on the Fig. 1.24(b). Different regimes of operation occur, depending on how many core modes are coupled to the high-index (HI) rods modes. At longer wavelengths, several core modes are guided and interfere, explaining the strong oscillating tendency observable on the spectrum. On the MM1 region, only the fundamental mode and one HOM are propagated in the core and interfere, resulting in a slightly oscillating intensity in this spectral range. Then, the last HOM is coupled out to the cladding, resulting in a singlemode operation on a narrow spectral band. Finally, at shorter wavelength, no core modes are propagated. In inset of the Fig. 1.24(b), an effective indices representation is reported, allowing to understanding when occur the coupling of the core modes to the HI rods ones. The spectral filtering shown by these fibers is also beneficial to filter the ASE, allowing to reduce the noise in fiber amplifier.

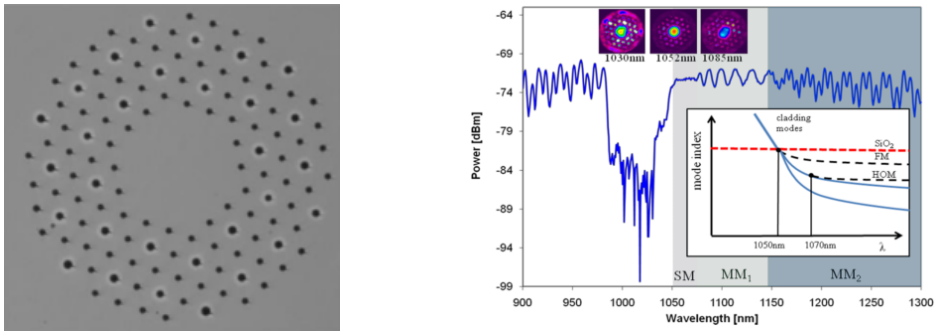


(a) (b)

**Figure 1.24:** (a) Microscope pictures of a Distributed Mode Filtering fiber (high index layers in white, pure silica in grey, and air holes in dark). (b) Transmitted spectrum collected after propagation through a passive DMF having a 85 $\mu$m core [Laurila11]. In insets: measured near field distribution at three different wavelength and a representation of the modes effective indices (fundamental modes, core HOMs and cladding modes.

The first demonstration was done in 2011 by Alkeskjold *et al.* [Alkeskjold11].

They got a singlemode operation from a passive 100 $\mu$m core fiber but also in an Yb doped DMF exhibiting a MFD of approximately 59 $\mu$m after 50 cm of propagation. In Q-switch regime, up to 104 W average power at 1.03 $\mu$m was obtained, providing 2.7 mJ at low repetition rates (10-30 kHz) [Laurila11]. Hence, second (515 nm) and third (343 nm) harmonic generation has also been successfully achieved.

Although numerical investigations have shown that a 85$\mu$m core DMF should exhibit modal instabilities for emitted power exceeding 371 W [Johansen13], the output average power obtained experimentally is limited to 292 W before the inset of modal instabilities [Laurila12], degrading the beam quality. Unfortunately, thermal induced effects blue-shift the emitted wavelength. This can be reversely used to determine the temperature increase on the fiber. A 44% power improvement have been noticed before the onset of modal instabilities by operating initially in the leaky regime, letting the thermal induced phenomenon blue shifted the spectrum and enable a singlemode operation at this wavelength [Laurila12]. The diffraction-limited operation was confirmed by a $C^2$ measurement [Laurila13a]. Finally, a recent experiment has demonstrated that DMF can deliver an efficient amplification of 25 ps pulses [Laurila13b].

Summarizing, several strategies have been efficiently applied to optical fiber design so as to provide a robust singlemode emission thanks to a large HOMs discrimination: partial doping of the fiber core, use of selective bending losses, resonant coupling of the HOMs out of the fiber core, reduction of the core NA ... Now, four kinds of fiber appear really performing for large mode area singlemode operation: DMFs, LPFs, LCFs and rod-type PCFs (Table 1.25). All of them can exhibit MFD larger than 60 $\mu$m but require a core refractive index matching that of silica. Unfortunately, standard manufacturing process do not provide a sufficient control on the refractive index of the RE-doped material. Thus, the RE-doped material refractive index being higher than that of the pure silica, this core material is commonly stacked together with fluorine rods and then drawn several times to access sub-

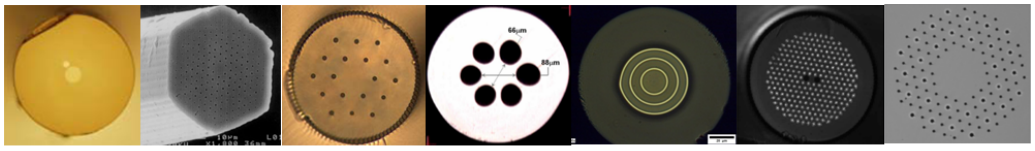

| | CCC | PCF | LPF | LCF | Bragg | 2D PBG | DMF |
|---|---|---|---|---|---|---|---|
| MFD | 21 µm | 85 µm | 90 µm | 63.4 µm | 33 µm | 36 µm | 60 µm |
| MFA | 350µm² | ~5500 µm² | > 6000 µm² | 3160 µm² | 870 µm² | ~ 1020 µm² | ~ 2800 µm² |
| M² | 1.07 | 1.3 | Modal instabilities! | 1.3 | 1.12 | ~ 1.1 | Modal instabilities! |
| Core index | > silica | = silica | = silica | = silica | = silica | = silica | = silica |
| Pump absorption | 5dB/m | ~30dB/m | ~24dB/m | ~ 12 dB/m | - | - | ~ 27dB/m |
| Manufacturing process | MCVD | MCVD + Multiple Stack and draw | MCVD + Multiple Stack and draw | MCVD | MCVD | MCVD | MCVD + Multiple Stack and draw |
| Bending sensitivity | ~30 cms | > 1 m => Rod type | > 1 m => Rod type | Down to 76 cms | Down to 15 cms | Down to 30 cms | > 1 m => Rod type |

**Figure 1.25:** Sum-up of the characteristic for the above-mentioned fibers: the largest Mode Field Diameter and Area reached by these fibers, the beam quality, the requirement on the core refractive index, the pump absorption, the use or not of the multiple stack-and-draw technique, and the critical bending radius achievable.

micronic dimensions, making the procedure time and money-consuming. Moreover, this results in a partial doping that limits the absorption capabilities of the RE doped area. Furthermore, these structures of interest, except the LCF, have to be drawn as rod type in order to avoid macro-bending mode distortions, limiting their integration. Even if an efficient singlemode operation has been reported from large core, some disruptive effects limit the beam quality: avoided crossing and modal instabilities. From now on, a special care must be carried on this phenomenon during the development of optical fibers for the high power regime. This is one of the main objective of this thesis.

### 1.5.5 Conclusion

In this first chapter, the interest of optical fibers as laser gain medium and waveguide was highlighted for high power fiber laser. An overview concerning the optical fiber manufacturing has been provided and their potential/restrictions for future fibers development were evidenced. Recent investigations also evidenced that the fiber composition has to be defined with care in order to avoid the temporal evolution of background losses called photodarkening. Then, optical limitations for power scaling have been discussed and current strategies to overcome them were presented. To sum up, fiber lasers are useful for power delivering but also for high power emission. Their optical efficiency can reach up to 80% for Yb-doped fiber laser and their abilities for laser micro-machining were demonstrated, in particular their high beam quality. In counterpart, the small volume of active core limits the energy storage contrary to solid state lasers and makes fiber sensitive to thermal and NL effects. The variety of active dopants usable has contributed to place them as a serious candidate in several spectral bands: around 1$\mu$m for material processing, 1.55$\mu$m for telecommunications or 2$\mu$m for medicine. Nevertheless, several challenges paved the way to push further the performances of LMA singlemode fibers. First, non-linear processes damage the optical beam, disturbing their spatial, temporal and spectral properties. So, to mitigate their occurrence, researchers focus on the achievement of a singlemode emission from very large cores (100 times the wavelength). The fiber length has also to be shortened, leading to the development of strongly RE-doped LMA fibers. However, large core fibers tends to support more and more guided modes and strategies has to be employed to ensure a singlemode emission. In this way, numerous cladding microstructuration have been imagined and fabricated. The challenge consists to efficiently favour the fundamental mode using tailored inner cladding structures taking into account the presence of the external pump cladding that make the structure highly multimode and the strong potential for modes couplings. Moreover, for this kind of microstructured fibers, a rigorous index

matching of few $10^{-5}$ has to be achieved between the active and the background material. However, conventional manufacturing processes (CVD) exhibit a poor accuracy only in the range of $5.10^{-4}$ to the best and their homogeneity does not fit the requirements for fabrication of large preform. Currently, a multiple stack and draw is achieved to increase the material homogeneity but this method is quiet time-consuming and expensive. Finally, it was demonstrated that the heat load has a strong impact on the fiber optical properties (modification of the refractive index change, appearance of modal instabilities ...). Thus, an efficient thermal management and dissipation is required.

Enriched by the knowledges of weaknesses and assets of current fibers, we aim to develop novel and competitive fiber structures, basing our work on the following points:

- the simplification of the manufacturing process and the reduction of its cost,
- the reduction of the core refractive index constraints, allowing a strong RE ions concentration and to prepare a darkening-free material,
- the development of all-solid fibers, facilitating their integration and offering an efficient heat dissipation,
- the strengthening of the mode discrimination by acting on the inner clad structuration,

In this context, the outline of the work reported here is the development of innovative LMA microstructured optical fibers exhibiting a robust singlemode emission, and sweeping three main topics: the waveguide design, its fabrication and its characterization. The following chapter is dedicated to the validation of our simulation procedure on a well-known air/silica LPF and to study of their performances. This will enable to get a reference for my further study relative to the design of microstructured optical fibers and to understand the guidance mechanism into fibers based on the "modal sieve" concept.

Chapter 2

# Simulation protocol: description and validation using a well-known state-of-the-art leaky fiber structure

Contents

The dramatic increase of the average optical power (in CW) and energy (in pulsed regime) delivered by fiber lasers and amplifiers remains a key issue which faces some disturbing phenomena. Indeed, a strong power density implies the onset of non-linear processes, degrading the spatial, spectral and temporal properties of the emitted beam; and potentially the dielectric breakdown. Thus, to push further the threshold of appearance of these harmful effects, the power density shall be lowered by enlarging the fiber core size. This has led to the development of VLMA fibers exhibiting a MFA exceeding 50 $\mu$m.

In this context, an essential criterion governing the development of high power fiber laser/amplifiers concerns their beam quality, it means the robustness of the singlemode emission. Nevertheless, VLMA fibers sustain undoubtedly a large core modal content: more and more modes acquire the ability to be guided when the fiber core size is increased. Thus, some efforts has to be achieved in order to design fibers presenting a large modal discrimination in their core.

By this way, it is required to define parameters describing the guided modes behaviour and to choose the most relevant to underline the singlemode tendency of designed waveguide structures. Among them, one can cite for instance the confinement losses, describing the losses undergone by modes leaking out the fiber core, and the overlap factor. The latter represents the overlap of the modes intensity distribution with the gain region of the fiber. Commonly, active fibers are composed of a double clad ensuring the pump power propagation. In this situation, core modes as well as cladding ones are loss-less guided. As a result, confinement losses have no longer meaning here. Therefore, in this chapter, the parameter chosen is the modes overlap factor.

Thus, modes guided in the fiber core can be identify and the overlap of their intensity distribution with the gain region compared in order to characterize the robustness of the singlemode emission. Thanks to this parameter, the guidance mechanism of VLMA fibers will be investigated in details in order to acquire the

knowledge to improve further their performance. For this, the attention will be focused on the study of leaky structures, such as the LCFs and LPFs, on which we will observed the impact of the air-hole sizes. In LCFs, the large air holes allow a slight mode leakage whereas in LPFs, the smaller holes act as a modal sieve.

This chapter deals with the description of our numerical *modus operandi* and with the demonstration of its reliability using a well-known state-of-the-art VLMA fiber described in the previous chapter as a reference.

## 2.1 Wave theory and fiber modes

First, it is required to theoretically define the behaviour of the light travelling through the fiber core. The propagation of electromagnetic waves through a dielectric waveguide is clearly described by the scalar Helmholtz equation (seen as a reduction of the Maxwell equations):

$$\nabla^2 E + k^2 E = 0 \tag{2.1}$$

$$\nabla^2 H + k^2 H = 0 \tag{2.2}$$

where E (resp. H) is the electric (resp. magnetic) field, k = $\frac{2\pi}{\lambda}$ is the wave vector and $\nabla^2$ is the Laplace operator. Considering the propagation of an optical wave along a conventional step-index fiber, equations are defined in the cylindrical coordinates (r,$\varphi$), with r being the position on the fiber radius and $\varphi$ the angle. In this case, the Helmholtz equations describing the z component of the electric field becomes:

$$\nabla_t^2 E_z(r,\varphi) + (n_1^2 k_0^2 - \beta^2) E_z(r,\varphi) = 0 \quad for\ r \leq a \tag{2.3}$$

$$\nabla_t^2 E_z(r,\varphi) + (n_2^2 k_0^2 - \beta^2) E_z(r,\varphi) = 0 \quad for\ r \geq a \tag{2.4}$$

Here, 'a' represents the core radius, $n_1$ (resp. $n_2$) is the core (resp. cladding) refractive index (RI), $k_0$ is the wave vector into the vacuum, $\beta$ is the propagation

constant and $\nabla_t^2$ is the transverse Laplace operator. For convenience, the transverse propagation constants can be defined as:

$$\beta_{t1}^2 = n_1^2 k_0^2 - \beta^2 \tag{2.5}$$

$$\beta_{t2}^2 = n_2^2 k_0^2 - \beta^2 \tag{2.6}$$

In the core (r<a), $\beta_{t1}$ is a real number and radial solutions of the electric field are ordinary Bessel functions of the first kind: $J_q$ ($\beta_{t1}$.r) whereas in the cladding (r>a), $\beta_{t2}$ is an imaginary value and radial solutions of the electric field are modified Bessel functions: $K_q$ ($\beta_{t2}$.r) approaching zero close to the outer cladding interface (r$\Rightarrow \infty$). Hence, the normalized transverse wave-numbers are noted as:

$$u = \beta_{t1}\ a = a\ \left(n_1^2 k_0^2 - \beta^2\right)^{1/2} \tag{2.7}$$

$$w = |\beta_{t2}|\ a = a\ \left(\beta^2 - n_2^2 k_0^2\right)^{1/2} \tag{2.8}$$

Then, the complete pair solutions of the Hemholtz equation related to the electric field can be written as:

$$E_z = A\ J_q\left(\frac{u\ r}{a}\right)\ sin(q\varphi)\ exp(-j\beta z)\ for\ r < a \tag{2.9}$$

$$E_z = C\ K_q\left(\frac{w\ r}{a}\right)\ sin(q\varphi)\ exp(-j\beta z)\ for\ r > a \tag{2.10}$$

where A, and C are constants. The others components of the electric and magnetic field ($E_r$, $E_\phi$, $H_r$, $H_\phi$, $H_z$) can be deduced from $E_z$. The eigenvalues of the guided modes are characterized by unique sets of u, w and $\beta$ matching boundary conditions, insuring the continuity of the tangential field components at the interface between the core and the cladding. The resulting modes are classified using their radial (m) and azimuthal (q) mode number. Transverse electric modes ($TE_{0m}$) have their electric field component $E_z$=0 whereas the transverse magnetic modes ($TM_{0m}$) have their magnetic field component $H_z$=0. Otherwise, if $E_z$ and $H_z \neq 0$, modes are

called hybrid modes and are labelled $EH_{qm}$ and $HE_{qm}$ depending on the major field component (respectively the electric and magnetic field). In the weakly guiding limit ($\Delta \approx \frac{n_1-n_2}{n_1}$ «1%), all these modes are referred as transverse electromagnetic modes (TEM): $E_z$=$H_z$=0 (Fig. 2.1) and their intensities follow those of the Laguerre-Gaussian modes (right part of the Fig 2.1).

Moreover, in this limit and for a cylindrically symmetric index profile, the solution of the scalar Helmholtz equations can be greatly simplified. The dispersion curves of each of the TEM modes families degenerate to a single curve, implying that all modes constituting each family share the same propagation constant for a given frequency. Furthermore, the different TEM modes belonging to the same family can be gathered to give birth to "Linearly Polarized" (LP) modes of different spatial distributions. This is the basis of the LP classification of the modes guided in an optical fiber. Note that the $LP_{lm}$ modes are transverse and have an intensity distribution in agreement with the Hermite-Gaussian modes. They are identified by two indices: $LP_{lm}$, where 'l' is half the number of maxima existing in the intensity pattern when the azimuthal angle $\varphi$ varies of $2\pi$ radians, and 'm' is the number of maxima in the intensity pattern occurring along the radial coordinate. The relation between the LP modes and the degenerated TEM ones is as follows:

- $LP_{0m}$ are composed of the $HE_{1m}$ modes,
- $LP_{1m}$ are composed of the $TE_{0m}$, $TM_{0m}$ and $HE_{2m}$ modes,
- $LP_{lm}$ are composed of the $HE_{l+1,m}$, and $EH_{l-1,m}$ modes.

A synthetic review of the first four LP modes and their associated TEM modes is displayed in Tab. 2.1. Now that modes denominations have been reviewed, a description of our simulation procedure will be done and its application to a state-of-the-art fiber will be achieved in order to demonstrate its relevance.

**Table 2.1:** The left part of the table refers to the name of the degenerated TEM modes and depicts the field distributions of the degenerated mode of each LP modes, on which are reported the field direction (black arrows). On the right part, the associated LP modes and their mode field distributions.

| Degenerated TEM modes | Mode field distributions | Corresponding LP modes | Mode field distributions |
|---|---|---|---|
| HE11x | 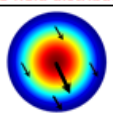 | LP01x | 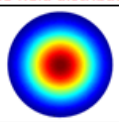 |
| HE11y | 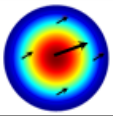 | LP01y | 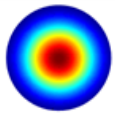 |
| TE01 + HE21x | 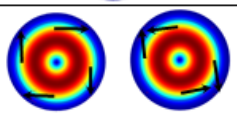 | LP11x | 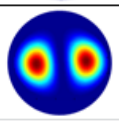 |
| TM01 + HE21x | 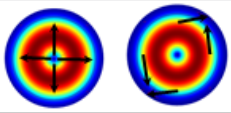 | LP11y | 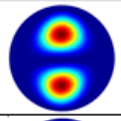 |
| HE31x + HE31y | 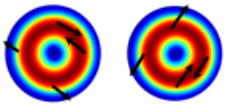 | LP21x | 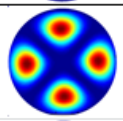 |
| EH11x + EH11y | 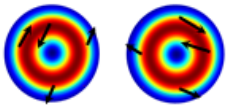 | LP21y | 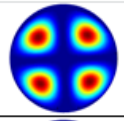 |
| HE12x | 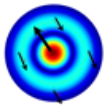 | LP02x | 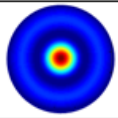 |
| HE12y | 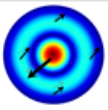 | LP02y | 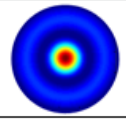 |

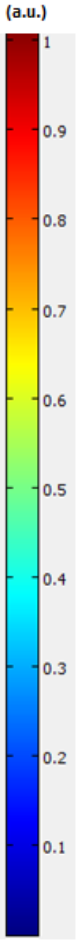


## 2.2 Modus operandi for our numerical investigations

In order to describe the modal content of a fiber core, it means the number of guided modes into it, with as much as accuracy as possible, numerical simulations are mandatory. Our approach relies on the computing of propagated modes in the studied structures and the definition of their overlap with the gain region. Then, a second software is used to model the laser dynamics and more precisely, the modal competition between the most competitive guided modes. The simulation parame-

ters are critical issues to ensure the reliability and the accuracy of results. This will be a focus in this section.

### 2.2.1 Solving of the Helmholtz equation

These simulations have been led using a software based on a full-vector finite-element method (FEM) that is commercially available. First, the fiber design is generated and opto-geometrical parameters are defined (design dimensions, working wavelength, refractive index (RI) profile...). Simulation conditions (mesh densities, elements type...) have to be chosen with care in order to get a reliable and realistic description of 1/ the modal content of the structure and 2/ the intensity distribution of each mode. For this, the fiber geometry is decomposed in a patchwork of sub-wavelength dimension domains called finite elements [Brechet00]. Then, partial differential Helmholtz equations (PDE) are solved in the transverse plane defined by the fiber cross-section, giving access to the modes content and their propagation constants. It is worth noting that this software computes the TEM modes, so a combination of these modes has to be achieved to get the true LP modes. Two parameters are used to describe the behaviour of the guided modes into the studied structures. First, the overlap factor (designated $\Gamma$ and expressed in percent), allows to quantify the overlap of the intensity distribution of a considered mode with the gain region located in the fiber core. It is computed using the following formula:

$$\Gamma = \frac{\iint\limits_{A_d} |E|^2_{gain}\ dS}{\iint\limits_{A_{tot}} |E|^2_{tot}\ dS} \tag{2.11}$$

E represent the electric field distribution of the considered mode, $|E|^2$ its intensity, $A_d$ and $A_{tot}$ are respectively the areas of the RE-doped and the pump cladding regions, and dS indicates the cross-sectional integration. Secondly, as the beam quality of a fiber laser is of great interest in the frame of high power fiber lasers, it is useful to define the modal content into the fiber core and hence deduce whether

the fiber is singlemode or not. Thus, we look for the larger overlap between the Fundamental Mode (FM) and the gain area, and conversely the lowest one for all other modes (core and cladding HOMs). The modal discrimination $\Delta\Gamma$ , and through it the singlemode behaviour, of the studied fiber structure is thus obtained by calculating the difference between the overlap factor of the FM/$LP_{01}$ mode (noted $\Gamma_{01}$)) and that of the most confined HOM (noted $\Gamma_{HOM}$) appearing as the most restrictive HOM:

$$\Delta\Gamma = \Gamma_{01} - \Gamma_{HOM} \tag{2.12}$$

Regarding the definition given in [Jø rgensen12], the singlemode operation occurs if $\Gamma_{FM}$ >80% and $\Gamma_{HOM}$ <50%. Therefore, a modal discrimination of about 30% could be sufficient to attest of a singlemode operation. Although widely accepted, this criterion is not universal because the experimental conditions of use of the fiber (in an amplifier or a laser cavity) can strongly influence the modal competition.

Hence, fiber structures can be rigorously compared using the parameter $\Delta\Gamma$ and we will look for the larger of modal discrimination, attesting of an efficient delocalization of HOMs out of the gain region. Then, an accurate modelling of the active laser behaviour will be the ultimate criterion.

### 2.2.2 Tests in laser configuration

To confirm the quality of their emitted beam, the studied fiber structures are also theoretically tested in a laser configuration. Thanks to a home-made program [Devautour09a], the evolution of the power carried by each considered mode during its propagation into the gain region are computed. First of all, the intensity profiles of the different TEM modes obtained previously are collected and combined in pairs to get the equivalent LP modes. Then, conditions governing the laser configuration forming a linear resonator are implemented (Fig. 2.1): the mirrors reflectivity $R_1$ and $R_2$, the gain medium properties (RE ions concentration $N_0$, length L, emission and absorption cross sections, attenuation) and the pump/signal powers and

wavelengths ($P_p$,$P_s$,$\lambda_p$,$\lambda_s$). Moreover, the gain area is transversally (dx,dy) and longitudinally (dz) sampled to accurately describe the gain dynamics and thus the modal competition.

Here, our study is focused on Yb-doped fibers which can be modelled as a quasi two energy level system. In this software, the pump absorption as well as spontaneous and stimulated emissions are considered. The wavelength dependency of cross sections is accurately described. Usually, the spectral band is sampled between 1000 and 1060 nm with a 1 nm pitch. The equations governing the evolution of the powers for different propagating waves (pump and ASE here) are complex, but for such two-level system, a simplification can be done, and equations can be thus written as follows:

$$\frac{dP_p^{\pm}}{dz}(z) = \pm \iint_{A_d} \Big[\sigma_e(\lambda_p).N_2(x,y,z) - \sigma_a(\lambda_p).N_1(x,y,z)\Big].\Gamma_p(x,y,\lambda_p).P_p^{\pm}(z).dx.dy - \alpha_p.P_p^{\pm}(z) \quad (2.13)$$

$$\frac{dP_{ASE}^{\pm}}{dz}(z) = \pm \iint_{A_d} 2.h.\frac{c}{\lambda_{ASE}}.\Gamma_{ASE}(x,y,\lambda_{ASE}).\sigma_e(\lambda_{ASE}).N_2(x,y,z).dx.dy \pm \iint_{A_d} \Big[\sigma_e(\lambda_{ASE}).N_2(x,y,z) - \sigma_a(\lambda_{ASE}).N_1(x,y,z)\Big].\Gamma_{ASE}(x,y,\lambda_{ASE}).P_{ASE}^{\pm}(z).dx.dy - \alpha_{ASE}.P_{ASE}^{\pm}(z) \quad (2.14)$$

where:

- $P_p^{\pm}$(z) and $P_{ASE}^{\pm}$(z) are respectively the pump and emitted powers at the longitudinal position z in both directions (in the +z and -z directions, as shown by the + and - superscripts),
- $A_d$ is the gain medium surface,
- $\sigma_e(\lambda_p)$ and $\sigma_a(\lambda_p)$ are the emission and absorption cross sections for the pump

at the wavelength $\lambda_p$,

- $\sigma_e(\lambda_{ASE})$ and $\sigma_a(\lambda_{ASE})$ are the emission and absorption cross sections for the laser emission at the wavelength $\lambda_{ASE}$,

- $N_1$(x,y,z) and $N_2$(x,y,z) are the population densities on the ground and excited state at the point (x,y,z),

- $\Gamma_p$(x,y,$\lambda_p$) and $\Gamma_{ASE}$(x,y,$\lambda_{ASE}$) are the overlap factors of the considered modes at the respective wavelength $\lambda_p$ and $\lambda_{ASE}$,

- $\alpha_p$ and $\alpha_{ASE}$ are the background losses respectively at the pump and laser wavelength,

- dx and dy are referred the radial pitch of the cross sectional integration.

- h is the Planck constant and c, the light velocity.

The transverse and longitudinal sampling (depicted in Fig. 2.1), coupled to the use of the fourth order Runge Kutta method enables to get an accurate solving of these equations along and across the fiber, and to describe reliably the population inversion and powers evolution. Moreover, the transverse sampling permits 1/ to take into account the local gain depletion called Transverse Spatial Hole Burning (TSHB), which can disturb the beam quality [Jiang08], and 2/ to transcribed faithfully the gain competition between all identified guided modes. Thus, a preferential/selective amplification of the FM can be demonstrated by quantifying the amount of the total power carried by this mode. According to [Pagnoux94], the emitted beam can be considered singlemode when at least 97.75% of the overall power ($P_{tot}$) is carried by the FM ($P_{01}$). Later, this rules will be used to define the beam quality (as depicted in Fig. 2.1).

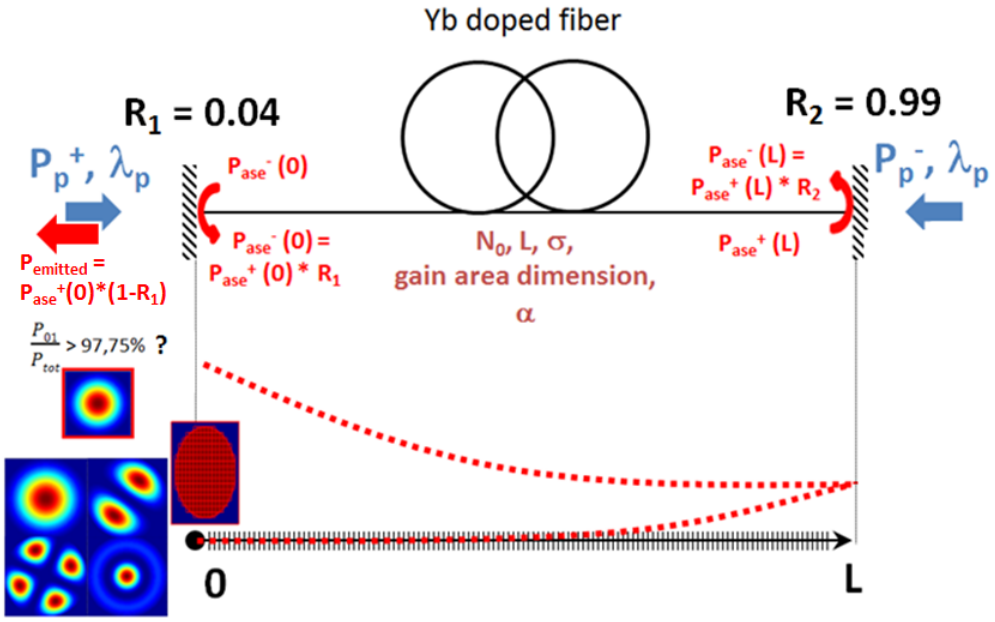


**Figure 2.1:** Schematic representation of a laser cavity with initial and boundary conditions: intensity distribution of the considered LP modes, co- and contra-propagative pump power and wavelength ... At the end, the singlemode behaviour is checked using the criterion defined in [Pagnoux94]: $P_{01}/P_{tot}$ >97.75%.

## 2.3 Description of the reference fiber

In order to valid the relevance of our modelling approach, we have considered a state-of-the-art fiber chosen as yardstick. The basic idea is to compare the results obtained with our simulation model with those published up to now in literature. A particular attention has been paid on the description of the modal content and the calculation of the modal competition.

The state-of-the-art Large Pitch Fibers (LPF) were chosen as reference because they exhibit outstanding performances in the high power regime (Subsection 1.5.4.5). Moreover, the potential of these fibers has been numerically investigated during the last few years [Jansen10, Jansen11, Limpert12b] and several statements were established. The first study was done to understand the influence of an index-depression between the actively doped region and pure silica one, which have to be ideally index-matched [Jansen10]. This work reports also on the optimal opto-geometric parameters offering a robust singlemode operation: considering a pitch

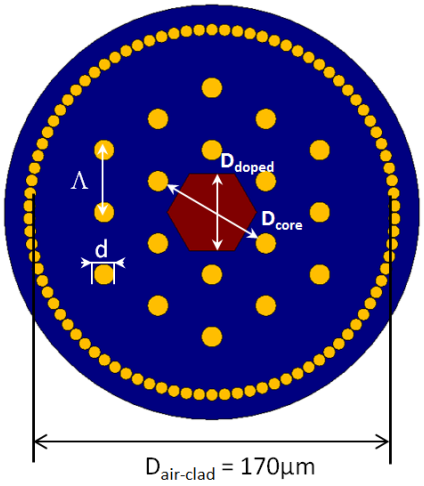


| Parameters | Values |
|---|---|
| Pitch Λ | 30 $\mu$m |
| d/Λ | 0.2 |
| $D_{core}$ | 54 $\mu$m |
| $D_{doped}$ | 40 $\mu$m |
| $D_{air-clad}$ | 170 $\mu$m |

**Figure 2.2:** On left: schematic representation of the modelled fiber with in red, the gain region, in dark blue, the pure silica, and in yellow, the air holes. On the right side: table listing the geometrical dimensions of the reference fiber.

of 30 $\mu$m, the optimal relative holes size (ratio between the air holes diameter and the holes spacing named 'pitch': $\Lambda$) is $\frac{d}{\Lambda} = 0.3$. Otherwise, an investigation of such fiber in regard to the modes confinement was reported in [Limpert12b], in which a relative holes size $\frac{d}{\Lambda}$ of about 0.2, a pitch of 30 $\mu$m and an air-clad diameter of 170 $\mu$m were considered (Fig 2.2(a)). These results have been used as starting point for our study. However, as informations concerning the shape and size of the gain medium have not been reported for these design, we consider an hexagonally shaped Yb doped region as in [Jansen10] having a radius of 20 $\mu$m.

The modal intensity distributions and modes overlap factors for the first five guided modes into this fiber are reported in [Limpert12b] and in Subsection 2.4.1. An efficient modal discrimination of 40% was obtained.

## 2.4 Application of our model to the reference fiber

To ensure the accuracy and reliability of our results, the modes intensity distribution, and so the modes overlap factor have been calculated. The simulations parameters (the mesh size and elements type) have been defined with rigour while mitigating the computational duration.

### 2.4.1 Mode intensity distributions/ Overlap factors

Modes intensity profile as well as their overlap factor with the actively-doped region have been computed using our simulation tools on the state-of-the-art LPF structure. Only the five modes reported in reference [Limpert12b] are depicted in Fig. 2.3. Thus the FM (which is the most confined in the active region) and first four HOMs are reported. For each of them, our results (bottom row) are in good agreement with those reported in the reference [Limpert12b] (see Fig. 2.3, top row). In particular, a perfect matching of the fundamental mode confinement is observed (≈75%). However, a slight difference appears on the overlap factor of the most competitive mode: $LP_{11}$-like ($\Gamma_{11}$=37% instead of ≈35%). We attribute this mismatching to our lack of informations concerning the gain region considered in the reference [Limpert12b] and to the fact that different numerical methods have been employed in the two studied. In the reference, they have used a full-vectorial finite-differences frequency domain mode solver. However, the overlap factor of the other HOMs agree with those of the publication. Therefore, we can affirm that these results confirm the reliability of our model.

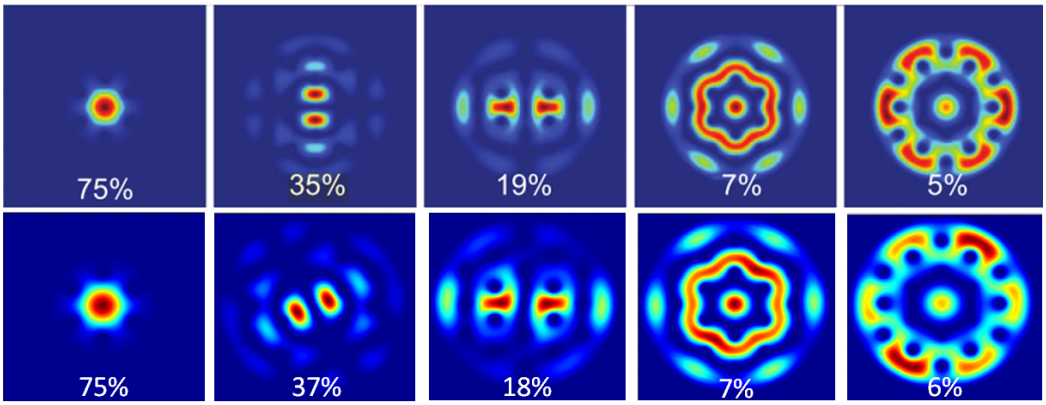


**Figure 2.3:** Representation of the calculated transverse mode intensity profiles for the five most competitive modes: those reported in [Limpert12b] (top row) and those obtained using our numerical approach (bottom row).

Furthermore, the adding of the air-clad structure into the model is time-consuming from a numerical point of view due to the fine mesh recommended by the

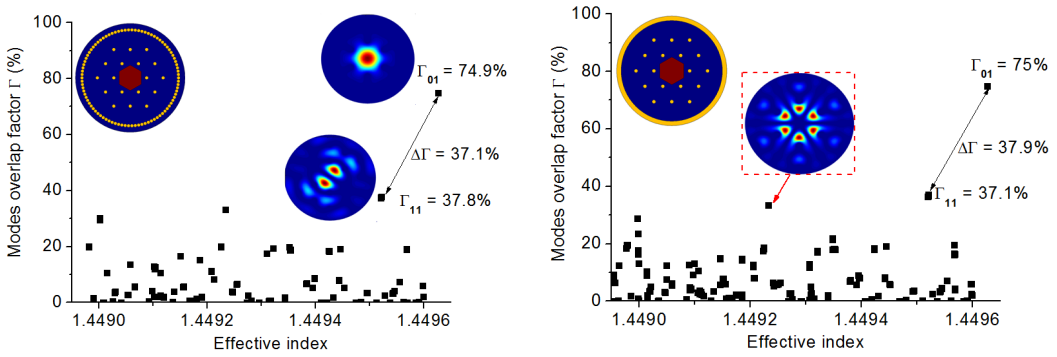


**Figure 2.4:** Computed overlap factors Γ for the first 300 guided modes versus their effective index in the reference fiber (a) with the air-clad structure and (b) with an equivalent air ring. The modal discrimination $\Delta\Gamma$ is also depicted in both cases. Insets: intensity distribution of the most confined HOMs: the $LP_{11}$-like and $LP_{31}$-like.

software for this large number of tiny air-holes. Thus, an investigation has been led in order to compare calculations done with the real air-clad structure (as shown on Fig. 2.2: air-clad with an inner diameter of 170 $\mu$m and composed of 90 air-holes) and those achieved with an equivalent air ring. The Fig. 2.4 reports the computed overlap factors Γ of the first 300 guided modes into the fiber structure in both cases. One can note that the modal discrimination $\Delta\Gamma$ is equal to 37.1% and 37.9% respectively for the air-clad structure and the equivalent air ring one. A small difference of 0.8% is noticed on the modal discrimination, demonstrating nevertheless that the approximation of the air-clad structure by an equivalent air ring can be applied and alleviates the computational time (reduction by a factor 3). Furthermore, it is worth noting that, although the modal discrimination appears to be only limited by the $LP_{11}$-like mode as explained in references [Jansen11, Limpert12b], we highlight here the existence of a second HOM: the $LP_{31}$ mode (see Fig. 2.4(b)), which could be a competitive mode for larger air holes and could impact the value of modal discrimination. Thus, during our following studies, 300 modes will be computed in order to take care of this mode.

### 2.4.2 Tests in laser configuration

In addition, we have checked the beam quality of the emitted beam at the output of the LPF structure chosen as reference when the latter is used in a laser configuration. The four most confined modes ($LP_{01}$, $LP_{11x}$-like, $LP_{11y}$-like, and $LP_{31}$) are implemented as depicted in insets of Fig. 2.5. A laser set-up is considered whose the characteristic are listed in the Table 2.2 presented below. Note that some of them have been arbitrarily chosen. The notations remain the same as previously ($\sigma$ represent the cross sections, $\alpha$ refers to the background losses and $\lambda$ is the wavelength for instance).

**Table 2.2:** Description of the laser cavity characteristics regarding the pump radiation, the optical resonator and the gain medium/optical fiber properties.

| **Optical pumping** | **Optical resonator** | **Gain medium/ fiber** |
|---|---|---|
| Copropagative, Pp = 20W | $R_1$: cleaved fiber end facet at 0° | 1 m rod-type air/silica LPF |
| $\lambda_p$ = 976 nm, $\alpha_p$ = 50dB/km | Fresnel reflection: 4% | |
| **Emission wavelength** | $R_2$: dichroïc mirror = 99% | 54 µm core, 170 µm air-clad |
| | | Yb concentration: 3.35 at/m$^3$ $Yb_2O_3$ |
| $\lambda$ = 1030 nm, $\alpha$ = 50dB/km | **Emission and absorption cross sections** | |
| | $\sigma_{ap} = \sigma_{ep}$ = 2.5.10$^{-24}$ ions/m², $\sigma_{as}$ = 4.4.10$^{-27}$ ions/m², $\sigma_{es}$ = 2.9.10$^{-25}$ ions/m² | |

Fig. 2.5 underlines the fact that the FM benefits from the majority of the gain due to its very high overlap factor with the gain medium contrary to HOMs. In this

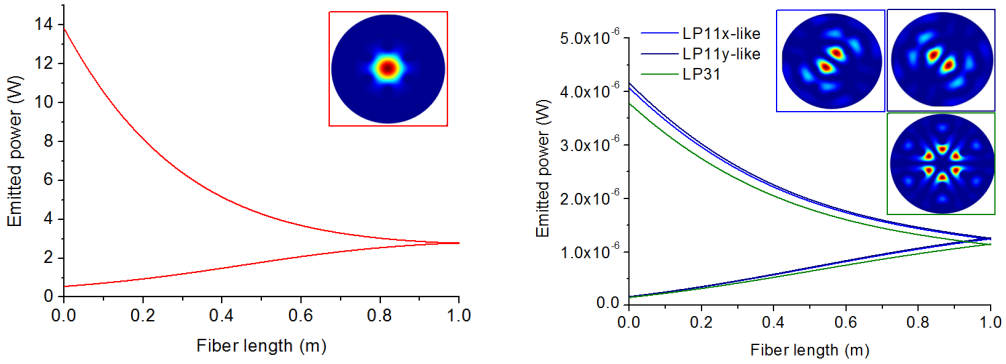


**Figure 2.5:** Longitudinal evolution of the laser power generated/carried by (a) the FM and (b) the three considered HOMs ($LP_{11x}$-like, $LP_{11y}$-like, and $LP_{31}$) after 20 round trip paths in the laser cavity integrating a 1 m long piece of LPF ($D_{core}$=54 $\mu$m core, $D_{air-clad}$=170 $\mu$m and d/$\Lambda$ = 0.2). Insets: transverse intensity distributions of the four considered modes.

situation, the FM carries more than 99.9% of the whole emitted power at 1.03 $\mu$m after 20 round trip paths in the laser cavity, so the laser beam is singlemode. Later, this software will be used to attest that the emitted beam is singlemode and to identify the boundaries at which a multimode operation starts to occur.

## 2.5 Avoided crossing

Typically, in a conventional straight step-index fiber, core and cladding modes are independent as their effective indices are clearly separated. Nevertheless, if we now consider very opened leaky structures as LPF designs surrounded by a double clad, core and cladding modes are embedded in the same waveguide, the double clad, although the air holes contributes to confine some modes in the core (see Fig. 2.6). By this way, an interaction between a core mode and a cladding HOM becomes possible as core modes leak out to the cladding and conversely, cladding modes overlap partially the gain region.

In these conditions, two phenomena can occurred: the "crossing" and the "avoided-crossing" (also called "anti-crossing"). At a crossing, a cladding HOM exhibits the same effective index $n_{eff}=\frac{\beta}{k_0}$ than a core mode but there is no overlap between them, i.e. their transverse mode profiles are orthogonal to each other. Therefore, no interaction occurs between these two "crossed" mode, and the crossing can be seen as a fortuitous coincidence of the modes effective indices. On the contrary, avoided-crossings rely on the overlap of the modes field/intensity distributions whereas the modes effective index is not perfectly identical. This implies a progressive energy transfer between the two 'coupled' modes which ultimately reverse their role. Then, their modes effective index will divergence. This effect is undoubtedly detrimental into singlemode fiber as it can occur on the fundamental mode, degrading the beam quality through the modification of the FM intensity distribution. Moreover, avoided-crossings occur for specific fiber dimensions and can also be induced by bending or a mismatching between the core and the highest

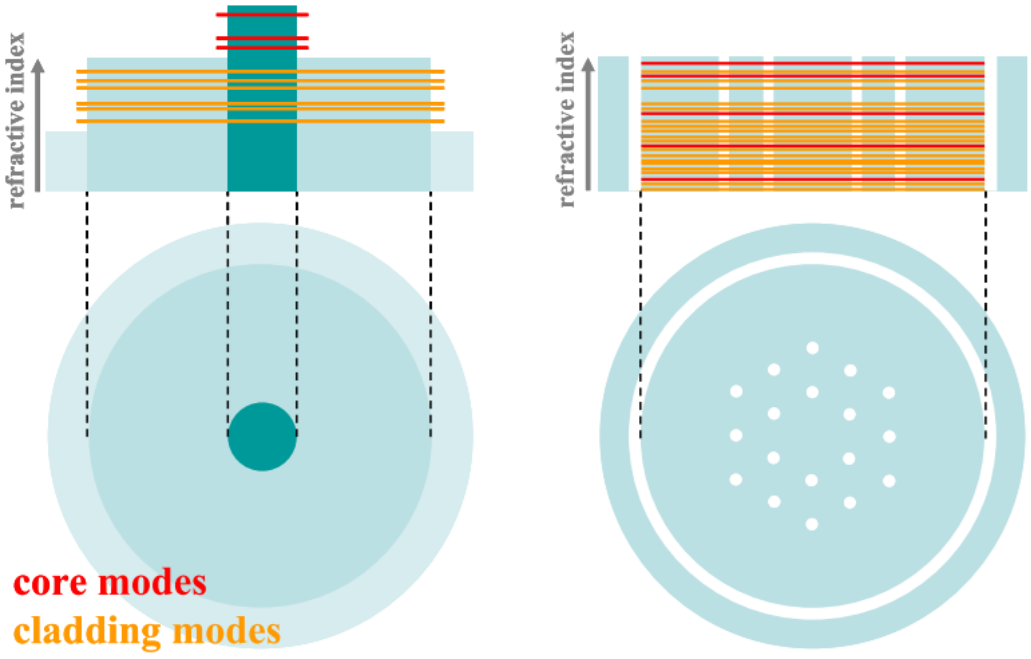


(a) (b)

**Figure 2.6:** Schematics representation of the RI profile (top row) and distribution (bottom row) of (a) a step-index and (b) a LPF. The effective indices of the core and cladding modes are depicted respectively in red and orange on the RI profiles. Representation stemming from [Jansen11].

index of the cladding [Jansen11]. Obviously, a special care has to be carried on this phenomenon during the development of double clad VLMA leaky fibers.

Thus, we have conducted a study in order to understand how this process works and allow to set us free of an avoided crossing on the FM during our further fiber development. First, we have considered a LPF structure similar to the reference fiber chosen previously (see Fig. 2.2(a)) with a relative hole diameter of d/Λ=0.2. Such small air holes size favour the spreading of the FM into the cladding. Hence, we have observed the evolution of the FM effective index and that of the cladding HOM participating to the process of avoided-crossing by varying the air-clad diameter from $D_{air-clad}$=140 $\mu$m to 210 $\mu$m. As evidenced earlier, an air ring is used on the calculation to alleviate the computational time. Intuitively, an increase of the air-clad diameter should not impact drastically the effective index of the fundamental

core mode as its interaction with the air-clad is moderated. However, the effective index of the cladding HOM is more significantly affected by this variation. At a certain point, the effective index of a particular cladding HOM tends toward that of the fundamental core mode and a deformation of the two modes profiles due to the avoided-crossing can be noticed. The intensity distribution of these two 'coupled' modes converge toward an identical shape, from which modes reverse their roles: the initial fundamental core mode, designated as mode 1 here, becomes the cladding HOM and conversely (see Fig. 2.7). In our range of variation for the air-clad diameter, only one avoided-crossing appears between the fundamental core mode and an annular cladding HOM. However, others can be observed for larger diameters [Jansen11].

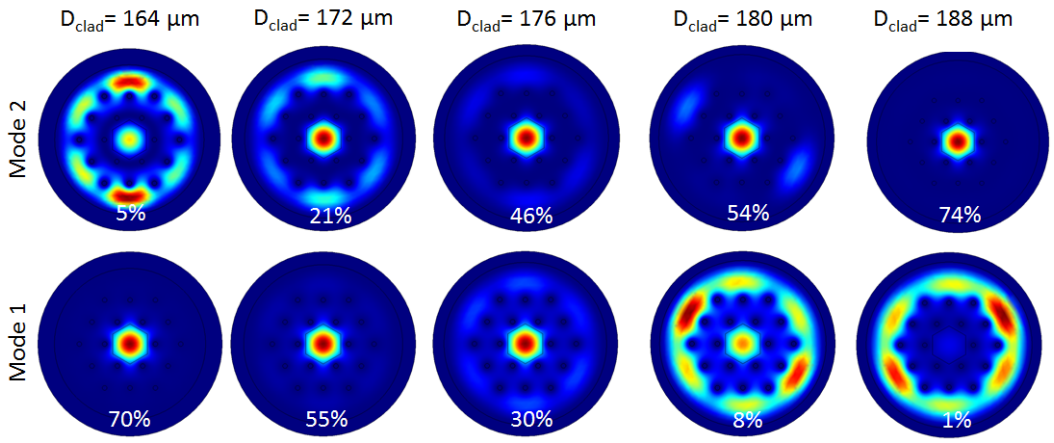


**Figure 2.7:** Evolution of the intensity distribution for the two modes involved in an avoided crossing for an air-clad diameter varying from 164 to 180 $\mu$m. In each case, the computed overlap factor is reported.

To describe more precisely the behaviour of this avoided-crossing, Fig. 2.8 illustrates the evolution of the effective indices and the overlap factor of the two 'coupled' modes versus the air-clad diameter It is worth noting that this phenomenon occurs when the effective index of the cladding HOM is close to that of the fundamental core mode ($\Delta n_{eff}$ is only few $10^{-6}$). Moreover, the avoided-crossing effect can be broad and then spread over a diameter range of $\Delta D \approx 28$ $\mu$m. The parameter $\Delta D$ will be used as a criterion to define the strength of the avoided-crossing. Indeed, it

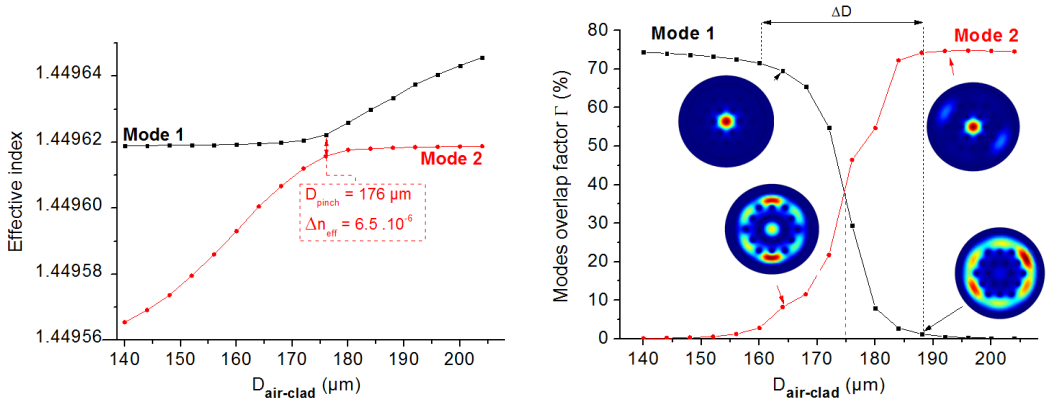


(a) (b)

**Figure 2.8:** (a) Evolution of the effective index and (b) the overlap factor for the two modes concerns by the avoided-crossing versus the air-clad diameter. It appears clearly that the former fundamental core mode (designated Mode 1) takes the role of the cladding HOM and conversely. In inset: intensity distributions for these two modes at specific air-clad diameter.

represents the range of air-clad diameter to avoid as the singlemode behaviour of the designed structure is no longer maintain due to the low overlap factor of the FM with the actively-doped region.

Furthermore, we have studied the influence of the normalized air holes size d/Λ

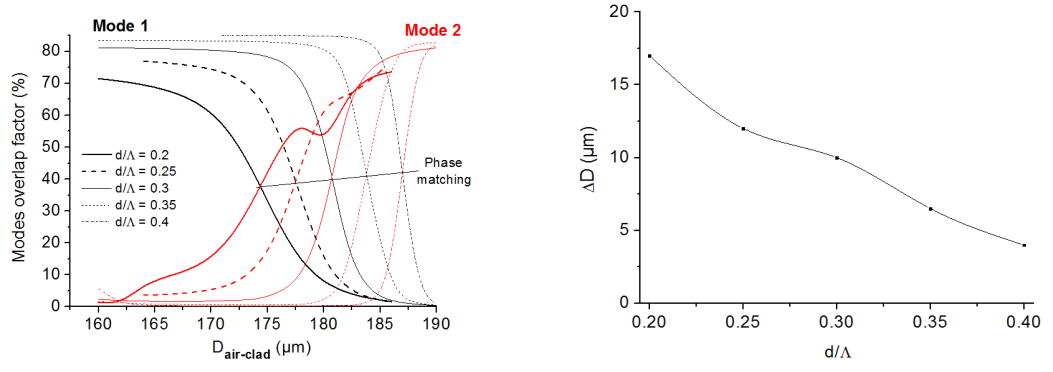


(a) (b)

**Figure 2.9:** (a) Evolution of the overlap factor Γ of the two 'coupled' modes for 5 different normalized air holes size d/Λ ranging from 0.2 to 0.4 depending on the clad diameter. (b) Representation of the range of air-clad diameter along which an avoided-crossing is observed and deteriorate the spatial beam quality.

for a constant $\Lambda$ of 30 $\mu$m on the following parameters: 1/ the air-clad diameter for which the avoided crossing is the most disturbing and 2/ the range of occurrence of the avoided crossing $\Delta$D. Results are presented on Fig. 2.9. One can observe that for larger air holes, corresponding to a larger d/$\Lambda$ value, the avoided-crossing becomes narrower ($\Delta$D decreases), as shown in Fig. 2.9(b). Indeed, larger hole sizes induce a stronger confinement of the FM and by the way minimize the overlap with a cladding mode. We have also observed that for larger air holes, the air-clad diameter value for which the avoided-crossing occurs is shifted as cladding modes has to exhibit a larger effective index to be coupled to the fundamental core mode (see Fig. 2.9(a)).

In conclusion, an avoided-crossing on the FM can be mitigated by designing a microstructured fiber having large inclusions and by properly defining the air-clad diameter. In any case, it is clear that the avoided-crossing issue has to be carefully addressed during the development of fiber design.

## 2.6 Investigation on the guidance in leaky structures

Hence, in order to imagine and develop new kind of VLMA microstructured fibers ensuring a robust singlemode emission, a good understanding of the guidance principle is required. Thus, we will studied in details the behaviour of air/silica LPFs, looking for useful statements enabling to push further their core modes content. The influence of each opto-geometrical parameters (number of air holes rings, normalized air holes size: d/$\Lambda$, doped core diameter, ...) will be investigated, allowing the understand of the "modal sieve" concept and providing a reference in term of performances for our further investigations. More precisely, our objective in this section will be to observe the characteristics of the FM and the evolution of the modal discrimination in such leaky structures, in order to take benefit from these results to propose novel all-solid leaky structures. In this section, we will first consider a 50 $\mu$m core fiber, partially doped with $Yb^{3+}$ ions ($D_{doped}$: 75% of the core diameter is actively doped)

and exhibiting a cladding diameter of 170 $\mu$m. These parameters are in agreement with those of the state-of-the-art LPF structures [Baumgartl11, Jansen11]. All our calculations are led for a emitted wavelength of 1.03 $\mu$m. The influence of the active region diameter will be also checked. Furthermore, the endlessly singlemodeness and the bending sensitivity of the fiber design will be studied. Finally, it has been mentioned earlier that LPFs have to present a rigorous index-matching between the gain region and the surrounding silica material in order to exhibit an efficient modal discrimination. So, to quantify this statement, the influence of an index mismatch will be investigated, establishing that the fabrication of such fiber design is a real challenge for the manufacturers.

### 2.6.1 1-ring leakage channels structure

Here, we focus first on the simplest leaky structure (LCF) composed of a 50 $\mu$m core surrounded by only one ring of six air holes (see Fig. 2.10(a)). The air-clad is replaced by an air-ring, as discussed earlier, and the pitch is varied with d/$\Lambda$ in order to maintain a constant core diameter. For a normalized holes diameter d/$\Lambda$ varying from 0.1 to 0.9, we have calculated the evolution of the overlap factor for the first 300 guided modes. The modal discrimination has been deduced from the previous results and its evolution is depicted in Fig. 2.10(b), together with the FM overlap factor. One can note that the FM is significantly more confined in the active core than the most competitive HOM ($LP_{11}$) even for d/$\Lambda$ as low as 0.1 (discrimination $\Delta\Gamma \approx$22%), demonstrating its inherent tendency to be easily confined. For an efficient amplification/larger linear gain and a stronger bend resistivity, it is obviously better to use larger air holes (larger d/$\Lambda$). Moreover, this structure is subject to avoided crossings between the $LP_{11}$ mode and a cladding HOM for normalized hole size close to 0.3 and 0.55 (see Subsection.2.5). It is clearly evidenced here that an avoided crossing impacting the most competitive HOM is beneficial for the modal discrimination.

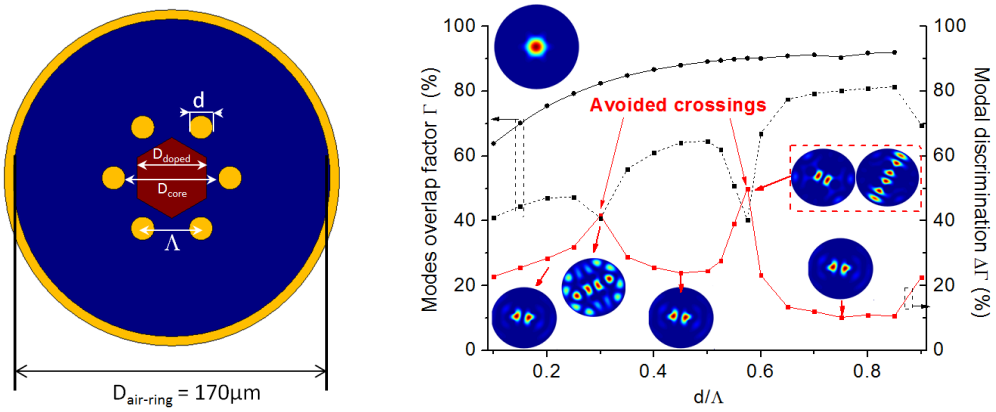


(a) (b)

**Figure 2.10:** (a) Schematic representation of a 1-ring leakage channels structure whose 6 air holes surround the 50 $\mu$m core, with $D_{doped}$ = 0.75 * $D_{core}$, $D_{air-ring}$ = 170 $\mu$m. (b) Evolution of the overlap factor for the two most competitive modes ($LP_{01}$: top black line, and $LP_{11}$: central black line), and of the modal discrimination. Inset: intensity distribution for these two modes.

Based on the singlemode criteria defined by Jorgensen *et al.* [Jø rgensen12], this 1-ring leakage channel structure will not be strictly singlemode as the modal discrimination is lower than 30%, except when a favourable avoided crossing occurs or when bendings contribute to increase the confinement losses of the HOMs. This structure is not really competitive due to the strong confinement of the $LP_{11}$ modes into the fiber core, limiting the modal discrimination around 25%, and the occurrence of avoided crossings [Dong09d], making it really sensitive to external perturbations (bending, fiber dimensions) and a RI mismatching induced during the fabrication. Nevertheless, 1-ring structures with a normalized air-holes size in the range of 0.7-0.9, called 'Leakage Channels Fibers', and whose the length exceeds 3 m, have already demonstrated the emission of a singlemode beam under strong bending radius [Dong09b].

### 2.6.2 2-rings leaky structure

We consider now a 2-rings LPF structure, still exhibiting the same core and clad dimensions. The dimension of the doped region is also kept constant

($D_{doped}$=0.75 * $D_{core}$) and the normalized holes size d/Λ is varying from 0.05 to 0.6. The RI repartition is depicted in inset of Fig. 2.11(a). The evolutions of the $LP_{01}$ mode overlap factor and the modal discrimination are shown in Fig 2.11(b). One can observe that the modal discrimination is significantly improved compared to the 1-ring structure, offering up to 54% of discrimination for an optimum d/Λ of 0.35. This optimum value is not the one usually used in literature [Jansen10, Baumgartl11, Jansen11]. Indeed, it is evidenced in Fig. 2.11(a) that this efficient discrimination of the competitive $LP_{11}$ mode benefits from a favourable modes coupling/avoided crossing with a cladding HOM ($LP_{11}$-like). Its is worth noting that these results are congruent with those reported in [Limpert12b], in which the most competitive HOM is the mode called here $LP_{11}$-like. However, this phenomenon makes the value of the modal discrimination particularly sensitive to variation of the dimension (d/Λ in this case).

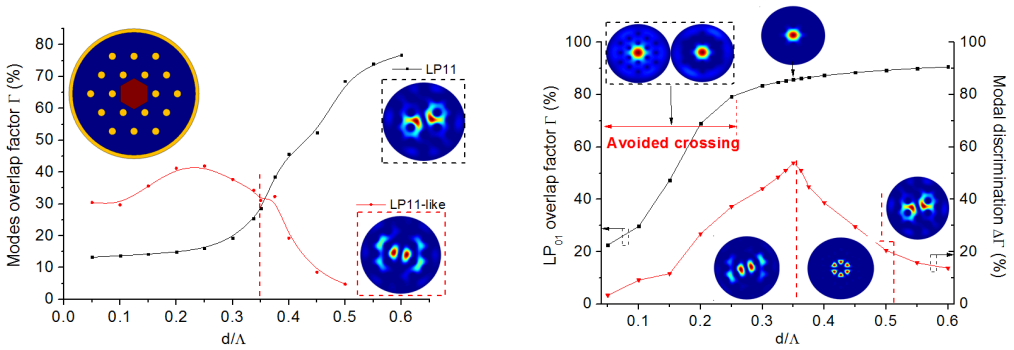


(a) (b)

**Figure 2.11:** (a) Evolution of the overlap factor Γ for the two coupled HOMs ($LP_{11}$ in black and $LP_{11}$-like in red) involved in the avoided crossing. In inset: schematic representation of a 2-rings LPF structure. (b) Evolution of the $LP_{01}$ mode overlap factor (black curve) and the modal discrimination ΔΓ (red curve). In inset: Intensity distribution of the FM (in the top) and the most disturbing HOMs ($LP_{11}$-like, $LP_{31}$ and $LP_{11}$).

For a d/Λ <0.25, an avoided-crossing appears and progressively reduces the FM overlap factor (see Subsection 2.5). However, for d/Λ >0.25, the FM confinement is less than 1% higher than that reported previously for a 1-ring leaky structure. This confirms that the $LP_{01}$ mode is mainly confined by the first ring of air inclusions.

This statement will be really useful for our further work.

Moreover, several modes are involved in the limitation of the modal discrimination depending on the d/Λ ratio. Although we have discussed earlier the impact of the "coupled" modes $LP_{11}$ and $LP_{11}$-like, for a d/Λ comprises between 0.35 and 0.525, the $LP_{31}$-like mode is the most disturbing HOM (Fig 2.11(b)). This evidences that a sufficient number of guided modes have undoubtedly to be computed to properly describe the modal discrimination and take into account this mode. Nevertheless, a singlemode emission has been obtained using our software, except when the FM is impacted by an avoided crossing.

### 2.6.3 Influence of the partial doping

To maximize the modal discrimination ΔΓ and optimize the linear gain of the sole fundamental mode, the dimension of the gain region has to be optimized regarding the core diameter of the fiber structure. Marciante *et al.* highlighted that a partial doping of the fiber core can be beneficial to selectively amplify the fundamental mode (see Subsection 1.5.4.1 and [Marciante09]). For instance, this intuitive principle has been experimentally reported in [Gaponov10] where the dimension of the doped region needed to be lower than 0.7 times the core diameter in order to avoid the amplification of five modes ($LP_{21}$, $LP_{02}$, $LP_{12}$, $LP_{01}$ and $LP_{11}$). To ensure a robust singlemode emission and improve the linear gain, the modal discrimination shall be systematically maximized by optimizing the repartition of the active dopant in the fiber core. Thus, the impact of the doped region size on the emitted beam quality, that is to say on the modal discrimination, has been observed and is depicted in Fig. 2.12. For that, the gain region is still considered as a unique hexagon whose the width is varied (see the fiber cross section in inset of Fig. 2.11(a)). Moreover, the d/Λ ratio is fixed to its optimal value: 0.35 (see Fig. 2.11).

Although the highest modal discrimination (ΔΓ=55%) is noticed for a partial doping (85% of the core diameter), a total doping of the fiber core should be ben-

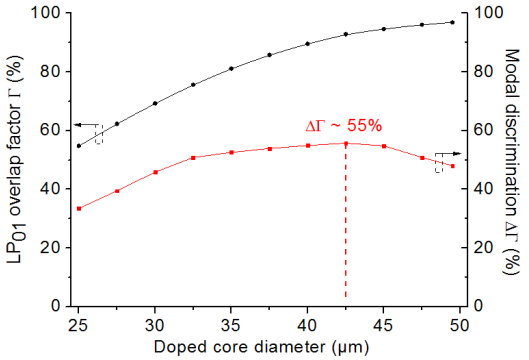


**Figure 2.12:** Evolution of the FM confinement (in black) and the modal discrimination (in red) versus the width of the actively doped region for a 50 $\mu$m core fiber and a d/$\Lambda$ value of 0.35.

eficial to get a large linear gain while maintain a significant modal discrimination ($\Delta\Gamma \approx 48\%$). Unfortunately, the manufacturing process of LPFs does not allow to fully doped the fiber core. Indeed, the fiber core is commonly manufactured by multiple "stacks and draws" of a set of fluorine doped canes and Yb doped ones in order to get a good homogeneity of the RI profile. Moreover, Yb doped canes are surrounded by a silica layers which is not removed before the "stack and draw" steps and a residual silica layer is always present between the gain material and the first ring of air-holes. This implies a reduction of the linear absorption and gain. In our study, we will develop structures circumventing these limitation.

### 2.6.4 Bending sensitivity

To improve the compactness of the laser sources, flexible fibers can be wrapped on a spool. Thus, their bending radius is close to 15 cm, what is common for standard fibers but can be detrimental for LMA ones. Indeed, in a bent fiber, the mode field patterns slip along the bending axis, leaking out of the gain region. In the case of leaky structures, the guidance mechanism implies an inherent sensitivity to the curvature, requiring the fabrication of rod-type fibers to be free of such perturbations. Nevertheless, from a developer point-of-view, the understanding of the bending-induced mode field deformations can allowed to imagine bend-resistive

fiber structures. In this way, the bending sensitivity of the LPF design chosen as reference is investigated.

These calculations are restricted to a bending induced on the Y-axis running between the air holes of the first ring (as shown in Fig. 2.13), so the axis on which the field can leak the most easily. The curvature is numerically realized by employing the following equation allowing to transcribe the mode field slipping induced by the fiber bending:

$$n(r,\theta) = n_{mat}(r,\theta) * \sqrt{1 + \frac{2r}{R_b}} \tag{2.15}$$

where $n_{mat}(r,\theta)$ is the initial RI distribution of the material, 'r' is the radial position and $R_b$ is the bending radius [Schermer07]. In Fig. 2.13, one can notice that the modal discrimination is strongly disturbed when the bending radius falls down to 2.5 m. In particular, avoided crossings occur on the FM, strongly degrading the beam quality. Thus, regardless the dimension of the gain region size, the critical bending radius is near 2.5 m. It demonstrates the strong sensitivity of LPFs to curvature, making them useless below this limit without showing mode distortions. This large bending sensitivity confirms also the requirement to manufacture fiber under a rod-type shape in order to relieve the constraint on bendings and micro-bendings.

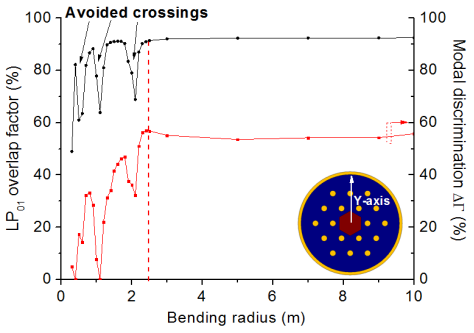


**Figure 2.13:** Influence of the bending radius on the FM confinement (black curve) and the modal discrimination (red curve) for a 50 $\mu$m partially doped core LPF ($D_{doped}$=0.85*$D_{core}$), presenting a $d/\Lambda$ = 0.35 and a cladding diameter of 170 $\mu$m. Insets: the bending axis is depicted on a LPF structure.

### 2.6.5 Endlessly singlemodeness

Furthermore, one of the main assets of the Large Pitch Fibers is their scalability, that is to say their ability to ensure a singlemode operation when: 1/ at a fixed wavelength, their dimensions are homothetically varied over a wide range and 2/ for fixed dimensions, the wavelength is varied over a broad spectral range. As an example, Limpert *et al.* have reported that the core size can be increased from 50 to 135 $\mu$m while maintaining a singlemode emission [Limpert12b]. As discussed in Chap. 1, leaky fibers (PCF, LPF,...) generally exhibit an endlessly singlemodeness while d/$\Lambda$ is kept smaller than 0.406, without consideration of the double clad. As the latter is used in our structures, the evolution of the modal discrimination is studied over a spectral range spanning from 400 to 2200 nm, so covering the visible range and the emission bands of the main rare-earth ions (1-1.1 $\mu$m for ytterbium, $\approx$ 1.55 $\mu$m for erbium, 1.6-2.1 $\mu$m for thulium and 1.9-2.2 $\mu$m for holmium). Fig. 2.14 illustrates that the FM confinement remains quasi-constant ($\approx$ 92.5%) over this range of wavelengths for the same fiber as previously. Moreover, the modal discrimination $\Delta\Gamma$ is relatively large (>54%) and quite constant. Simulations in laser configuration (not reported here) have demonstrated a singlemode emission over the entire spectral range: the power carried by the FM reaches 99.9% at the two extremity of the spectrum [Pagnoux94]. This tendency is a very attractive property we aim to

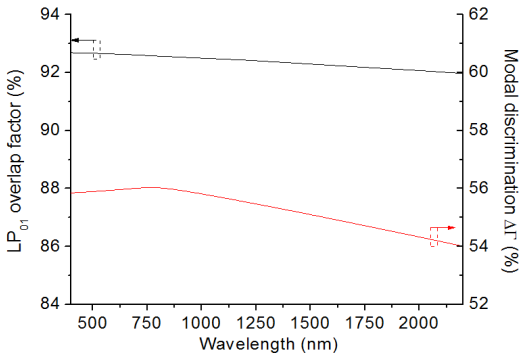


**Figure 2.14:** Spectral dependence of the FM overlap factor (in black) and the modal discrimination (in red) from 400 to 2200 nm for a 50 $\mu$m partially doped core LPF ($D_{doped}$=0.85*$D_{core}$).

provide to fibers developed in the next chapter.

### 2.6.6 Index mismatching

Despite some experimental demonstrations, the fabrication of such fibers remains a real challenge, making these fibers rare and expensive (see Subsection 1.5.4.5). Standard manufacturing processes enable to reach a RI control in the vicinity of $5 \cdot 10^{-4}$ to the best but microstructured leaky structures requires a quasi perfect index matching. Therefore, to be on a safe side, manufacturers often target an actively doped material whose RI contrast would be slightly lower than that of silica as this index depression can be compensate by a thermal induced RI change. However, it is absolutely required to know which degree of freedom is offered on the value of the RI mismatch 'dn' between the actively RE-doped region of the fiber core and the surrounding silica. Here, a position step-index mismatch can also be seen as an intuitive approximation of the thermal induced index change. Thus, we have observed the behaviour of our optimized air/silica LPF at an operating wavelength of 1.03 $\mu$m regarding a positive and negative step-index mismatch between the gain region and the surrounding silica which can stem from the material fabrication.

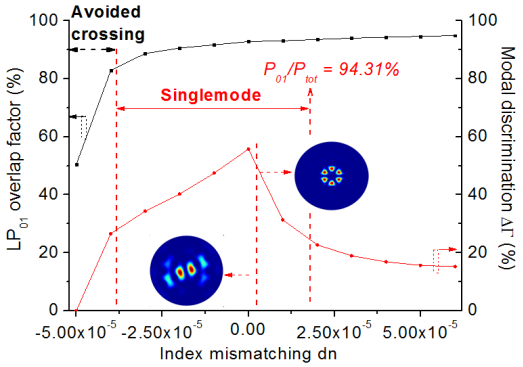


**Figure 2.15:** Influence of a RI mismatch on the FM overlap factor (in black) and the modal discrimination (in red) for a 50 $\mu$m core air/silica LPF whose the RE doping is partial ($D_{doped}$=0.85*$D_{core}$), the ratio d/$\Lambda$ = 0.35 and a double clad diameter of 170 $\mu$m. In inset: intensity distribution of the competitive HOMs.

Fig. 2.15 depicts the evolution of the FM confinement and the modal discrimination on a range going from dn=-$5 \cdot 10^{-5}$ to dn=+$6 \cdot 10^{-5}$. This result demon-

strates that LPF's exhibit a tolerance to an index mismatch of the gain region of about $6 \cdot 10^{-5}$ (-3.75 $\cdot 10^{-5} \Rightarrow < 2 \cdot 10^{-5}$) limited on one side by an avoided crossing occurring on the FM and, on the other, by the onset of the $LP_{31}$ mode drastically reducing the modal discrimination and contributing to a multimode emission. The use of this fiber, with a dn=$2 \cdot 10^{-5}$, in a laser configuration ha evidenced a multimode emission: the FM carries less than 97.75% of the whole emitted power ($P_{01}/P_{tot}$=97.31%). This tolerance is congruent with that reported in [Jansen10]: $5 \cdot 10^{-5}$.

However, such requirement on the RI accuracy is at least one order of magnitude smaller than current accuracies achievable with CVD processes. Nevertheless, thanks to the multiple 'stack and draw' technique, the fabrication of active leaky fibers have already been demonstrated. In the next chapter, we will systematically calculate the sensitivity of the designed fiber structures to a RI mismatch of the active material in order to estimate if our design can release slightly the constraint on this parameter. Moreover, we will take care of this disturbing $LP_{31}$ mode.

### 2.6.7 Opening on our proposal

The validation of our simulation procedure was done here by comparing our preliminary results with those reported in [Limpert12b]. Hence, a description of the strongly disturbing avoided crossings was provided, highlighting that modes can be coupled and suffer strong confinement changes. This phenomena is deleterious on the FM but can be beneficial if it occurs on the most competitive HOM, increasing the modal discrimination. Then, a detailed investigation of leaky structures was led to define an optimum design presenting the strongest singlemode robustness. This study has allowed to establish several statements:

1. the FM is mainly affected by the first ring of air holes,allowing to devised freely the inner cladding structuration,

2. a $2^{nd}$ ring contributes to improve the modal discrimination and limits the impact of avoided crossings occurring on the competitive HOMs,

3. a partial doping of the fiber core can enhance the modal discrimination. However, this reduces the linear absorption and gain.

The sensitivity to bending was also discussed underlining the requirement to drawn these leaky structures as rod-type fibers. Moreover, the endlessly singlemodeness was confirmed and the request on the material manufacturing was also described by observing the influence of an index mismatching between the doped core material and the surrounding silica. It has been highlighted that the tolerance to an index mismatch ($\approx 6 \cdot 10^{-5}$) is lower than what is achievable with common CVD fabrication processes ($5 \cdot 10^{-3}$ to $1 \cdot 10^{-3}$).

Besides the validation of our numerical approach and the thorough investigation of the leaky fibers, this study has allowed us to understand the assets of the LPF structure (efficient discrimination of the HOMs, robust singlemode operation over a wide spectral range,...) as well as their weaknesses: a strong sensitivity to the bending, a low tolerance to an index mismatch of the core material, ... Moreover,

the manufacturing process of these fibers compels the doping of the gain region. Indeed, the RE doped material has to index-match the surrounded silica, limiting the concentration in rare-earth ions. Moreover, as the CVD techniques does not permit to reach a sufficient RI accuracy, manufacturers resort to multiple 'stack and draw' steps on a combination of fluorine and RE doped canes to increase the material homogeneity and fulfil the requirement on the RI matching. This complex fabrication procedure significantly impacts the price of the LPFs, making them really expensive. This partial doping of the core material also means that the optical properties (absorption and linear gain) of the gain region are not as large as expected.

Enriched of the findings cited above, we will investigate in Chap. 3 a breakthrough fiber design taking advantage of:

- an alternative fabrication process of raw material allowing the synthesis of large and homogeneous volume of doped silica glass for both core and cladding, making it cost-effective,
- the degrees of freedom offered by the stack and draw technique to develop novel kind of all-solid LMA leaky fibers allowing an efficient modal discrimination in all-solid structures ;
- the relief of the core and cladding RI through the development of active and passive index-matched materials, giving us the ability to strongly doped the gain region, improving the linear gain, and offering the potential to use darkening-free material composition.

Thus, the Chap. 3 focuses on the development of all-solid leaky fibers aiming to provide a robust singlemode emission.

Chapter 3

# Development of original all-solid microstructured fibers

Contents

The main goal of my work was the development of innovative and performing Very Large Mode Area (VLMA) optical fiber designs, exhibiting a robust singlemode emission and overcoming the limits of air-silica microstructured fibers used in high power laser sources. In this third chapter, it is first essential to define the frame of this study. Indeed, my objective was to design realistic fiber structures based on the requirements derived from the manufacturing process: the properties of the raw material, the stack and draw process... or relying on the expected optical performances (large modal discrimination for instance).

Our objective was to propose evolutions regarding the fiber geometry and structuration in order to enhance the performances of current fiber lasers. Therefore, I have identified the degrees of freedom offered by the manufacturing process and then studied the behaviour of a conventional all-solid LPF structure fulfilling our expectations. Thus, this investigation starts with the transposition of an air/silica LPF to an all-solid structure. In a logical and progressive approach, several examples of geometries aiming to improve the modal discrimination are then reported. Further, I will emphasize the interest of a symmetry reduction on the fiber structure to access an incomparable low core modes content. Finally, the performances of optimal fiber structures will be discussed regarding their modal discrimination, scalability, and sensitivity to an index mismatch of the actively doped material.

## 3.1 Guidelines

As a reminder, the development of fiber lasers for the further progress of the power scaling is limited in particular by non-linear effects, which can be efficiently mitigated by two strategies: the mode area scaling and the shortening of the fiber length. However, the latter requires an increase of the linear gain which cannot be easily achieved by increasing the RE concentration in state-of-the-art air/silica leaky fibers. Indeed, although the guidance mechanism of these structures allows an efficient modal discrimination, it implies an inherent sensitive of these structures

to an index mismatch between the gain region and the surrounding material. Thus, the gain medium has to present a rigorous refractive index (RI) matching with that of the surrounding silica (as highlighted in Subsection 2.6.6), restricting the concentration in rare-earth (RE) ions. Moreover, in current air/silica leaky fibers, the core is partially doped with RE as depressed-index silica-based rods (fluorine-doped silica for instance) are used to compensate the index rise induced by the presence of active ions (see Fig. 3.1(a)). Hence, in order to satisfy the requirement on the RI matching, the gain material is most of time obtained by successive "stack and draw" steps of this alternation of Yb-doped and depressed-index rods. This results in a sub-wavelength structured material, the RI of which is perceived as a homogeneous index profile matching that of silica. It is obvious that this procedure is time-consuming and expensive.

In this context, we chose to resort to an alternative manufacturing process based on the sintering and vitrification of doped silica powders (see Subsection 1.9). Unlike preforms fabricated by the MCVD process which exhibit ripples, this process enables to get a highly reproducible and homogeneous RI profile, even for large volumes of material. Moreover, the RI accuracy reachable using this method should be in the vicinity of few $10^{-4}$, increasing the potential to adapt the RIs of the gain medium and the surrounding material. Thus, we could be free of the above-mentioned multiple 'stack and draw' steps to produce the gain material, reducing the manufacturing cost and duration. Thereby, the fiber fabrication relies on only one 'stack and draw'.

We have also opted for the development of all-solid fibers in order to facilitate the fibers preparation (splicing, cleaving and polishing) and their integration in an all-fiber system. The heat dissipation from the gain region to the fiber outer boundary is also favoured, allowing an efficient thermal cooling. In addition, to relieve the restriction on the core RI, we have chosen to use high-index passively doped silica rods (alumino- or phospho-silicate glasses for instance) on the leaky region, instead of pure silica (see Fig. 3.1). Thus, the gain medium has no longer to match the

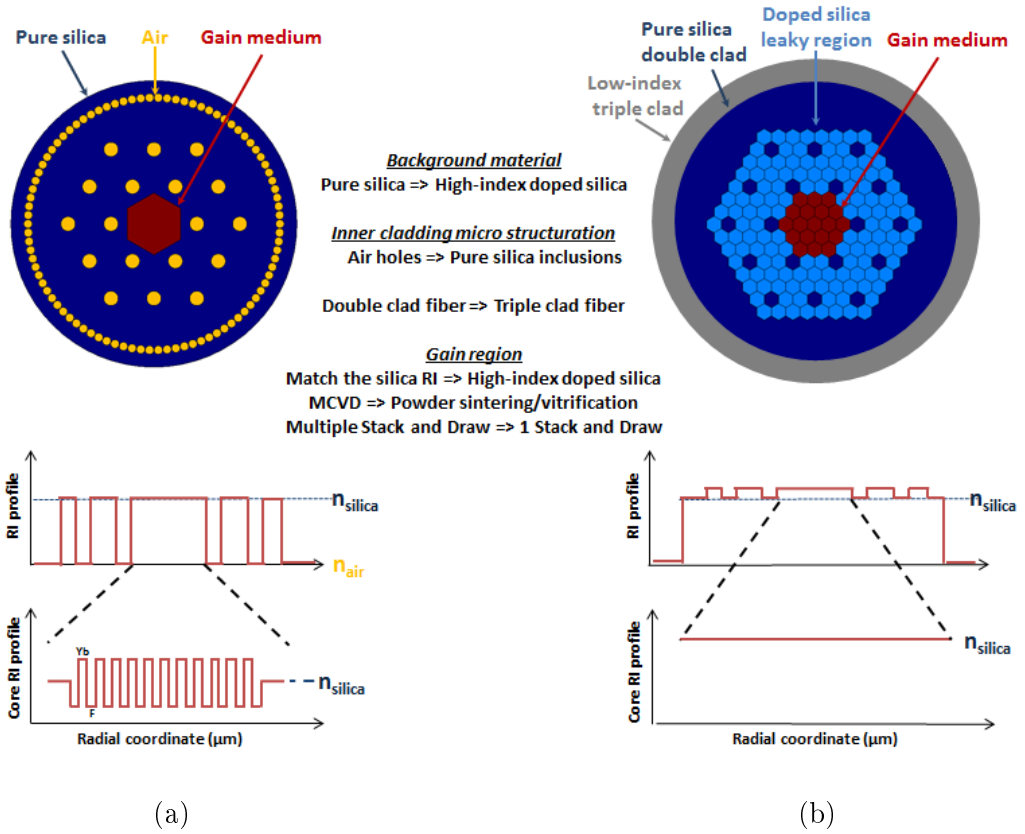


(a) (b)

**Figure 3.1:** Comparison of the structure RI distribution (in the top), their RI profile (in the middle) and a zoom on their core RI profile (in the bottom) for (a) a state-of-the-art air/silica LPF and (b) our proposed all-solid LPF. The core RI profile of the air/silica LPF is composed of an alternation of high-index RE doped material and low-index fluorine doped canes whose the final size is sub-wavelength whereas that of our all-solid LPF should be homogeneous. Complementary informations relative to the structures composition and fabrication are added in the middle.

silica RI but rather that of these passive rods which can be defined arbitrarily. Thus, high concentrations of RE ions are now usable without the need to compensate the core RI, offering a large linear gain and potentially resulting in a shortening of the fiber length. Moreover, as the RI of these two materials can be adjusted, we can also resort to specific material compositions presenting a significant resistance to photo- and radio-induced darkening (co-doping with Cerium or Phosphorus for instance, see Subsection 1.4.4 and [Jetschke12,Vivona12]). Hence, the inner cladding microstructuration can be composed of pure silica inclusions, allowing an efficient discrimination of HOMs. One can underline that the optimization of the inner

cladding microstructuration is the milestone of this work.

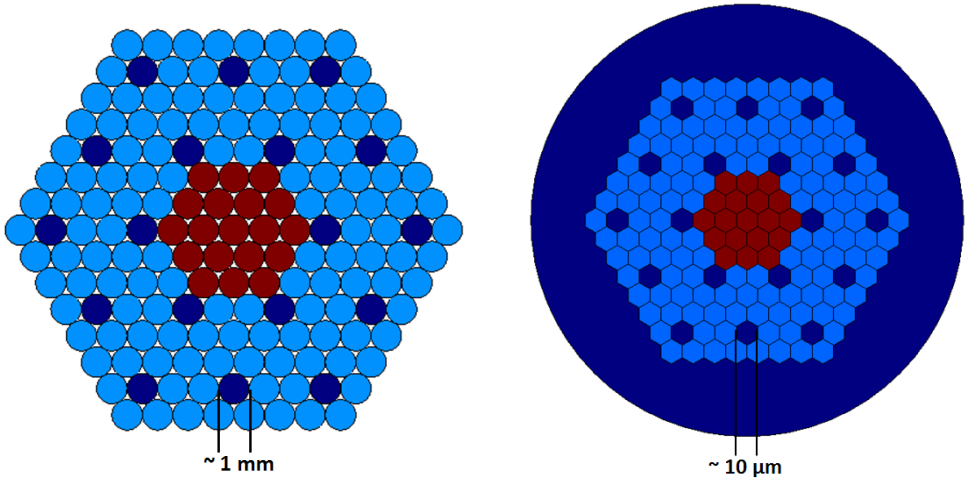


(a) (b)

**Figure 3.2:** Schematic representation of our fiber geometry: (a) first, a set of 1 mm circular canes produced by powders sintering and vitrification is stacked. Then, this stack will be placed in a silica tube. (b) After drawing, the interstitial air holes are collapsed and we consider that it leads to an array of micrometer-scale hexagonal-shaped cells. Throughout this manuscript, red hexagons refer to the gain region, clear blue areas represent the index-matched material and navy domains are the pure silica.

Initially, the preform stack is composed of circular canes assembled with respect to the final RI distribution. This stack is then placed in a silica tube before drawing for its maintain. Thereby, a silica layer covers the inner cladding fiber microstructuration (also called leaky region, colored in clear blue in Fig. 3.2), acting as a second clad and so influencing the modes confinement (see Fig. 3.1(b)). In this situation, interstitial air holes are strewed within the stack, but they will be collapsed during the fiber drawing, modifying the shape of the elementary cells. Although the final shape of the micro-structure depends mainly of the properties of the different materials (their viscosity notably), i will consider hereafter the ideal case of a homogeneous reshaping of the structure, leading to an array of micrometer-scale hexagonal-shaped elements (Fig. 3.2(b)). Finally, a low-index layer (air clad or fluorine layer) is added to confine the pump radiation (see Fig. 3.1(b)). In the following, this triple clad will not be represented as i have observed that it does not

affect inner cladding modes.

**Table 3.1:** Sum-up about the state-of-the-art air/silica fibers properties and comparison with our proposal versus the manufacturing process, the strategies to push away the non-linearities, the core refractive index, the method to provide a high beam quality and the fiber hardening. Assets/weaknesses of each proposals are respectively reported in green/red.

| **Topic** | **State-of-the-art air/silica fibers (DMF, LPF, LCF)** | **Our approach** |
|---|---|---|
| Manufacturing process | Multiple stacks and draws for the gain medium + final one for the whole fiber structure | Powder sintering technology + Unique 'Stack and draw' step |
| Non linearities | Core size scaling (from 40 $\mu$m to 135 $\mu$m) | Large fiber core: $>$ 50 $\mu$m |
| Core refractive index | $n_{core} = n_{silica} \Rightarrow$ Limited gain | $n_{core}$ is not restricted $\Rightarrow$ Potential for large gain and fiber length shortening |
| Core RE doping | Partial | **Total** |
| Singlemodeness | Modal discrimination using a periodic triangular-lattice cladding microstructuration | **Optimization of the inner cladding microstructuration by symmetry breaking** |
| Darkening sensitivity | Depends on the gain medium composition, which has to match the silica index | Can be mitigated by a judicious choice of dopants |

To summarize, Table 3.1 lists the properties of the state-of-the-art air/silica fibers and constitutes a basis for comparison with our proposal. The strengths (weaknesses) of each structure, regarding the manufacturing process, the fiber composition, and the opto-geometrical properties (core size, refractive index and singlemodeness), are highlighted in green (red). This evidences our wish to propose

solutions overcoming current performances, notably by using an alternative manufacturing process. This allows to drastically reduce the fabrication cost and duration, to release the restriction on a fully doped fiber core and optimize the fiber micro-structuration.

## 3.2 Investigation on the performances of an all-solid LPF

First, I will applied our above-mentioned considerations on a LPF design and study the behaviour of an all-solid LPF structure. Many parameters will be varied (RI contrast $\Delta$n, fiber dimensions ...) in order to evidence their influence on the guided modes and highlight the limit for a further improvement of the modal discrimination.

### 3.2.1 Modal discrimination

In our case, the pump cladding is made of a low index layer (fluorine layer for instance) surrounding both the high index microstructured region (in clear blue on Fig. 3.3(a)) and a pure silica layer (in navy) delimiting the leaky region of core modes. The pump cladding will not be depicted hereafter as i have checked that it does not affect the confinement of modes guided in the high-index leaky region. In facts, the dimensions of this pump cladding can be adjusted freely in order to fit the optical properties of the pump beam (spot size and numerical aperture) and maximize the launched pump power.

Moreover, the RI contrast between the passively doped leaky region/gain medium and the pure silica inclusions is first arbitrarily fixed to $\Delta$n=$6.10^{-3}$. This value is realistic considering the RI of the current RE-doped materials. It is important to underline that this RI contrast is drastically decreased compared to the previously studied air/silica LPF ($\Delta n \approx 0.45 \Rightarrow 0.006$), increasing the mode leakage.

Fig. 3.3(b) reports the computed overlap factors of the first 300 modes with the gain region into a 50 $\mu$m core all-solid LPF. Due to the use of solid materials and the stack and draw process, only discrete value of the ratio d/$\Lambda$ are available:

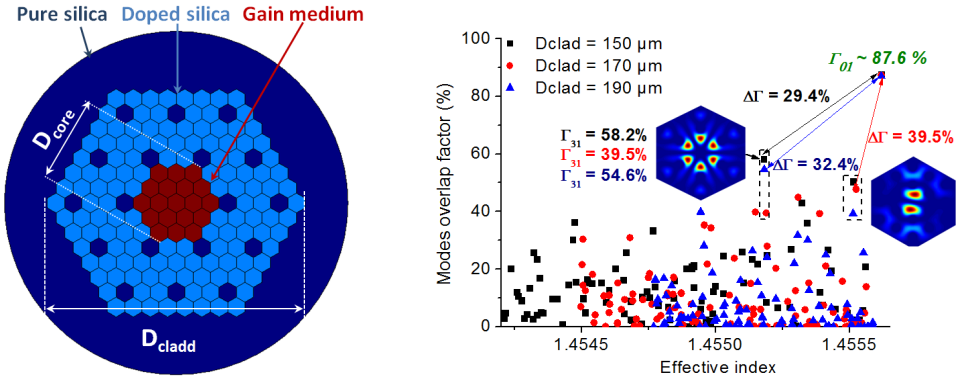


(a) (b)

**Figure 3.3:** (a) RI repartition for our all-solid hexagonally microstructured LPF. The RE-doped core region is in red, the index-matched leaky area in clear blue and the pure silica double clad in navy. (b) Overlap factor of the first 300 guided modes for a RI contrast of $6 \cdot 10^{-3}$. Insets: intensity distributions for the most competitive HOMs ($LP_{11}$-like and $LP_{31}$-like).

0.5, 0.33, 0.25, 0.16... depending on the number of RE-doped rods composing the fiber core (respectively 1, 7, 19, 37 ...). In order to be close to the optimum d/$\Lambda$ value evidenced in Chap. 2, we fixed it to 0.33. Thus, the size of an elementary cells is 10 $\mu$m (flat-to-flat) and the pitch is fixed to 30 $\mu$m. In this case, the peak-to-peak dimension of the leaky region $D_{clad}$ can be 150, 170 or 190 $\mu$m depending on the number of doped silica material layers (respectively 5, 6 and 7). In this configuration, the core size remains constant, as it can be seen in Fig. 3.4.

Fig. 3.3(b) shows that the FM is well confinement in the fiber core regardless the size of the leaky region ($\Gamma_{01}$=87.6%), although the reduction of the RI contrast compared to an equivalent air/silica LPFs induces a decay of 5% ($\Gamma_{01}$=92.6%). It is worth noting that the FM is free of avoided crossing in this case. However, the value of modal discrimination strongly varies from 29.4 to 39.5% due to the large fluctuation of the $LP_{31}$-like mode confinement. It is important to notice that its confinement is quiet unintuitive, as it is not leakier and leakier when the size of the leaky region is extended. On the contrary, it is well discriminated for a 170 $\mu$m high-index region ($\Gamma_{31}$=39.5%) whereas it appears re-confine for a larger dimension

($\Gamma_{31}$=54.6% at 190 $\mu$m). Thus, a real care should be carried on the impact of this disturbing mode and a detailed study should be led to understand its behaviour.

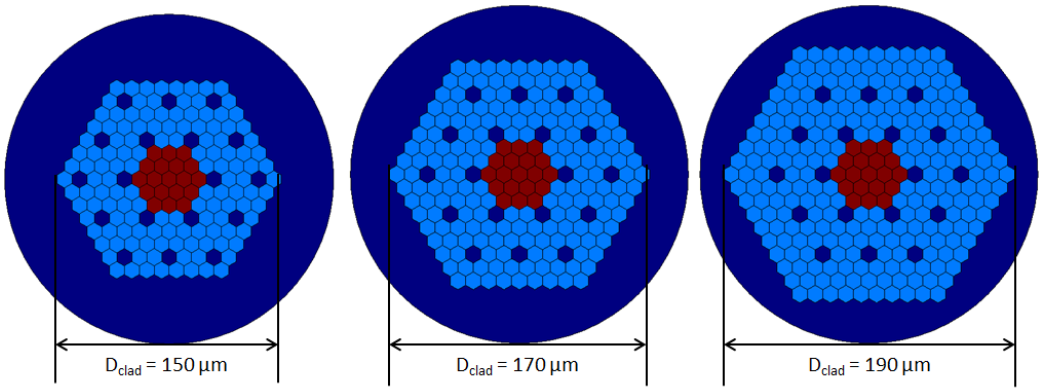


**Figure 3.4:** Representation of an all-solid LPF structure whose the dimension of the high-index region is tuned by adding layers of passively doped material (clear blue): (a) 150 $\mu$m - 5 layers, (b) 170 $\mu$m - 6 layers and (c) 190 $\mu$m - 7 layers. One can note that the size of the micro-structure remains constant (core size and pitch).

Hence, it is useful to observe in more details the behaviour of this mode and thereby the modal discrimination. For this, i fixed the dimension of the leaky region to 5 layers of high-index cells in order to minimize the amount of manufactured material. In the configuration of Fig. 3.3(a), i applied a homogeneous enlargement of the fiber structure, increasing the fiber core diameter from 50 to 70 $\mu$m, and by the way extending the leaky region dimension from 150 to 210 $\mu$m. The evolution of the modal discrimination versus the fiber core size has been calculated (see Fig. 3.5(a)). One can note that the homogeneous enlargement of the fiber dimensions does not affect significantly the modes confinement. It is almost constant for the three different fiber dimensions, demonstrating the scalability of this structure. Nevertheless, the level of discrimination is particularly low and has to be enhanced.

Furthermore, the influence of the RI contrast $\Delta$n has also been studied on a 50 $\mu$m core all-solid LPF (see Fig. 3.5(b)) by increasing together the RI of the passively doped leaky region and that of the gain medium. Here, $\Delta$n is varied from

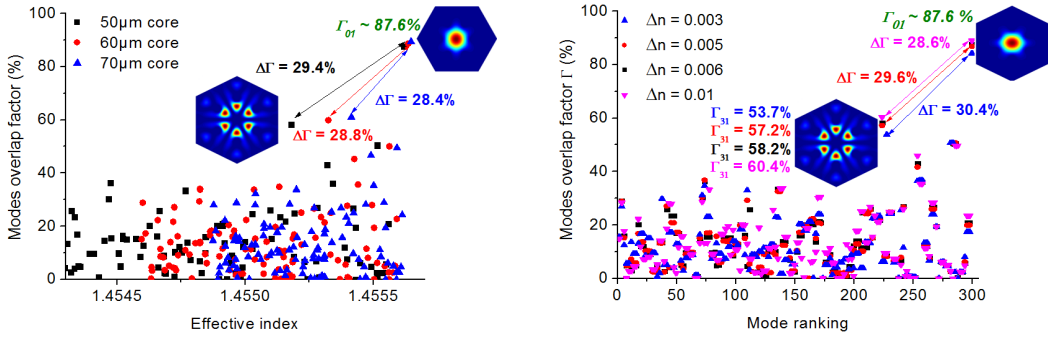


(a) (b)

**Figure 3.5:** (a) Overlap factor of the modes guided in an all-solid LPF whose the fiber dimensions are varied homogeneously (Core size varying from 50 to 70 $\mu$m). (b) Evolution of the modes overlap factor in a 50 $\mu$m core all-solid LPF whose the RI contrast spans from 0.003 to 0.01. Insets: intensity distribution for the $LP_{01}$ and the competitive $LP_{31}$-like modes.

$3 \cdot 10^{-3}$ to $10 \cdot 10^{-3}$. As the core RI is varied, it is no longer judicious to represent the modes overlap factor versus their effective index. In Fig. 3.5(b), the modes overlap factor are referred to their modes ranking: the $300^{th}$ mode being the FM and the first one is the highest order mode. It is worth noting that such variation of the RI progressively increases the FM confinement. However, the disturbing $LP_{31}$-like mode is clearly reconfined ($\Gamma_{31}$ from 53.7% to 60.4%) and reduces the modal discrimination. Later, it should be necessary to propose a solution to efficiently discriminate this HOM. However, i will first go beyond on the study of this all-solid LPF by investigating its general properties: its endlessly singlemodeness, its bending sensitivity and its tolerance to an index mismatch between the high-index passive material and the gain region.

### 3.2.2 Endlessly singlemodeness

When air/silica PCF whose the fiber core is created by omission of one air holes exhibits a normalized holes size $d/\Lambda$ lower than 0.406 and an infinite pattern, they shown an endlessly singlemode behaviour [Kuhlmey02]. It means that regardless the operating wavelength, the emitted beam presents a Gaussian-like intensity profile.

This tendency is checked in our proposed all-solid LPF ($d/\Lambda = 0.33$), whose the microstructuration is delimited by a double clad. I have calculated the evolution of the modal discrimination over a large spectral band ranging from 400 nm to 2200 nm, covering thus the emission bands of the main RE ions. Results are reported in Fig. 3.6.

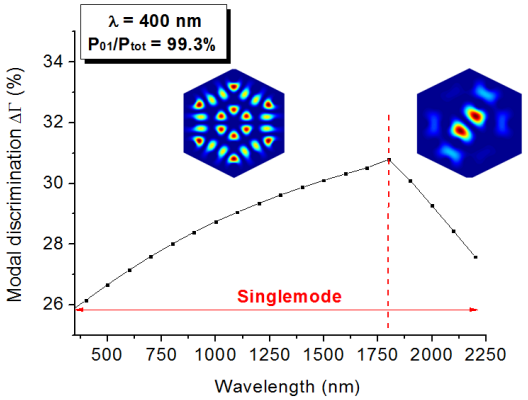


**Figure 3.6:** Evolution of the modal discrimination over a spectral range going from 400 nm to 2200 nm. In inset, the intensity distribution of the most competitive modes is reported.

Either side of 1800 nm, two different HOMs are competitive: the $LP_{31}$-like mode for shorter wavelengths and the $LP_{11}$ for longer wavelengths (see insets of Fig. 3.6). The values of modal discrimination obtained here are at the edge of the singlemode domain ($\Delta\Gamma$ from $\approx$ 26 to 31%). Following the approach described in Subsection 2.4.2, laser simulations have been performed over the spectral range of investigation. The five most confined modes have been implemented. According to the criterion defined in [Pagnoux94], the emitted beam appears singlemode from 400 to 2200 nm. However, the wavelength should be decrease only below 300 nm ($\Delta\Gamma \approx 25.5\%$) to get a multimode emission: the power carries by the FM ($P_{01}$) falls down to 97.75% of the whole emitted power $P_{tot}$. Thus, the modal discrimination should to be improved to provide a robust singlemode emission.

### 3.2.3 Bending sensitivity

Despite being critical for laser integration, VLMA leaky fibers suffer very high bending losses. Nevertheless, it is interesting to evaluate this sensitivity. Here, I consider that the curvature is applied on an axis running between two low-index inclusion surrounding the core (Y-axis in Fig. 3.7). This is the worst scenario as the bending is induced along a leakage channel. The FM overlap factor as well as the modal discrimination have been calculated for various bending radii. It is worth noting that when the bending radius is reduced, the modal discrimination is first enhanced as HOMs leak faster than the FM. Then, the FM starts to leak significantly, weakening the value of discrimination. Thus, the optimal situation is for a bending radius of 1.8 m. Moreover, as for air/silica LPF, a mode coupling appears on the FM, degrading the beam quality and placing the critical bending radius around 1.5 m. Although the RI contrast was significantly lowered compared to air/silica LPF, the inherent leaky nature of these structures is the source of modes coupling and avoid to maintain a robust singlemode emission under bendings. Thus, this confirms the needed to fabricate these fibers on a rod-type shape, making them less dispose to macro-bending and preserving its beam quality.

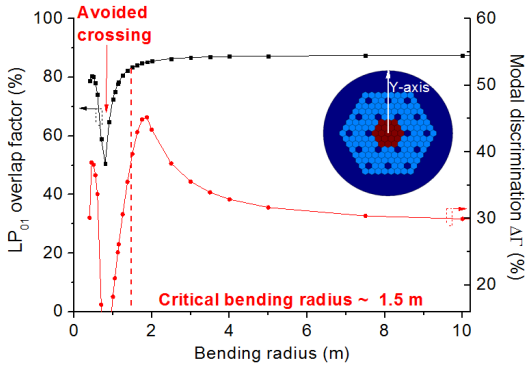


**Figure 3.7:** Evolution of the FM overlap factor and the modal discrimination for various bending radii (from 10 to 0.4 m).

### 3.2.4 Influence of an index mismatching

As I aimed to model fiber structures by taking into account experimental inaccuracies, as well as the constraints and opportunities offered by the fabrication technology, I have to consider the influence of a potential index mismatch between the gain medium and the passively doped region. Indeed, it represents a real challenge to perfectly match these two material and the interest of our fiber structure depends of their tolerance to this critical issue. Due to their relatively low RI contrast compared to that of the air/silica LPFs, it is straightforward to expect a lower tolerance of our all-solid fibers to this parameter. To check this intuitive assumption, the evolution of the modes confinement into the all-solid LPF has been studied over a range of index mismatching values going from -5 $\cdot 10^{-5}$ to +5 $\cdot 10^{-5}$. Several statements can be extracted from the Fig. 3.8. First, it is obvious that depending on the sign of the index mismatching, the modes leakage is inherently different. An index rise leads to a re-confinement of the modes, in particular for the $LP_{11}$ mode which becomes the most competitive HOM. On the contrary, an index depression contributes to a larger mode leakage out of the gain region, notably the $LP_{01}$ mode. Here, the modal discrimination is restricted by the $LP_{11}$ mode from dn=-4 $\cdot 10^{-5}$ to -1 $\cdot 10^{-5}$. Elsewhere, the $LP_{31}$-like mode is dominant. Moreover, because of the low

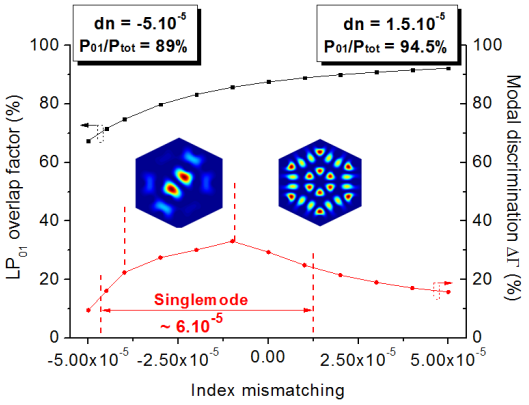


**Figure 3.8:** Evolution of the modal discrimination versus the index mismatching between the gain area and the silica doped region. Insets: Intensity distributions of the most competitive HOMs.

modal discrimination attributed to this all-solid LPF structure, its tolerance to an index mismatching is relatively low: approximatively $6 \cdot 10^{-5}$ (from dn=-$4.75 \cdot 10^{-5}$ to dn=$1.25 \cdot 10^{-5}$), making them really complicated to manufactured. The boundary of the singlemode emission are defined by simulating the laser behaviour of the fiber. Thus, following the criterion discussed earlier [Pagnoux94], the limit of the singlemode emission is considered when less than 97.75% of total emitted power is carried by the FM (see Inset of Fig. 3.8). Nevertheless, it has been shown in Chap. 2 that air/silica LPF are not more resistance to this mismatching as the FM can suffer mode coupling.

Hence, it is now require to understand how the disturbing $LP_{31}$-like modes behave in order to propose solutions aiming to efficiently delocalized it out of the gain region and so improve the modal discrimination in all-solid fibers. By the way, this could slightly increase the tolerance to an index mismatching, making the fabrication more affordable.

## 3.3 Understanding of the modes confinement

In this part, the objective is to understand the reason of the strong confinement of the LP31-like mode in order to propose innovative fiber structures maintaining an efficient confinement of the FM in the fiber core and strongly delocalizing the HOMs out of the region. For this, I will evidence the occurrence of avoided crossing on the disturbing HOMs. Then, I will focus my attention on the $LP_{31}$ and highlight its inherent confinement on the fiber core.

### 3.3.1 Avoided crossing on HOMs

Here, I am pursuing the previous investigation on the impact of the index mismatch between the gain region and the surrounding high-index material. It has been evidenced above that mainly two HOMs are competing: the $LP_{11}$-like and the $LP_{31}$-like. Thus, these two modes are considered with care here, starting with the

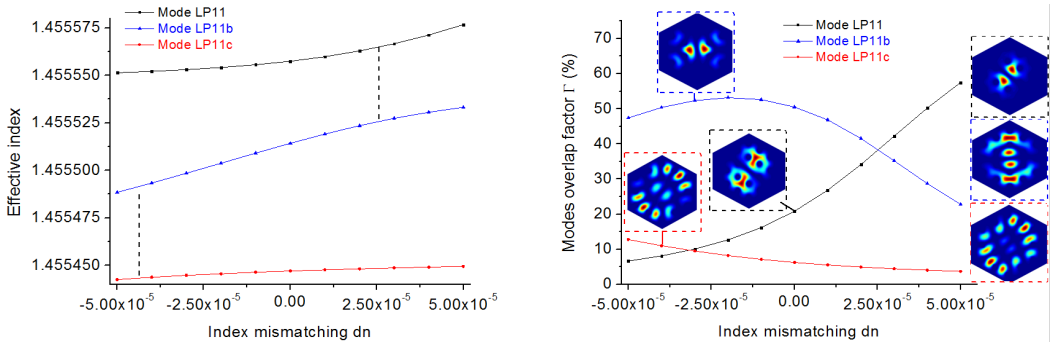


(a) (b)

**Figure 3.9:** (a) Evolution of the effective indices and (b) the overlap factor for the three $LP_{11}$-like modes involved in an avoided-crossing mechanism. Their intensity distribution is depicted in insets.

$LP_{11}$-like. On the range of investigation (dn=$-5 \cdot 10^{-5}$ to $+5 \cdot 10^{-5}$), I have observed that three $LP_{11}$-like modes are involved in an avoided crossing. Fig. 3.9 reports the evolution of their effective index, their overlap factor and their intensity distribution in insets. These results are in agreement with those of the Subsection 2.5. One can note two energy transfers occurring between modes exhibiting an overlap of their intensity patterns and an effective index in the vicinity one of the other (for dn≈$-4 \cdot 10^{-5}$ and $3 \cdot 10^{-5}$). Thus, the mechanism evidenced here is an avoided crossing. For the larger positive index mismatch, the true $LP_{11}$ can be clearly identify (black curves). Then, when 'dn' is reduced, this mode leaks, overlapping the $LP_{11b}$ mode, and transferring progressively its energy to this mode. In counterpart, the overlap factor of the $LP_{11b}$ mode with the gain medium is thus enhanced, making it competitive. A further reduction of the gain region RI will lead to the coupling of this mode with another cladding mode ($LP_{11c}$). Thus, it is once again evidenced that avoided coupling are ubiquitous in leaky fibers, although the FM can be relatively insensitive to this process due to its strong confinement into the fiber core.

Moreover, an avoided crossing is also highlighted on the $LP_{31}$-like mode (see Fig. 3.10). One can observe in Fig. 3.10(b) that the mode called $LP_{31}$-like up to now is in fact the true $LP_{31}$ mode. Due to its leakage in the inner cladding, its shape

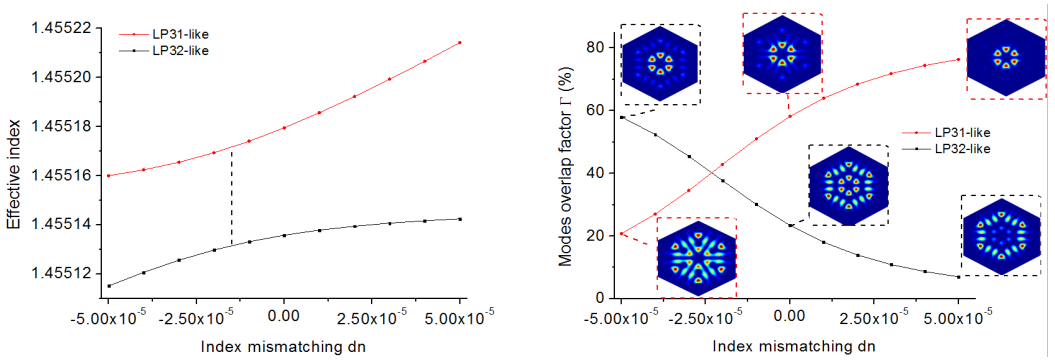


(a) (b)

**Figure 3.10:** (a) Evolution of the effective indices and (b) the overlap factor for the two coupled $LP_{31}$-like modes. Insets: Intensity distribution of these two modes.

is slightly modified and tends to exhibit an second ring of lobes. In the following, the notation is simplified and this mode is denominated $LP_{31}$. Otherwise, it is clear on the Fig. 3.10(a-b) that the $LP_{31}$ mode transfers its energy progressively to the $LP_{32}$-like mode. This transfer is more efficient when the effective indices of the two modes are the closest. Hence, its overlap with the gain region is significantly reduced but the modal discrimination is now limited by the $LP_{32}$-like mode whose the overlap factor is increased. Moreoever, it is worth noting that the $LP_{31}$ mode appears inherently well confined in the fiber core ($\Gamma_{31}$ approaches 60% for dn=0), being detrimental for the modal discrimination.

Although avoided crossings occurring on the FM are deleterious as they degrade the beam quality, they could be beneficial for an improvement of the modal discrimination if they impact HOMs. Indeed, when the energy transfer is the most efficient, the two coupled mode share equitably their energy and are then discriminated. Thus, it will be useful to investigate the impact of the microstructuration on the confinement of this mode and by the way, on the avoided crossing. A rigorous microstructuration of the leaky region should allow to tune the effective index of the cladding modes, favoring an efficient mode coupling for a perfect index matching.

### 3.3.2 1-ring structure

To go further, I decided to observe the influence of the first ring of six low inclusions. Here, the same geometrical considerations are kept as previously: the 50 $\mu$m active core is composed of 19 cells and the ratio d/$\Lambda$ = 0.33. Moreover, the diameter of the leaky region is varied from 150 $\mu$m (5 layers of high-index material) to 190 $\mu$m (7 layers). Fig. 3.11 depicts the RI repartition of this initial design and the modes overlap factor. First, one can observe that the FM can subject to a mode coupling (see insets of Fig. 3.11(b)). Thus, the microstructured should be extended in order to reduce the density of mode guided in the leaky region and makes the FM less sensitive to avoided crossing. Nevertheless, for the two dimensions of the leaky regions, this mode exhibits an overlap factor reaching 85%, highlighting that the first layer of low index inclusions mainly contributes to efficiently confine the FM. This statement is of major interest for the further development of microstructured fibers. It means that the cladding microstructuration can be devised freely to discriminate the HOMs. Otherwise, all others modes are significantly delocalized out of the fiber core ($\Gamma_{HOM}$ <50%), except for the persistent $LP_{31}$ mode, whose the overlap factor value $\Gamma_{31}$ appears strongly influenced by the dimension of the high-index region, as observed in Fig. 3.11(b) ($\Gamma_{31}$=50%, 74% and 63% respectively for a high-index dimension of 150, 170 and 190 $\mu$m). This behaviour is explained by its inherent confinement on the gain region and an avoided crossing: as the dimension of the leaky region are enlarged, the effective index of the cladding modes are shifted, implying a modification of the $LP_{31}$ mode coupling dynamic, occurring thus with different modes depending on the dimensions.

Moreover, this 1-ring all-solid structure cannot be a final design for several reasons. The leaky region sustains a very large number of guided modes, so the probability of mode coupling with the FM remains significant even for favourable dimensions of the leaky region. Furthermore, the modal discrimination is not really high ($\Delta\Gamma$ = 35% to the best) and has to be improved by efficiently weakening the

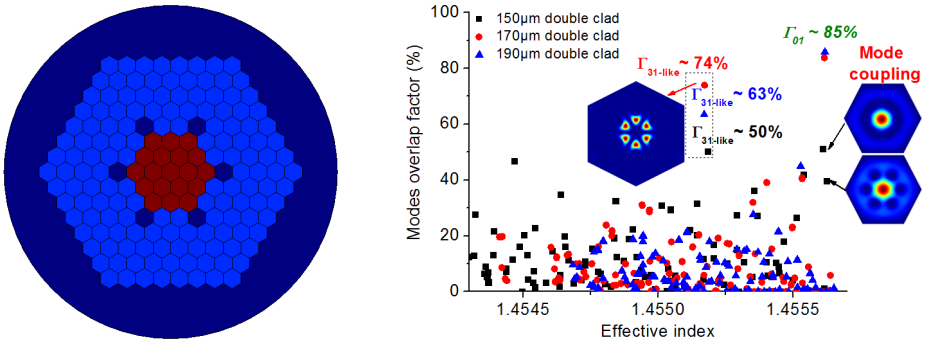


(a) (b)

**Figure 3.11:** (a) RI repartition of the 1-ring structure. (b) Representation of the modes overlap factor regarding their effective index for three dimensions of the high index region: $D_{clad}$. In insets: intensity distribution of the $LP_{01}$ under mode coupling and the $LP_{31}$.

$LP_{31}$ mode in particular. Otherwise, its bending sensitivity should be quite large due to the limited number of inclusions which can contribute to retain the mode leakage outside the fiber core. Thus, in order to develop a fiber laser exhibiting a robust singlemode emission, additional pure silica inclusions are required in the leaky region. However, this operation has to be achieved with care to avoid the reconfinement of the HOMs in the fiber core. For this, the $LP_{31}$ mode confinement is studied further in the next subsection.

### 3.3.3 $LP_{31}$ mode confinement

In this subsection, the evolution of the $LP_{31}$ mode field distribution is observed for two dimensions of the leaky region, with and without the first ring of pure silica inclusions. Thus, we should be able to understand the dynamic of its confinement.

At first, the high-index region is free of pure silica inclusions. This fiber looks like a step-index one whose the cladding is constituted by the pure silica layer. By this way, modes spread over the entire inner cladding. Among them, one mode appears similar to the $LP_{31}$ mode observed in a 1-ring structure. Fig. 3.12 shows the spatial intensity repartition of the $LP_{34}$-like cladding mode and its radial electric field distribution (solid lines), going from the center of the core to a corner of the

leaky region. One can note that the intensity of the mode field is quite similar in each lobe (see insets) and the mode overlap factor $\Gamma_{34}$ does not exceed 20%.

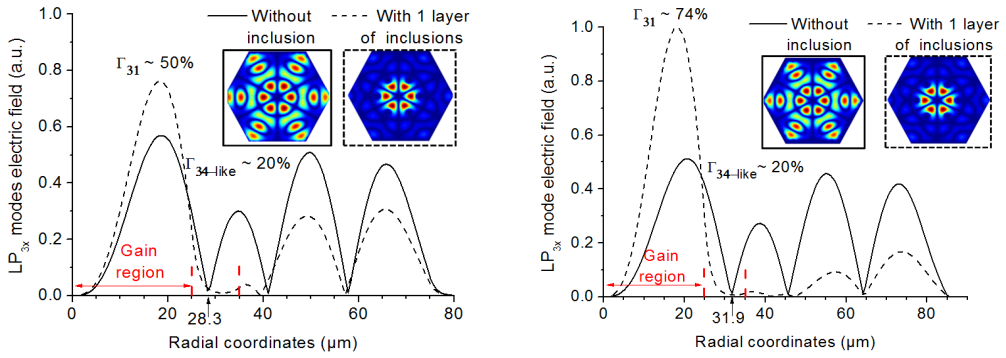


(a) (b)

**Figure 3.12:** Radial distribution of the modes electric field for the $LP_{34}$-like cladding mode into a step index fiber (solid lines) and the $LP_{31}$ mode in a 1-ring structure (dashed lines) for two diameters of the high-index region: (a) 150 $\mu$m and (b) 170 $\mu$m. Modes intensity distributions are added in insets. Red dashed lines denote the position of the inclusions.

Then, the single layer of six pure silica inclusions is added to delimit the fiber core, constituting a 1-ring structure. Maxima of the electric localized beyond the inclusions are strongly attenuated whereas the central lobes appears reinforced (see Figs. 3.12). In this case, the mode looks like the $LP_{31}$ mode and its effective index is only slightly modified. Let us remark that the relative dimension of the leaky region and the position of the low-index inclusions strongly impact the radial electric field distribution. In particular, when the overlap of the central lobes of the $LP_{34}$ mode with the position of the inclusions increased, the overlap factor of the final $LP_{31}$ in the 1-ring structure is more important. Thereby, it exhibits an overlap factor as large as $\Gamma_{31}$=74% in a 1-ring structure whose the size of the leaky region is 170 $\mu$m, as the inclusions contributes more to the confinement of the electric field in the fiber core than with a 150 $\mu$m leaky region.

So, in order to limit the overlap of this mode with the fiber core, the position of the additional inclusions should be placed in regions where the mode field distri-

bution is the lowest, limiting its reconfinement in the fiber core but acting on the cladding modes effective index. Thus, the dynamic of modes coupling should be impacted. By appropriately positioning the additional inclusions, I intend to limit the overlap factor of this mode by limiting its inherent confinement and coupling it to a cladding mode.

## 3.4 Advanced cladding microstructuration

Starting with the standard LPF structure discussed above, I will take benefit of the several statements highlighted previously to judiciously design the inner cladding and enhance the modal discrimination. First of all, I would like to summarize the different rules established up to now which will be useful for the further fiber development:

1. one layer of six low-index inclusions is sufficient to ensure a strong confinement of the FM, so the inner clad can be devised freely to efficiently delocalized the HOM out of the gain region. Whether a sufficient number of inclusions paved the inner clad, the modes coupling observed previously on the fundamental mode should disappear.

2. the leakage channels shall be large enough to let HOMs leak out the gain region.

3. avoided crossings are ubiquitous on HOMs guided in leaky structure. Thus, i would like to take benefit from this process to favour a strong energy transfer from the $LP_{31}$ mode and a cladding mode. This is achievable by tuning the effective index of the cladding modes through the addition of silica inclusions on the electric field minima of the $LP_{31}$ modes.

Using this three guidelines, I afford to devise microstructured leaky fibers whose the core exhibits a low modal content. In order to enhance the mitigation of the

disturbing HOM, I will highlight that a reduction of the microstructure symmetry is beneficial.

### 3.4.1 Six-fold symmetry structures

Initially, the six-fold symmetry of conventional air/silica LPFs was kept. Moreover it was chosen to restrict the dimensions of the leaky region in order to limit the request on the material fabrication. Thus, although it does not appear as the most favourable case regarding the previous results, the number of passively-doped silica layer was fixed to 5. In this way, a 50 $\mu$m core fiber exhibits a 150 $\mu$m leaky region. Then, to study the region of the inner cladding where the most disturbing modes are delocalized, the latter was divided in six identical sections. Each cell in a section is associated with the five cells at the same position in the other sections, forming a set of subdomains, as shown in Fig. 3.13. Then, the analysis of the electric field density localized in each group of cladding subdomains for all modes considered, and separately the $LP_{31}$ mode, has made possible to strive towards an optimum cladding microstructuration for HOMs discrimination.

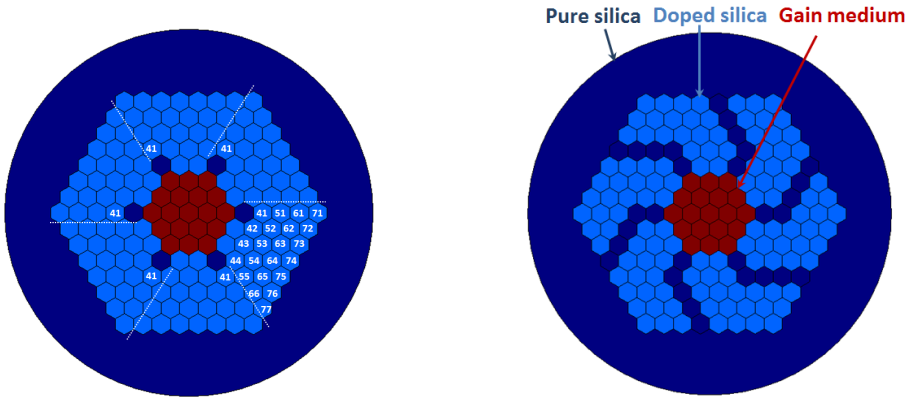


(a) (b)

**Figure 3.13:** (a) Representation of the 1-ring structure with the subdomain numbering used to design the inner clad. (b) RI repartition for the "Vortex fiber".

Using this approach, novel fiber structures can be proposed, demonstrating a

serious improvement of the modal discrimination in comparison to the all-solid LPF structure. Here, only the most relevant solution is reported. This design, called "Vortex fiber", is composed of six arms of silica inclusions (Fig. 3.13(b)). The RI contrast is still kept equal to $6 \cdot 10^{-3}$. Moreover, the fiber dimensions were homogeneously increased, enlarging the fiber core from 50 to 70 $\mu$m and by the way the size of the leaky region from 150 to 170 $\mu$m, to observe the evolution of the modal discrimination. Fig. 3.14(a) shows that the FM confinement has been slightly enhanced ($\Gamma_{01}$=87.6% $\Rightarrow$ 90%) and the modal discrimination clearly improved up to $\Delta\Gamma$ = 45.8% for a 50 $\mu$m core Vortex fiber compared to $\Delta\Gamma \approx 29\%$ for a 50 $\mu$m all-solid LPF. This has been made possible thanks to the weakening of the $LP_{31}$ mode, placing in this case the $LP_{11}$ as the most competitive HOM. However, the avoided crossing evolves significantly when the fiber dimensions are increased ($\Gamma_{31} \approx 42\%$ for a 50 $\mu$m core and $\Gamma_{31} \approx = 52.2\%$ for a 70 $\mu$m core), and thus the modal discrimination is reduced. The avoided crossing occurring on the $LP_{31}$ mode is depicted in insets of Fig. 3.14(a) for a 60 $\mu$m core Vortex fiber.

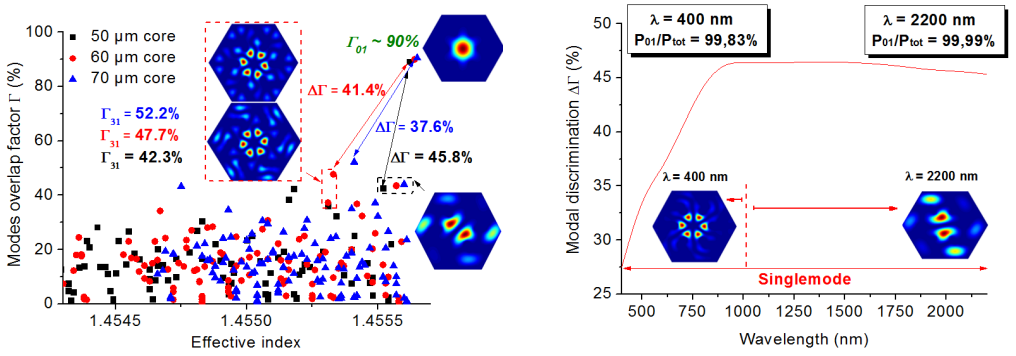


(a) (b)

**Figure 3.14:** (a) Computed modes overlap factor into the Vortex fiber for different fiber dimensions (here, the RI contrast $\Delta$n is equal to $6 \cdot 10^{-3}$). Insets: intensity distributions of the $LP_{01}$, $LP_{11}$ and the two-coupled $LP_{31}$ modes. (b) Spectral evolution of the modal discrimination. In inset, intensity distributions of the most competitive HOMs.

A complementary investigation (not reported here) based on the influence of the RI contrast ($\Delta$n from 6 to $20 \cdot 10^{-3}$) has allowed to demonstrate that the lowest

value of modal discrimination achievable into the 50 $\mu$m core Vortex fiber is 38% for a $\Delta_n = 13 \cdot 10^{-3}$, pointed out that a real improvement has been provided and that the resonance of the $LP_{31}$ is inherently weaken in this novel structure. Indeed, the surface of interaction of this mode with the edge of the leaky region is lowered because of the 6 arms of inclusions.

In order to push further this study, the spectral evolution of the modal discrimination has been observed in the 50 $\mu$m core Vortex fiber (Fig. 3.14(b)). As previously, the spectral range of investigation covers the visible wavelengths and the emission bands of the main rare-earth ions (from 400 nm to 2200 nm). Laser simulations has also been achieved to clearly evidence whether the emitted beam is singlemode or not. A singlemode emission is demonstrated over the whole range of investigation ($P_{01}/P_{tot}$>97.75%), on which the minimum modal discrimination is 27.5% at 400 nm. Moreover, depending on the operating wavelength, the most disturbing HOM can be the $LP_{11}$ or the $LP_{31}$-like but it is worth noting that the modal discrimination is relatively high and stable from 900 nm to 2200 nm, making it really interesting for a transposition to the main RE doped fiber lasers (Yb, Er, Tm and Ho).

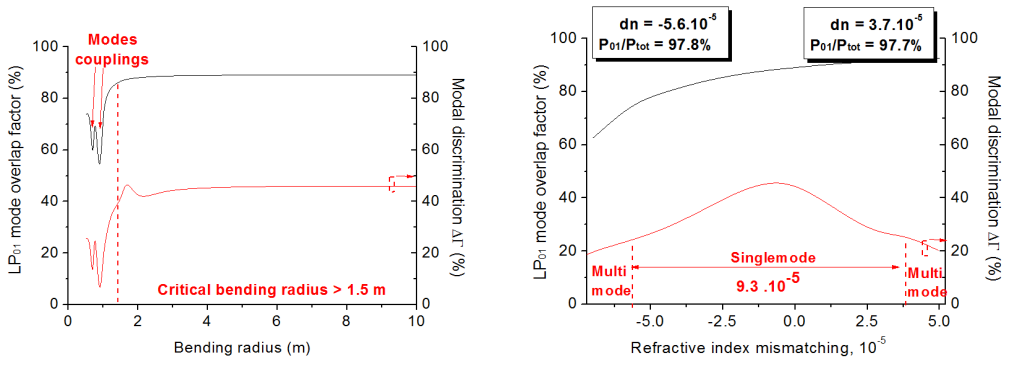


(a) (b)

**Figure 3.15:** (a) The modes overlap factor in this structure for different core diameter. In inset: intensity distribution of the $LP_{01}$ and $LP_{31}$-like modes. (b) Evolution of the fundamental mode overlap and the modal discrimination regarding the index mismatching between the gain region and the background material.

Furthermore, the bending sensitivity of the Vortex fiber has been studied. Fig. 3.15(a) shows the evolution of the FM confinement and the modal discrimination versus the bending radius. Although the FM confinement is strengthened in the Vortex fiber, modes couplings are still noticed on the FM for bending radius lower than 1.5 m, strongly impacting the modal discrimination, and by the way, the singlemodeness. Finally, another asset of this fiber design in comparison to an all-solid LPF is its larger insensitivity to an index mismatching 'dn' between the gain medium and the silica doped background material. Based on the criterion define in [Pagnoux94] and used previously, the tolerance of the 50 $\mu$m core Vortex fiber to an index mismatch of the gain region reaches $9.3 \cdot 10^{-5}$ (from dn=-$5.6 \cdot 10^{-5}$ to $3.7 \cdot 10^{-5}$), so almost twice that of the all-solid LPF, making it slightly easier to manufacture.

In conclusion, a careful observation of the modes leakage and then an appropriate positioning of the silica inclusions have contributed to devise a novel microstructured fiber in which the modal discrimination has been drastically improved up to 45%. The 50 $\mu$m Vortex fiber exhibits a modal discrimination as large as an equivalent air-silica fibers investigated in Chap. 2. However, the avoided crossing impacting the most disturbing HOM and restricting its overlap factor in a 50 $\mu$m core Vortex fiber does not allowed to maintain this strong weakening of the $LP_{31}$ mode when the fiber dimensions are homogeneously increased. Nevertheless, an endlessly singlemodeness has been evidenced with a large modal discrimination above 900 nm ($\Delta\Gamma \approx 45\%$) and its tolerance to an index mismatch of the gain region has been doubled compare to a conventional LPF. Hence, to go further and get an all-solid fiber competing with state-of-the-art leaky fibers, new improvements are required. For this, i will take benefit of a statement stemming from the Vortex fiber: a reflection plane does not exist in the Vortex fiber. In the following, the influence of the microstructured cladding symmetry will be discussed and investigated.

### 3.4.2 Discussion on the reduction of the fiber symmetry

Commonly, microstructured optical fibers (PCFs for instance) are based on a periodic lattice of air-holes, forming a hexagonal array. This microstructuration confers to the fiber a $C_{6\nu}$ symmetry: 6 reflection planes and a 6-fold rotational symmetry. As discussed earlier, this kind of fiber presents the advantage to provide an efficient mode leakage and thus a good discrimination of the HOMs. Due to their leaky tendency, core modes escape the core region and interact with the next interface (air clad in air/silica LPFs and the edge of the leaky region in our all-solid LPFs). Previously, it has been highlighted that a coherent contribution of the two waveguides (the microstructured inner cladding and the surrounding silica layer) can lead to a strong confinement of HOMs into the fiber core (see Subsection 3.3.3). Moreover, core modes leaks into the cladding and partially overlap cladding modes. Thus, potential avoided crossings/modes couplings can occur between them (see Subsections 2.5 and 3.3.1). Thereby, the inner cladding microstructuration shall be designed in order to favour as much as possible the leakage of HOMs into the inner cladding and allow a beneficial avoided crossing to coupled out the competitive HOMs (at least the $LP_{31}$ mode).

For this purpose, my strategy is to break the fiber symmetry. In this way, I intend to increase the leakage of the competitive HOMs by providing them different conditions of resonant either side of the fiber core, resulting in asymmetric modes. Moreover, the avoided crossing will be impacted as well. Three approaches can be followed to fulfil this objective:

1. shifting the fiber core,
2. acting on the inner cladding microstructuration,
3. modifying the shape of the leaky region.

To date, only few works report on the use of these methods to favour a singlemode propagation or emission. Agruzov *et al.* have demonstrated the development of

passive fibers promoting a strong attenuation of the HOMs. They have initially used a conventional PCFs (large number of tiny air holes) in which the fiber core have been shifted [Agruzov09]. Then, a PCF exhibiting two sizes of air holes have been fabricated, by managing the pressure applied in each group of air holes, resulting in a three-fold symmetry fiber ($C_{3\nu}$ symmetry). Along 20 m of these fibers, selective losses has allowed to efficiently attenuate the HOMs, providing a Gaussian emitted beam. Moreover, Limpert *et al.* have recently numerically transposed this principle to LPF structures [Limpert12a]. The fiber design, called "Spiral fiber" and presenting a 3-fold symmetry, has been announced to increase the modal discrimination up to 52% (79% of overlap factor for the fundamental mode and 27% on the $LP_{11}$). Nevertheless, the influence of resonant cladding modes, such as the $LP_{31}$-like, has not been discussed. Otherwise, an alternative non-hexagonal design has also been proposed by this group [Stutzki11]. A pentagonal lattice was proposed for the improvement of modal discrimination allowing the extension of the MFD up to 125 $\mu$m.

In the case of all-glass fibers, the manufacturing process requires to stack canes of the same dimensions. So, to develop a fiber structures exhibiting two sizes of low index inclusions, it would be necessary to prepare canes composed of two materials: a pure silica rod surrounded by a layer of high-index material for instance. To mitigate the constraints on the fiber manufacturing, it is decided to take others approaches.

### 3.4.3 Shifted core all-solid LPF

The first strategy has been to shift the periodic lattice along the horizontal X-axis (Fig. 3.16(a)). Thus, the center of the fiber core is also shifted, becoming closer to one edge of the leaky region than to the other. In this configuration, a coherent reflection can not take place symmetrical on the two sides of the fiber core. Through this, it is expected to weaken the overlap factor of modes interacting with the edge

of the leaky region, such as the $LP_{31}$ mode.

In Fig. 3.16(b), the intensity pattern of the FM and the most competitive HOMs are depicted. It is clearly shown in inset of this figure that the $LP_{31}$-like mode gets favourable resonant conditions on one side of the fiber core, promoting its field on the central lobes, whereas on the other side, the mode remains leaky. By this way, its overlap factor with the fiber core is reduced, improving the modal discrimination by approximatively 10% in comparison to an all-solid LPF ($\Gamma_{31}$ =58% $\Rightarrow$ 47%). Here, no avoided crossing has been clearly identified on the $LP_{31}$ mode. A homogeneous enlargement of the fiber dimensions modify the conditions of resonance and implies a slight increase of the $LP_{31}$ mode confinement. However, this solution is relevant although its overlap factor is not as large as in a Vortex or air/silica LPF.

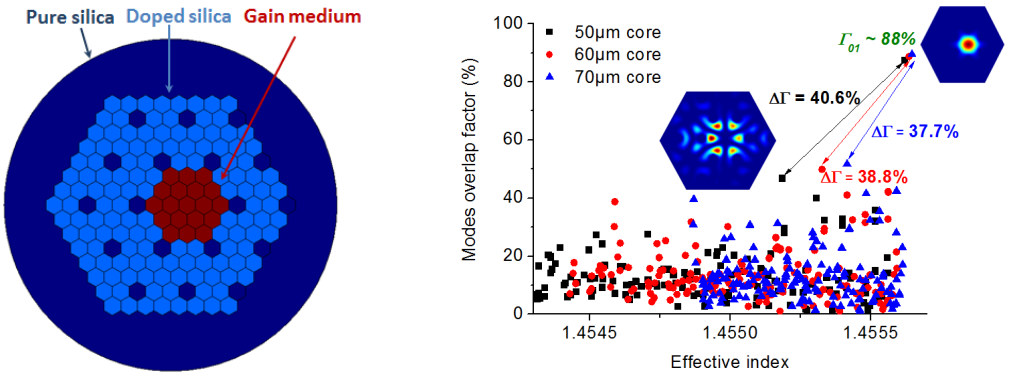


(a) (b)

**Figure 3.16:** (a) RI repartition for a shifted core all-solid LPF. (b) Related modes overlap factor for a homogeneous enlargement of the fiber dimensions (fiber core diameter ranging from 50 to 70 $\mu$m). In inset: intensity distribution for the FM and the most competitive HOM.

### 3.4.4 Rotated lattice all-solid LPF

On the other hand, the second idea was to rotate the periodic lattice inside the leaky region (Fig. 3.17(a)). In this case, and as for the Vortex design, no reflection plane exists but the 6-fold rotational symmetry is maintained ($C_6$ symmetry). Due

to the rotation of the periodic pattern and the hexagonal arrangement of the stack, the spacing/pitch between two inclusions is reduced to $\Lambda \approx 26$ $\mu$m for a structure composed of 10 $\mu$m rods and thus, the ratio d/$\Lambda$ tends to 0.4, narrowing the leakage channels. To retrieve a fiber core of 50 $\mu$m (from one inclusion to another), the size of the each elementary cell is increased up to 11.55 $\mu$m, enlarging consequently the size of the high-index region. In order to compare rigorously the results obtained on this rotated all-solid LPF to those got on a conventional all-solid LPF and on the Vortex fiber, I choose to maintain a constant core size and by the way, an identical gain area.

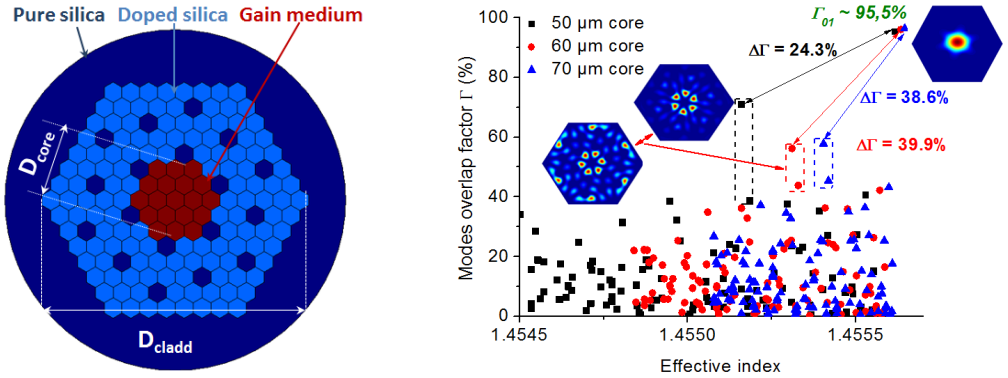


(a) (b)

**Figure 3.17:** (a) RI repartition of a rotated lattice all-solid LPF. (b) Modes overlap factor into this fiber design for different core diameters (from 50 to 70 $\mu$m). In insets: intensity distribution for the $LP_{01}$, the competitive $LP_{31}$ mode and its coupled cladding mode.

This rotation, and by the way the narrowing of the leakage channels, has contributed to enhance the confinement of the FM up to 95.5% (7% more than for the standard all-solid LPF design), enabling to benefit from a stronger interaction between the emitted radiation and the gain region and so a larger linear gain. Moreover, the $LP_{31}$ is still the most competitive HOM, in particular for a 50 $\mu$m core structure in which its overlap factor reaches $\Gamma_{31}$= 71.1%. However, it is drastically weakened when the fiber dimension are homogeneously varied as it transfers part of its energy to a cladding mode (see insets of Fig. 3.17(b)), becoming even more inter-

esting for larger core size ($\Delta\Gamma \approx 39\%$). As for the Vortex fiber, the value of modal discrimination is significantly influenced by a modification of the fiber dimensions. Except for a 50 $\mu$m core, this design demonstrates the same level of modal discrimination but allow a stronger confinement of the FM. Thus, I intend to optimize this proposal. To minimize this effect and favour an avoided crossing for a 50 $\mu$m core, the shape of the leaky region will be modified by extending the periodic pattern up to the interface with the silica layer.

### 3.4.5 Extension of the rotated lattice

In order to modify the condition of resonance for the $LP_{31}$ and act on its coupling with a cladding mode, the periodicity of the rotated LPF lattice is extended up to the edge of the leaky region (Fig. 3.18(a)). In Fig. 3.18(b), one can observe that the $LP_{11}$-like mode is now the most competitive one, limiting the modal discrimination to 41.5% for a 50 $\mu$m core structure. The homogeneous enlargement of the fiber dimensions allows to progressively and slightly improve the modal discrimination, reaching up to $\Delta\Gamma = 48.3\%$ for a 100 $\mu$m core fiber (not reported here). Indeed, the effective index of the well-confined $LP_{11}$-like mode gradually comes closer to

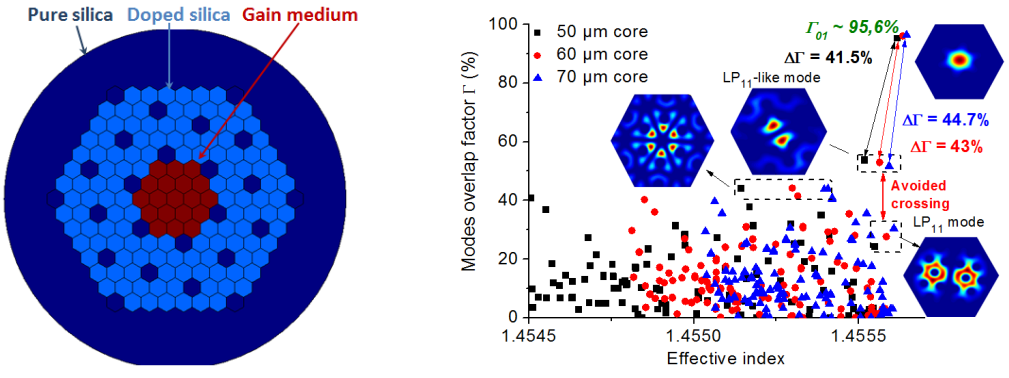


(a) (b)

**Figure 3.18:** (a) RI distribution for an all-solid LPF whose the inner cladding lattice is rotated and extended. (b) Modes overlap factor in this fiber design for different size of the fiber structure. The core diameter is thus varied from 50 to 70 $\mu$m. In inset: intensity distribution for the FM and the most competitive HOMs.

that of the leaky $LP_{11}$, allowing to transfer it more and more energy, as shown in Fig. 3.18(b). Moreover, it is worth noting the weakening of the $LP_{31}$, whose the overlap factor is felt down to 43%. Thus, inclusions placed on the corner of the high-index region contribute to reduce the overlap of the $LP_{31}$ but does not affect the $LP_{11}$-like mode. To increase further the modal discrimination, these two modes have to be discriminated simultaneously. For this, I will set the fiber structure free of its 6-fold symmetry by inserting additional silica inclusions in an asymmetric way to attenuate the disruptive HOMs, leaving one region of the inner cladding intact for an efficient evacuation of these HOMs out of the gain region. Thus, I intend to favour a strong discrimination on the two above mentioned competitive HOMs and maximize the modal discrimination.

### 3.4.6 Symmetry free fibers

In order to weaken the overlap of the two most competitive modes ($LP_{11}$-like and $LP_{31}$) with the gain region, i choose here to combine two principles: 1/ avoid the cooperative and symmetric resonances and 2/ save the periodic rotated LPF lattice for an efficient HOMs leakage and a strong confinement of the FM. Hence, additional pure silica inclusions are used to tune the effective index of the cladding modes in such way to get favourable avoided crossings on the competitive HOMs. Hence, a wide variety of fiber structures can be realized following these guidelines. However, only the two most relevant will be reported here. These structures exhibit an inner cladding free of symmetry: neither reflection plane nor rotational symmetry, impacting symmetric leaky modes. These designs are called "Hexagonal Symmetry Free fibers": $HSF_x$, with the '$x$' index referring to the number of additional inclusions. The term 'Hexagonal' is related to the shape of the first layer of pure silica inclusions.

As shown above, the addition of inclusions on the corner of the double clad contributes to slightly reduced the $LP_{31}$ mode overlap factor. Here, I propose to

use only few inclusions in this position to influence the $LP_{31}$ mode, letting it leak out the core in the opposite directions. Moreover, some other inclusions will be inserted on the inner clad microstructuration to reinforce the structure asymmetry and favour an efficient avoided crossing on the $LP_{11}$-like mode.

#### 3.4.6.1 Modal discrimination

On this principle, I propose two fiber structures demonstrating outstanding performances. The $HSF_4$ fiber has been developed by inserting two inclusions in the corner of the leaky region (acting on the $LP_{31}$ mode) and two others behind the second ring of periodic inclusions. The latters are positioned on regions where the electric field of the $LP_{31}$ mode is minimum, influencing mainly the effective index of the pure cladding modes. Moreover, all these inclusions have been placed in such way to leave one side of the inner cladding intact, letting the leaky HOMs preferentially escape the fiber core towards this area. In Fig. 3.19(a), the 4 added inclusions are evidenced by white hexagons. Interestingly, the modal discrimination of the $HSF_4$ fiber reaches 54.1% in a 50 $\mu$m core $HSF_4$ fiber, outperforming the all-solid LPF, but

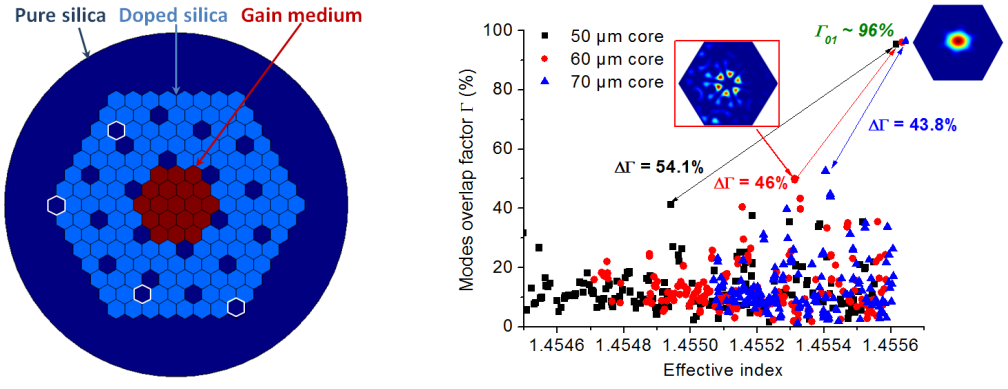


(a) (b)

**Figure 3.19:** (a) RI distribution for $HSF_4$ fiber and (b) overlap factor of the mode guided in this structure for three different three fiber dimensions: $D_{core}$= 50, 60 and 70 $\mu$m across inclusions. The intensity distribution of the FM and the competitive modes are reported in inset.

also that of air/silica LPFs reported in literature (Fig. 3.19(b)). The avoided crossing occurring on the competitive $LP_{31}$ mode is optimal here for a 50 $\mu$m core fiber. For larger core size, the overlap factor of this mode increases, limiting the modal discrimination. One can note that the $LP_{31}$ mode appears slightly asymmetric.

My second proposal, called $HSF_5$, has been devised by inserting 5 silica inclusions, 3 in a triangular shape to act on the modes coupling and 2 on the horizontal line to weaken the $LP_{31}$. These modifications are highlighted by white hexagons in Fig. 3.20(a). Once again, this symmetry free fiber exhibits a significant modal discrimination, exceeding 48% for a core size ranging from 50 to 70 $\mu$m across inclusions and reaching up to 56.2% for a 50 $\mu$m core $HSF_5$ structure (Fig. 3.20(b)). The $LP_{31}$ mode is still the most disturbing HOMs but is efficiently weakened. From now on, it appears more difficult to enhance further the modal discrimination by this approach as a large number of HOMs presents an overlap factor $\Gamma$ in the vicinity of 40%. It is demonstrated here the more performing discrimination reported up to now. A further improvement should be achieved by modifying the fiber structure (use of a pentagonal first ring for instance). Nevertheless the performances of these

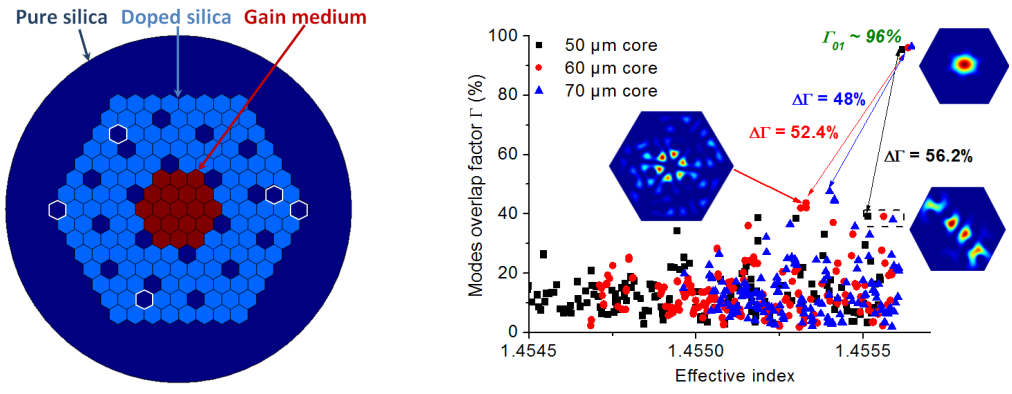


(a) (b)

**Figure 3.20:** (a) RI distribution for $HSF_5$ fiber and (b) overlap factor of the modes guided in this symmetry free fiber for three fiber dimensions: $D_{core}$= 50, 60 and 70 $\mu$m across inclusions. In inset: intensity pattern of the FM and the competitive HOMs ($LP_{11}$ and $LP_{11}$-like).

two symmetry free fibers surpass those of the published state-of-the-art air/silica LPFs.

Hence, it is interesting to observe the evolution of the modal discrimination for core sizes larger than 70 $\mu$m, in order to reinforce the potential of these fibers for the use in high power regime. The two above-mentioned symmetry free fibers have thus been investigated for core diameters spanning from 45 to 100 $\mu$m across inclusions (and by the way, the dimension of the leaky region increased proportionally). Fig. 3.21 shows that the overlap factor of the $LP_{31}$ mode increases as the fiber dimensions are homogeneously enlarged. However, the modal discrimination remains larger than 40% while the core size does not exceed at least 80 $\mu$m in diameter.

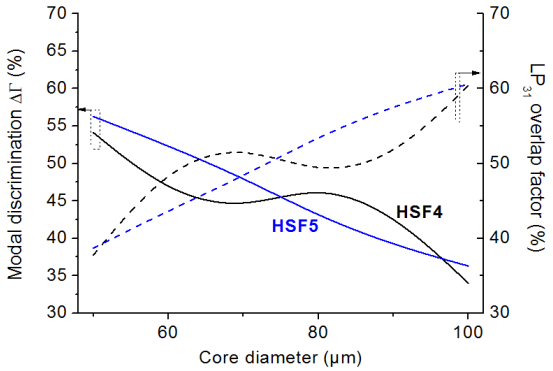


**Figure 3.21:** Evolution of the modal discrimination and the $LP_{31}$ overlap factor in $HSF_x$ fibers on a range of core dimensions going from 45 to 100 $\mu$m.

This demonstrates that the method employed here to design novel microstructured fibers is a convenient approach but can not provide a universal solution as the most disturbing HOMs are involved in avoided crossing processes whose the strength varies with the effective indices of the coupled modes. Indeed, as the modes coupling is influenced by an increase in fiber dimensions, it is not possible to develop a fiber structure which is the most performing regardless the operating wavelength and the dimensions of the high index region. Thus, this method should be applied for each particular fiber dimensions in order to get the most discriminative microstructuration. However, under the consideration of this study, we have successfully devised an asymmetric inner cladding offering a modal discrimination as large as 55%. More-

over, this approach has also been validated to design a 100 $\mu$m fiber whose the modal discrimination is equal to 55% at 1 $\mu$m.

To complete the study of the $HSF_x$ structures, their endlessly singlemode tendency, sensitivity to the bending and tolerance to an index mismatching between the gain area and the index matched region will be evaluated.

#### 3.4.6.2 Endlessly singlemodeness

The wavelength bandwidth of investigation is the same as previously (400 nm $\Rightarrow$ 2200 nm). Modellings are done for a RI contrast of $\Delta n = 6 \cdot 10^{-3}$ and the fiber core size is varied to observe the spectral evolution of the modal discrimination. In Figs.3.22(a-b), one can note that 50 $\mu$m core HSF fibers demonstrate a discrimination larger than 50% from 900 nm to 2200 nm, confirming their potential for RE doped fiber lasers and amplifiers. However, when the fiber core is enlarged, the spectral evolution of the modal discrimination is red-shifted. Indeed, the enlargement of the fiber core size enhance the ability of modes to be guided in this region and so, their leakage is curbed. To retrieve an equivalent modes leakage, the wavelength has to be increased in the same proportion. For 100 $\mu$m core HSF fibers, the emission

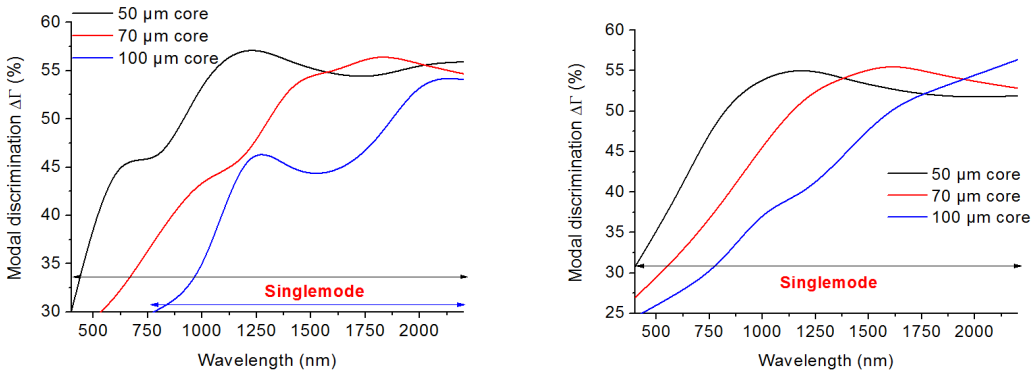


**Figure 3.22:** Spectral evolution of the modal discrimination in the (a) $HSF_4$ fiber and (b) $HSF_5$ fiber for three fiber core diameters: 50 $\mu$m (in black), 70 $\mu$m (in red) and 100 $\mu$m (in blue).

should be multimode for wavelengths below approximatively 800 nm as the modal discrimination is significantly reduced at short wavelengths. Here, it is worth noting the relatively small variation of the modal discrimination around 2 $\mu$m, making these designs strongly scalable for Tm- and Ho-doped fiber lasers. On the contrary, it is evidenced that the fiber structures can not be scaled indefinitely at 1 $\mu$m. When the fiber core exceeds 75 $\mu$m, the modal discrimination starts to be reduced ($\Delta\Gamma \approx$ 44.5%) and the robustness of the singlemode emission is thereby impacted. Thus, our approach should be applied on a 100 $\mu$m core all-solid LPF for instance in order to offer an efficient discrimination at 1 $\mu$m for larger core size. These two symmetry free fibers display quite similar performances and are both relevant solutions for the development of robust singlemode high power fiber lasers.

### 3.4.6.3 Bending sensitivity

Although it was demonstrated earlier that the bending resistance of all-solid fiber is mainly restricted by the occurrence of avoided crossing on the FM, I intend to observe the influence of the insertion of additional inclusions. Figs. 3.23(a-b) report on the evolution of the FM confinement and modal discrimination versus the bending radius. On the two symmetry free fibers, no real improvement of the

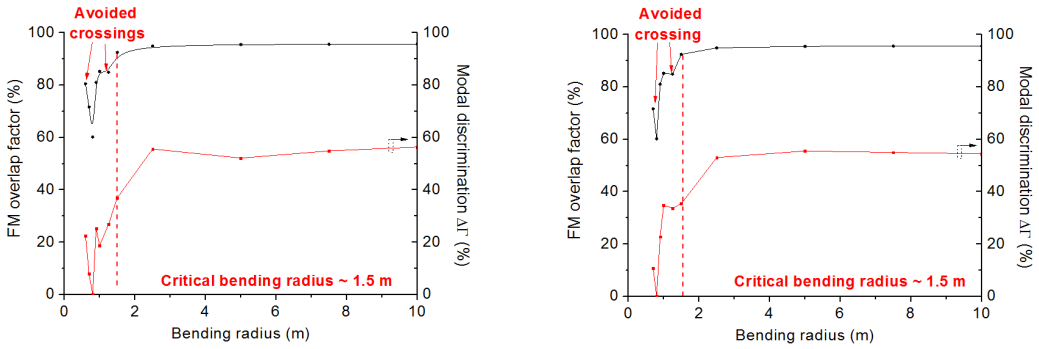


(a) (b)

**Figure 3.23:** Evolution of the FM confinement (in red) and modal discrimination (in black) versus the bending radius in the (a) $HSF_4$ fiber and (b) $HSF_5$ fiber for a core diameter of 50 $\mu$m and a RI contrast of $\Delta n = 6 \cdot 10^{-3}$.

bending resistance is noticeable. The critical bending radius is still limited around 1.5 m due to avoided crossings. Thus, these fibers should be drawn as rod-type to avoid the macro-bendings.

#### 3.4.6.4 Influence of an index mismatching

Finally, i have studied the tolerance of these symmetry free fibers to an index mismatching between the gain region and the passively doped material. This section is one of the most important to quantify and evaluate the impact of manufacturing inaccuracies. This investigation is reported below for the two 50 $\mu$m symmetry free fibers ($\Delta n = 6 \cdot 10^{-3}$). The HSF fibers demonstrate a tolerance to an index mismatch of the gain region in the range of $8 \cdot 10^{-5}$ (from dn≈-4.5 $\cdot 10^{-5}$ to dn≈3.5 $\cdot 10^{-5}$) so larger than for all-solid and air-silica LPF. Due to their large modal discrimination (efficient mode coupling), a larger index mismatch is required to reconfine the $LP_{31}$. Thus, it facilitates their fabrication.

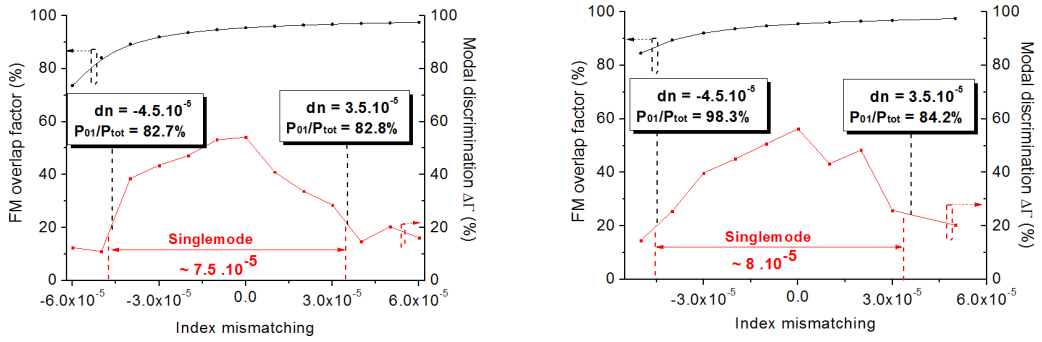


(a) (b)

**Figure 3.24:** Evolution of he FM confinement and the modal discrimination for an index mismatching between the gain region and the passively doped material in 50 $\mu$m core (a) $HSF_4$ fiber and (b) $HSF_5$ fiber whose the RI contrast with the pure silica inclusions is $\Delta n = 6 \cdot 10^{-3}$.

### 3.4.7 Spiral LPF

#### 3.4.7.1 Design description and modal discrimination

To lead this theoretical work to its outcome, I finally removed the initial periodicity of the structured cladding to prevent the existence of all symmetric modes ($LP_{31}$ mode for instance). Thus, I expect an additional reduction of the high-order modes confinement into the fiber core (gain region) through an annihilation of the cladding symmetries. In this aim, low-index inclusions are placed in a spiral way. Due to the gradual increase of the distance to the center along a spiral, no symmetry can exist regarding the core center, favoring the mode leakage out of the core and by the way, out of the gain region. The fiber devised on this principle is depicted in Fig. 3.25(a). The gain region remains composed of 19 Yb-doped cells but inclusions surrounding the fiber core are no longer hexagonally arranged but rather describes an irregular pentagonal shape. The refractive index contrast is still $\Delta n = 6 \cdot 10^{-3}$.

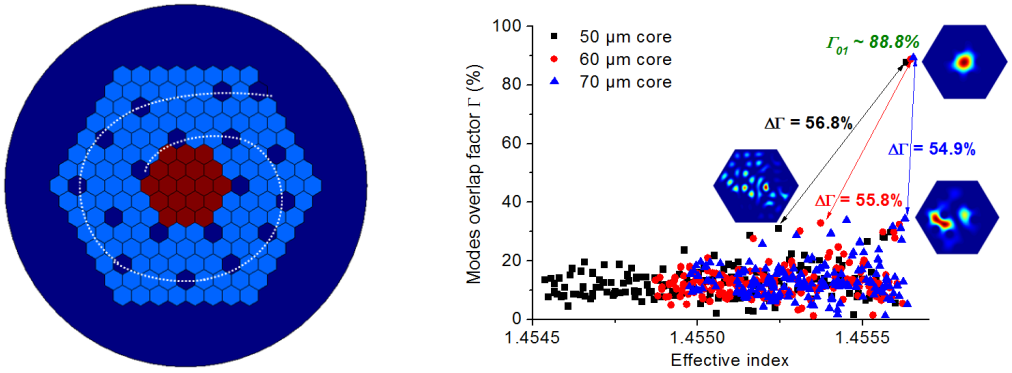


(a) (b)

**Figure 3.25:** (a) Cross sectional representation of a Spiral LPF: the gain region is in red, the clear blue region stand for the passive index-matched material and pure silica is depicted in navy. (b) Overlap factor of the first 300 guided modes into the Spiral LPF whose the core diameter across inclusions is: 50, 60 and 70 $\mu$m. The intensity distribution of the FM and the two most disturbing HOMs are reported in insets.

The modification of the inner cladding microstructuration, and in particular the position of inclusions in vicinity of the gain region, impacts obviously the mode leakage and thereby, the fundamental mode confinement. In this Spiral LPF, the

FM overlap factor does not exceed $\Gamma_{01} = 88.8\%$, like in the all-solid LPF (see Fig. 3.25(b)). So the linear gain is consistently lowered compared to above mentioned HSF$_x$ fibers for instance: $\Gamma_{01} = 96\%$. One can observe in inset of Fig. 3.25(b) a slight deformation of the FM intensity distribution. However, this fiber structure demonstrates a modal distribution larger than that of all-solid fibers discussed in this report and state-of-the-art air/silica LPFs: $\Delta\Gamma = 56.8\%$ for a 50 $\mu$m core. This evidences an efficient delocalization of HOMs through an integral suppression of the structure symmetry: neither the whole inner cladding microstructuration, nor individual inclusions are symmetric referring to the core center. Thus, the inner cladding can no longer sustain symmetric modes. The modal discrimination is here limited by the leaky LP$_{11}$ mode and a pure inner cladding mode (bottom insets of Fig. 3.25(b)). It is also worth noting a weak increase of the HOMs overlap factor for a 60 and then 70 $\mu$m core, denoting the robustness of this fiber design.

Then, I achieved a complementary investigation by extending the dimensions of the leaky region. Although it was addressed in our guidelines a limitation of the requested material volume, this study mainly intends to validate the relevance and

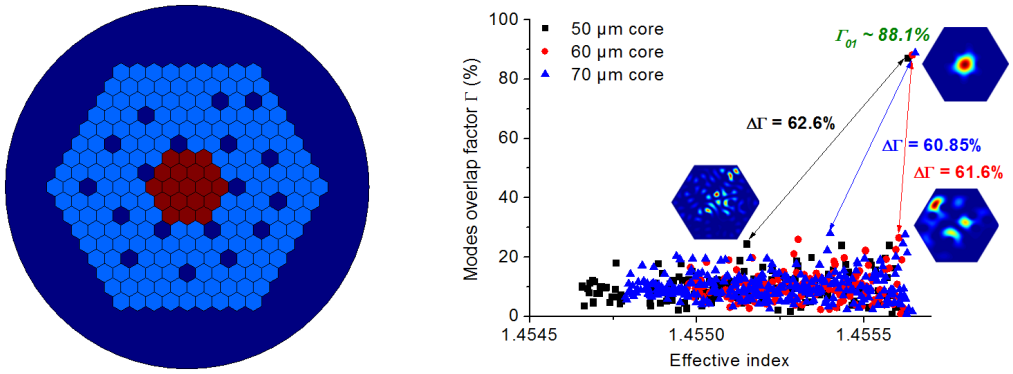


(a) (b)

**Figure 3.26:** (a) Transverse RI distribution of the extended Spiral LPF: one layer of passive high-index rods has been added to the microstructuration. (b) Overlap factor of the first 300 guided modes into the extended Spiral LPF whose the core diameter is: 50, 60 and 70 $\mu$m from flat to flat of the gain region. The intensity distribution of the FM and the two most disturbing HOMs are reported in insets.

robustness of this fiber structure. As depicted in Fig. 3.26(a), the position of pure silica inclusions is kept identical and one layer of passive high-index rods is added to extend the dimensions of the leaky region. Thus, pure cladding modes, as well as leaky core mode, spread farther the fiber core and should be more efficiently discriminated than previously. This is evidenced in Fig. 3.26(b) through another increase of the modal discrimination, exceeding now 60%, whereas the FM undergoes only a really small reduction of its confinement with the gain region ($\Gamma_{01} = 88.1\%$). The most competitive HOMs remain quiet similar to those observed previously. Then, the modal discrimination of these two Spiral LPFs was investigated up to 100 $\mu$m in core size and compared to the $HSF_5$ fibers (Fig. 3.27).

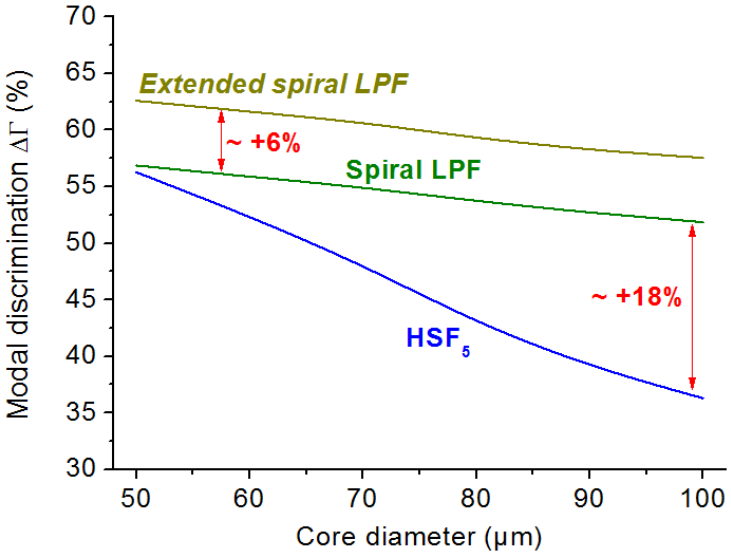


**Figure 3.27:** Comparison of the modal discrimination into the $HSF_5$ fiber, reported as a reference, and the Spiral fibers for core dimensions spanning from 50 to 100 $\mu$m.

The main advantage of these Spiral LPFs relies on the slow reduction of their modal discrimination when the fiber dimensions are homogeneously enlarged. This demonstrates an inherent and efficient delocalization of the HOMs out of the gain region. To the contrary, it has been highlighted earlier that fiber structures based on a periodic array of inclusions are heavily disturbed by the strongly resonant $LP_{31}$ mode. In particular, the modal discrimination of the $HSF_5$ fibers is drastically

weakened when the fiber dimensions increase. Here, the geometry of the Spiral LPF does not allowed to sustain $LP_{31}$-like mode(s). Thus, their performances appears more robust: $\Delta\Gamma = \ > 50\%$ for $D_{core} < 115$ $\mu$m. The reduction of the modal discrimination is only due to the enlargement of the fiber dimensions, inherently providing to the fiber core a higher ability to guide modes. These fibers represent the outcome of our theoretical work as they exhibit an incomparably strong and robust modal discrimination.

#### 3.4.7.2 Spectral tendency

Moreover, I have quantify the variation of the modal discrimination over the wavelength range of the main rare-earth ions (from 400 to 2200 nm). This study, led on 50 $\mu$m core structures, is reported below. Over the whole range of investigation, these designs should provide a robust singlemode emission as their modal discrimination exceeds 45%. It is worth noting that the Spiral LPF appears more stable than the extended Spiral LPF. Indeed, the modal discrimination is relatively constant from 1 to 2 $\mu$m. Moreover, although the extended Spiral LPF has demonstrated the best performances below 1.4 $\mu$m, its modal discrimination is clearly impacted

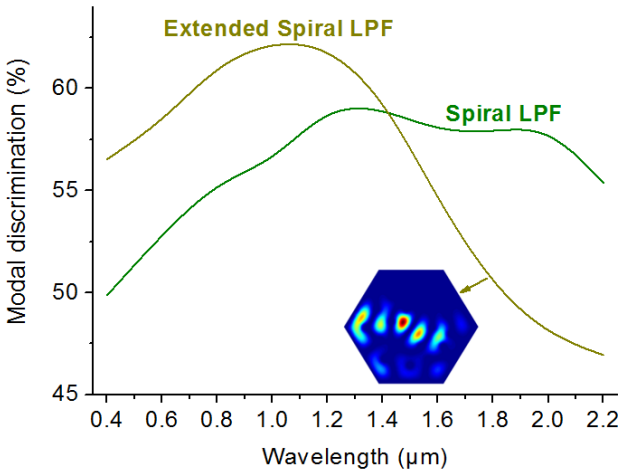


**Figure 3.28:** Spectral evolution of the modal discrimination in 50 $\mu$m core Spiral LPFs for a RI contrast of $\Delta n = 6 \cdot 10^{-3}$. In inset: intensity distribution of the most disturbing mode in the extended spiral LPF.

by a $LP_{12}$-like modes for a wavelength larger than 1.1 $\mu$m. Thus, the interest of an additional layer of passive rods is not so significant and must be considered with clear-sightedness, depending on application. For larger core sizes, the evolution of the modal discrimination is only red-shifted proportionally to the dimensions increase. Here, the performances of these fibers under curvatures are not discussed as there is no noticeable statement.

#### 3.4.7.3 Tolerance to an index mismatch

Finally, I checked the manufacturing feasibility of these fibers by determining their tolerance to an index mismatch between active and passive high index regions. This study was led on the two Spiral LPFs presented in this section. First, the evolution of the fundamental mode confinement and the modal discrimination were computed for two dimensions of the Spiral LPF (30 and 50 $\mu$m core). In Fig. 3.29(a), one can observe a larger tolerance of this fiber structure to an index mismatch compared to previously discussed 50 $\mu$m core all-solid fibers, in particular the $HSF_x$ fibers. Here, the tolerance reaches $\approx 1.2 \cdot 10^{-4}$ (from $-4 \cdot 10^{-5}$ to $8 \cdot 10^{-5}$). However, in a 50 $\mu$m core Spiral LPF, two successive avoided crossings are noticed on the fundamental mode for index depressions of the gain region larger than $-4 \cdot 10^{-5}$, strongly impacting its mode field distribution. So to fight against these impairments, I choose to increase the difference in effective indices between the fundamental mode and the two cladding modes implied on the avoided crossing. For this, a reduction of the fiber dimensions is achieved to reduce the size of the inner cladding regions where cladding mode having an effective index close to that of the fundamental mode are localized. Thus, their effective indices are largely modified. In the 30 $\mu$m core Spiral LPF, it is worth noting an absence of avoided crossings on the FM, offering a tolerance to an index mismatch at least 2 times larger. Indeed, the tolerance exceeds now $2.7 \cdot 10^{-4}$. This significant improvement of the tolerance is beneficial and match the precision of the RI control achievable on optical fiber.

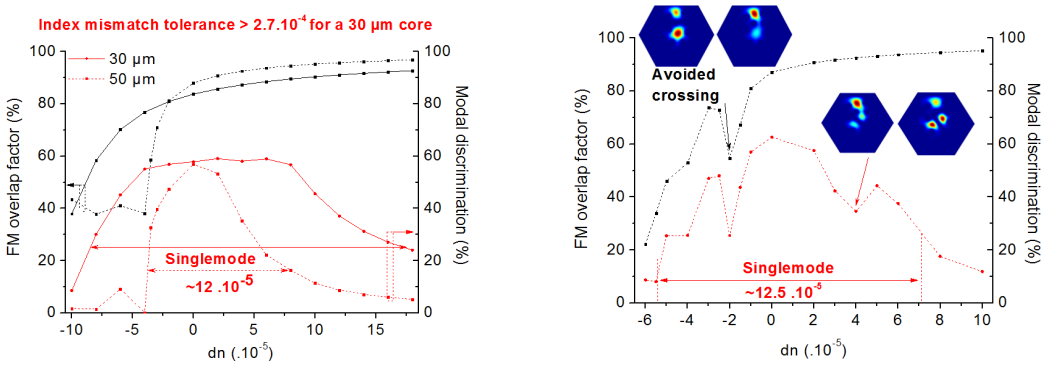


(a) (b)

**Figure 3.29:** Evolution of the fundamental mode overlap factor (black curves) and the modal discrimination (red curves) in (a) a Spiral fiber and (b) an extended spiral fiber. Solid lines refers to a 30 $\mu$m core whereas dashed one are related to a 50 $\mu$m core.

Furthermore, I also checked the influence of an index mismatch on a 50 $\mu$m extended spiral LPF (see Fig. 3.29(b)). Here, only one avoided crossing is noted on the fundamental mode. Nevertheless, it occurs for a particular value of index mismatch: $\mathrm{dn} = 2 \cdot 10^{-5}$. Thus, it is not consider as a limiting factor to delimit the range of singlemodedness. With the achievement of laser simulations, a tolerance of $1.25 \cdot 10^{-5}$ has been computed. This value agrees with that obtained in the Spiral fiber. Thus, the latter is our optimal solution as the volume of material required is mitigated while maintaining a large modal discrimination.

## 3.5 Conclusion

Throughout this chapter, the design of novel kinds of microstructured optical fibers aiming to increase the modal discrimination has been achieved. First, a transposition of the air/silica LPF concept to an all-solid structure has been realized and has allowed to demonstrate that all-solid LPFs exhibit a relatively low modal discrimination (around 28%). However, they represent a real manufacturing challenge as their tolerance to an index mismatching is quite low: $5 \cdot 10^{-5}$. Hence, several improvements of this design has been proposed in order to efficiently delocalize the

HOMs out of the gain region: 1/ breaking the fiber symmetry to avoid symmetric resonances and weaken the disturbing HOM and 2/ benefit from a favourable avoided crossing on HOMs. First, I have proposed the Vortex fiber on which no reflection plane exists. This fiber has enabled to enhance the modal discrimination at least up to 45.8% in a fully doped 50 $\mu$m core and to partially relieved the tolerance on the index mismatching: $\approx 8 \cdot 10^{-5}$. Then, symmetry free fibers based on a hexagonal periodic lattice have been devised to favour the discrimination of the $LP_{31}$-like mode in particular, which is the most disturbing mode in the previous structure. This evolution of the inner cladding microstructuration has permit to reach outstanding modal discriminations in the vicinity of 55% at 1 $\mu$m, surpassing the performances of the current air/silica LPFs, and increasing the tolerance to an index mismatching: $8 \cdot 10^{-5}$ compared to partially doped air/silica LPFs. Finally, a suppression of the inner cladding periodicity was achieved to enhance the degree of asymmetry. This has led to the development of the Spiral LPF which, once again, has overcame the performances of both the state-of-the-art air/silica fibers but also our previously proposed all-solid LPFs. This fiber design provides an impressive modal discrimination exceeding 50% (up to 62% for some particular operating points) for core diameter ranging from 50 to 100 $\mu$m at least and over the emission bands of the main rare-earth ions (from 400 to 2200 nm). This should ensure a robust singlemode. Moreover, I demonstrated a slight enhancement of the tolerance to index mismatch of the gain region, reaching $1.2 \cdot 10^{-4}$. Going further, a route has been proposed to reduce the sensitivity of leaky fibers to an index mismatch. Thus, the fabrication of all-solid LPFs exhibiting a RE-doped area extended to the whole core region should therefore be achievable and will be presented in the next chapter.

Chapter 4

# Fabrication and characterization of all solid microstructured fibers

Contents



Simultaneously to the theoretical study done on the optimization of the inner cladding microstructuration, some all-solid fibers have been manufactured to 1/ prove their feasibility, 2/ confirm the relevance of the selected manufacturing process, 3/ highlight potential manufacturing limiting aspects and 4/ demonstrate the optical performances of all-solid microstructured fibers. In this purpose, I will first evoke published results about the optical properties of optical fibers made by sintering and vitrification of doped powder (so-called Repusil process). Then, these characteristics will be confirmed on a highly-doped step-index fiber whose the core is destined to be use on our all-solid microstructured fibers. In this way, we aimed to quantify the attenuation/ absorption of the core material, but also its laser efficiency.

## 4.1 Performances of optical fibers made of Repusil material

Here, both core and cladding materials are manufactured by resorting to the sintering and vitrification of doped-silica powders known as Repusil process. This technique was selected because of its potential to withstand high pump powers and provide large volume of heavily doped silica glass (rods of 15 mm in diameter and 150 mm in length typically), whose the RI distribution is rigorously homogeneous and can be finely controlled (good predictability). Moreover, it enables a high batch-to-batch reproducibility.

Up to date, few publications report on the use of this method. Nevertheless, the outstanding properties of Repusil-made materials have been highlighted. The first demonstration was achieved by Langner *et al.* on an Ultra Large Mode Area fiber whose the core diameter was 150 $\mu$m [Langner08]. The latter was doped with a relatively high $Yb_2O_3$ concentration (0.25 mol%), and $Al_2O_3$ ions were inserted (1.5 mol%) to reduce the clustering of rare-earth ions, resulting in a RI of approximatively $4.75 \cdot 10^{-3}$ larger than the pure silica. Moreover, a fluorine-doped layer was deposited by POD (Plasma Outside Deposition), providing a NA of about 0.25. Despite the large RE concentration, very low background losses have been obtained ($\approx$ 20 dB/km at 1200 nm). Authors demonstrated that such material can sustain operation in a high power regime (up to 1.5 kW of pump power). Furthermore, it has been shown that 50 $\mu$m Repusil-made material can withstand up to 7 kW of pump power at 976 nm and provide 4 kW of emitted power without damage the fiber end facets [Langner12].

Additional experiments have been done to demonstrate in particular the laser efficiency on a double-clad 13 $\mu$m core step-index fiber [Leich11]. The fiber core composition was slightly different than for the former work: 0.2 mol% of $Yb_2O_3$ and 1.5 mol% of $Al_2O_3$. Here, the core is surrounded by a non-circular silica clad, covered by a fluorine-doped double clad deposited by POD. First, an excellent ho-

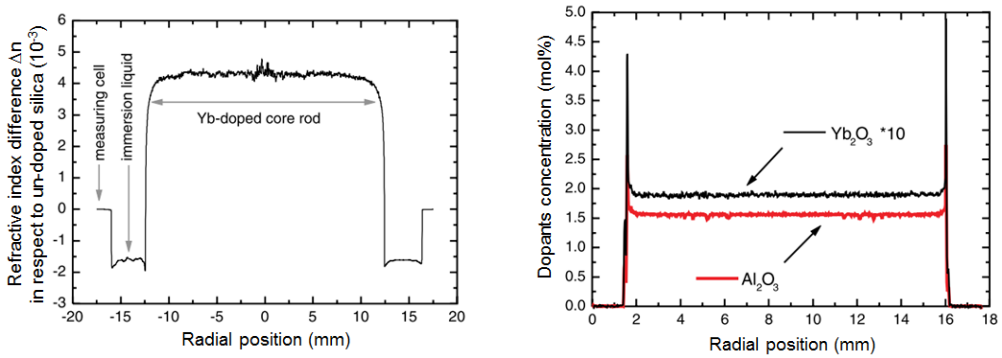


(a) (b)

**Figure 4.1:** (a) Measured RI profile and (b) electron microprobe analysis of the Yb/Al contents in the Yb-doped core rod used in [Leich11].

mogeneity of the material RI (Fig. 4.1(a)) as well as a uniform distribution of the dopants (Fig. 4.1(b)) were evidenced. These measurements were mainly limited by the precision of the preform RI analyzer ($4 \cdot 10^{-4}$). Then, a simple laser cavity was realized using a Fabry-Pérot resonator composed of a highly reflecting dichroïc mirror at the lasing wavelength and 0° cleaved fiber end facet (Fresnel reflection: 4%). A laser efficiency as high as 80% was reported for pump power reaching 230 W at 976 nm, highlighting the interest of this manufacturing process for high power fiber laser applications.

To complete this set of favourable properties for the development of fiber lasers,

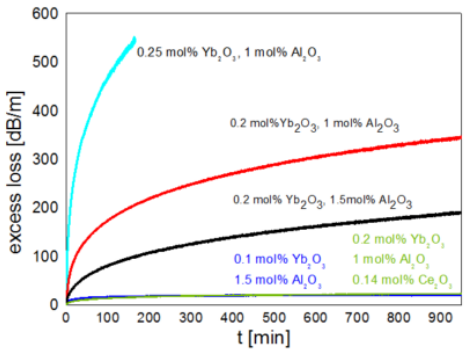


**Figure 4.2:** Temporal evolution of the photodarkening induced losses at 633 nm measured on 13 $\mu$m core fibers presenting different composition for core material [Langner12].

a synthetic study was led on the influence of the photodarkening induced losses at 633 nm [Langner12]. Several 13 $\mu$m core step-index fibers exhibiting different core compositions have been prepared. Thus, it was highlighted that significant photodarkening induced losses appears especially when the Yb concentration exceeds 0.1 mol%. However, this phenomenon was mitigated by introducing cerium ions in highly Yb-doped fiber (Fig. 4.2, green curve). Moreover, one can observe that an increase of the Al content contributes to slightly limit the darkening induced losses.

To summarize, the sintering and vitrification of doped-powders allows to benefit from:

- Low background losses: $\approx$ 20-50 dB/km,
- A high optical efficiency (80%),
- Operation in high power regime: several kW without fiber damages as end faces breaking or core melting for instance),
- High doping levels (for instance, up to 0.25 mol% of $Yb_2O_3$),
- An excellent material homogeneity as well as a uniform doping level, even for large volume of doped material,
- A high batch-to-batch reproducibility.

Due to these outstanding material properties, we have selected this technique for the fabrication of our novel all-solid microstructured fibers in the aim to demonstrate their technical feasibility and potentially reduce drastically the manufacturing cost of high power fiber lasers.

## 4.2 Step-index fiber made of Repusil core material

Despite all previously mentioned outstanding properties, the Repusil process is not controlled at an industrial level and it is necessary to characterize each fabricated

preform. Consequently, a material sample was systematically used to fabricate a test step-index fiber. The core composition was defined to allow a strong pump absorption and a mitigation of the photodarkening (PD) effect. Regarding the results of Fig. 4.2, we opted for the following core material composition:

- 0.2 mol% of $Yb_2O_3$ ions to provide a strong absorption of the pump radiation,
- the addition of $Ce_2O_3$ ions (0.14 mol%) for an efficient mitigation of the PD,
- and 1.5 mol% of $Al_2O_3$ ions to reduce the clustering and finely adjust the RI.

This step-index fiber is composed of a 7.81 $\mu$m circular core surrounded by a low-index cladding achieved by stacking pure silica canes (see Fig. 4.3(a)). Then, the stack has been placed into a silica tube polished after consolidation to get a D-shaped double clad, enhancing the pump absorption. From the material composition and the results provided in [Kirchhof03] on refractive index modifications induced by each dopants, the refractive index contrast in this fiber is expected to be close to $5.83 \cdot 10^{-3}$. It is depicted in Fig.4.3(b) that using this approach, a good refractive index predictability is obtained: $5.8 \cdot 10^{-3}$. However, the RI profiler provides a precision of about $2 \cdot 10^{-4}$.

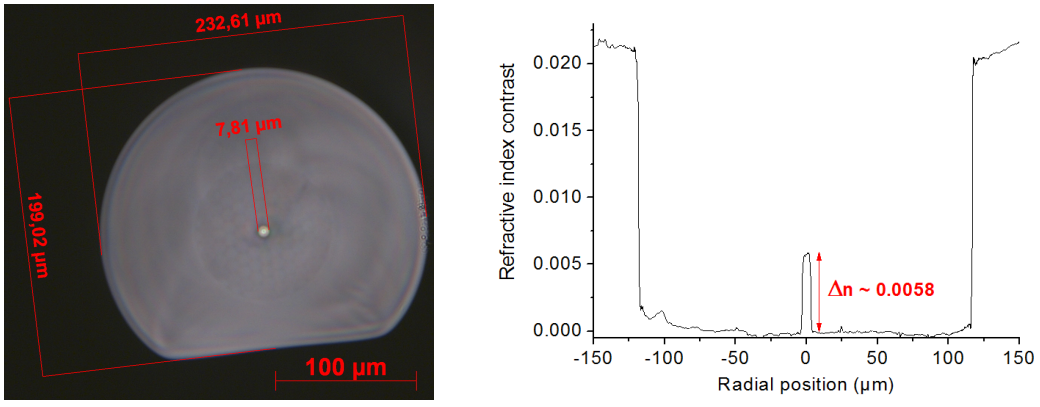


(a) (b)

**Figure 4.3:** (a) Microscope picture and (b) measured refractive index profile of our step-index fiber whose the core is made using the Repusil process.

Initially, this fiber was coated with a high-index polymer, in order to enable only the propagation of the light launched into the fiber core (simple clad structure) and to measure the background losses of the Repusil-made core material. This was achieved using the cut-back technique on a 75 m-long piece of fiber using a halogen white light source. For each fiber length, the transmitted spectrum was collected after several cleaves of the fiber end facet whereas the launching conditions remain unchanged all along this measurement. This ensures that the measured attenuation is free of the cleaves influence, allowing a rigorous definition of the material attenuation. Thus, background losses as low as 44 dB/km were measured at 1200 nm (Fig. 4.4(a)), which is congruent with the relatively low attenuation reported earlier.

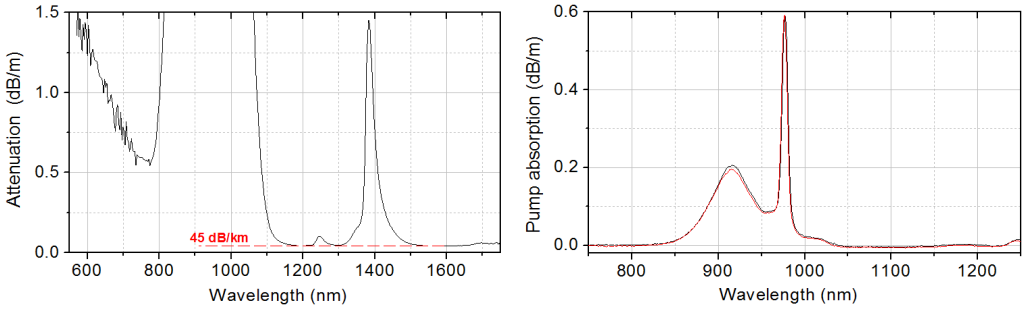


(a) (b)

**Figure 4.4:** (a) Attenuation and (b) absorption spectra of the Repusil-made step-index fiber. On the latter, the measurement is reported for two different 10 m-long samples.

Then, a second fiber sample has been drawn with a low-index polymer, acting as a double-clad and allowing a cladding pumping. The cut-back method was employed once again to define the fiber absorption (Fig. 4.4(b)). The small core to clad ratio of this fiber implies inherently a low fiber absorption ($\approx$ 0.2 dB/m at 917 nm and $\approx$ 0.6 dB/m at 976 nm). Furthermore, the absorption of the core material can be estimated using the ratio between the core and clad areas: approximatively 175 and 525 dB/m at respectively 917 nm and 976 nm. These results are almost in agreement with the material absorption of standard LMA fiber. Nevertheless, we

can expect to get a fiber absorption two times larger to that of standard air-silica LPFs (around 24 dB/m in a 50 $\mu$m core air/silica LPF [Baumgartl11]). Indeed, only 40 to 55% of the whole core area is actively doped in state-of-the-art LPF.

To go further in the investigation on the optical properties of the core material, the laser efficiency of the double-clad step-index fiber was determined using the simple laser setup depicted in Fig. 4.5(a). The pump radiation from a 25 W pigtailed multimode laser diode is collimated and focused by two lenses to properly launch it into the fiber cladding. The laser cavity is composed of two reflectors: the 0° fiber end facet (Fresnel reflection: R = 4%) and a dichroïc mirror $M_2$ (high reflectivity: 99.9% at 0°) to enable multiple round-trips of the laser radiation. Finally, a second highly reflecting dichroïc mirror ($M_1$) was used at 22.5° to extract the laser radiation. By this way, a laser efficiency exceeding $\eta$ = 75.1% was obtained with a 10 m-long fiber (Fig. 4.5(b)).

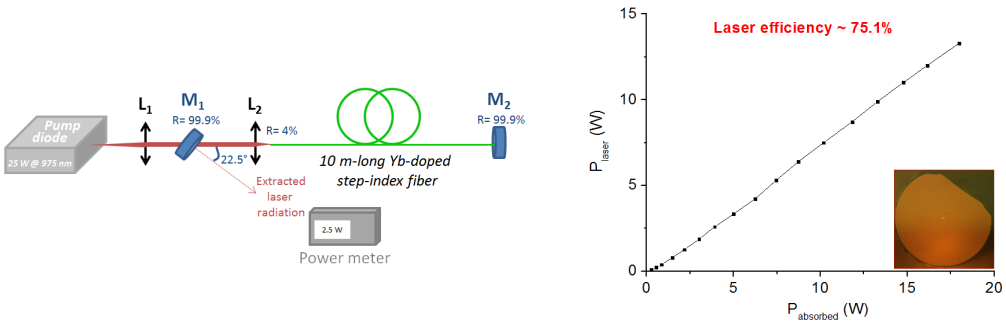


(a) (b)

**Figure 4.5:** (a) Schematic representation of the laser setup: two lenses (resp. $L_1$ and $L_2$) for the collimation and focusing of the pump beam and two dichroïc mirrors operating around the laser wavelength: $M_1$ allowing the extraction of the laser radiation and $M_2$ forming the laser cavity with the 0° cleaved fiber end facet. (b) Measured laser power versus absorbed power for the Repusil-made step-index fiber.

Briefly, results obtained in this section (attenuation, absorption and optical efficiency) are congruent with those reported in [Langner12, Leich11] and confirm the relevance of this manufacturing process for the fabrication of low-loss efficient material. Hereafter, all-solid fibers based on this manufacturing process are presented.

## 4.3 Fabrication of an All-Solid Large Pitch Fiber

For the first fabrication run, we opted for a direct transposition of the well-known air/silica LPF design into an all-solid structure. This structure is the simplest among those proposed and therefore its production can highlight potential problems with the manufacturing step. During the material preparation, a special care has been carried on the importance of a very good index matching between the core and cladding materials. In particular, the RI profiles of the material preforms were checked before stacking. However, the measurement accuracy (in the range of $10^{-4}$) is not sufficient to ensure that a perfect matching of the refractive indices is reached.

The fiber core was partially doped to reduce the required amount of Yb-doped material and more clearly identify the impact of the selective amplification on the mode field distribution. Thus, only the 7 central cells composing the fiber core were doped with ytterbium ions. For this first test, we used available b-doped material and the core composition was slightly different from that of the step-index fiber discussed above, lowering the material absorption and limiting the refractive index contrast with the silica inclusions to $4.12 \cdot 10^{-3}$ theoretically. The control of the RI contrast on a step-index fiber composed of the same core material has confirm the relatively good RI predictability ($\Delta n = 4.2 \cdot 10^{-3}$).

Moreover, two layers of pure silica rods were placed around the leaky region to extend the dimensions of the inner cladding. The pump cladding made of a fluorine layer provides a moderate NA of 0.265 but should results in an efficient fiber pumping. This layer contributes to get an all-solid fiber structure (Fig. 4.6). Aiming to achieve a rod-type fiber because of the strong sensitivity of leaky fibers to bending, the preform was first drawn into 3.35 mm canes (Fig. 4.6(a)).

Unfortunately, one can observe that the fluorine layer has caused the appearance of uncontrolled bubbles during the canes drawing (see Fig. 4.6(a)). It is worth noting that bubbles have been preferentially generated on the corners of the hexagonal stack, so in the region where the mechanical stresses are the largest during

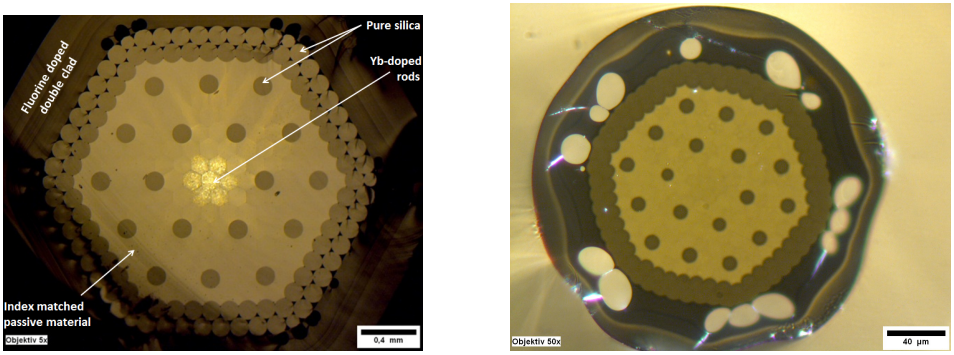


(a) (b)

**Figure 4.6:** Microscope pictures of the 50 $\mu$m core all-solid LPF structure: (a) the cane, (b) the flexible fiber. Only the seven central rods are actively doped.

the drawing. Despite this point, we have used some canes to prepare rod-type and flexible fibers for RI measurements. Whatever the drawing parameters and the preform preparation, bubbles have been expanded, resulting in a total and uncontrolled deformation of the fiber shape(Fig. 4.6(b)). As bubbles are still present and erratic, they disturb the optical properties of the optical fiber by inducing micro-bending and deformations on the fiber core and its environment. To avoid this perturbation on our future fibers and evidence the modal properties of the fiber core, the fluorine layer was then replaced by an air-clad structure. Additional works should be achieved in the future to make possible the use of a fluorine layer as pump cladding. Furthermore, silica inclusions have kept their circular shape during the drawing because of their lower viscosity compared to doped materials. Nevertheless, this does not rule out the relevance of my numerical work as I numerically checked the weak impact of the inclusions shape on the modes leakage.

As the rod-type fiber is strongly deformed, optical characterizations were focused on the flexible fiber. The fiber core size is 47 $\mu$m (peak to peak) and the dimensions of the inner clad are 125*145 $\mu$m. I first checked the optical properties of the material by measuring the attenuation and absorption (Fig. 4.7). For this, I used the cut-back procedure. Background losses as low as 18 dB/km at 1200 nm have

thus been measured. Moreover, the measured fiber absorption around 915 nm was 4.4 dB/m, so the absorption at 975 nm should be in the vicinity of 15 dB/m, which is lower than that of standard air/silica LPF ($\approx$ 25 dB/m).

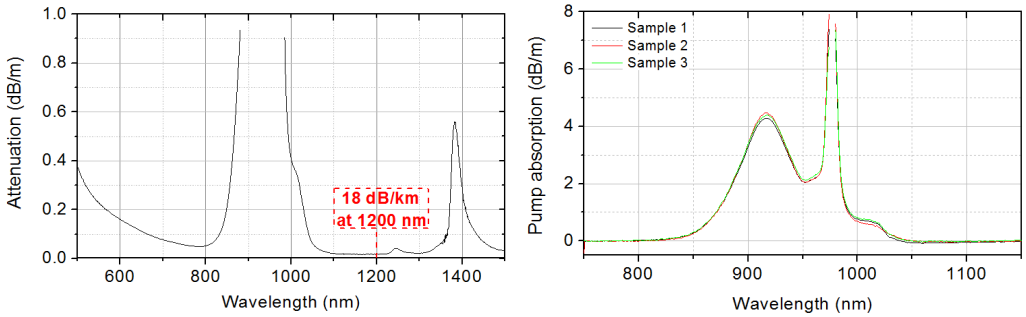


(a) (b)

**Figure 4.7:** (a) Attenuation and (b) absorption spectra of the all-solid LPF with conventional distribution of low-index inclusions. On the latter, the measure is reported for three different samples.

Then, the all-solid LPF was characterized in a laser configuration. The Fabry-Pérot resonator was composed of the input fiber end facet (Fresnel reflection) and a 99.9% dichroïc mirror (butt-joint with the fiber output end facet), totally reflecting the laser radiation (see Fig. 4.8(a)). Two f = 8 mm lenses were also used to couple efficiently the pump radiation into the fiber cladding. In facts, the focal lengths of the collimating and focusing lenses (resp. $L_1$ and $L_2$) are defined such as the pump beam exhibit an identical or lower etendue than the fiber cladding, it means the product between the spot size and the numerical aperture. Several lengths of fiber have been used in this experiment. Intensity distributions collected at the laser output using a 5.3 m-long fiber are depicted in Fig. 4.8(b). First, it is worth noting that the ASE is not well confined into the fiber core but rather spreads largely into the inner cladding. Then, a laser effect was obtained. Unfortunately, the emitted radiation appears delocalized into the cladding. Moreover, no intensity maximum was overlapping the gain region, letting think that the fundamental Gaussian mode is no longer confined into the fiber core. I obtained the intensity distributions

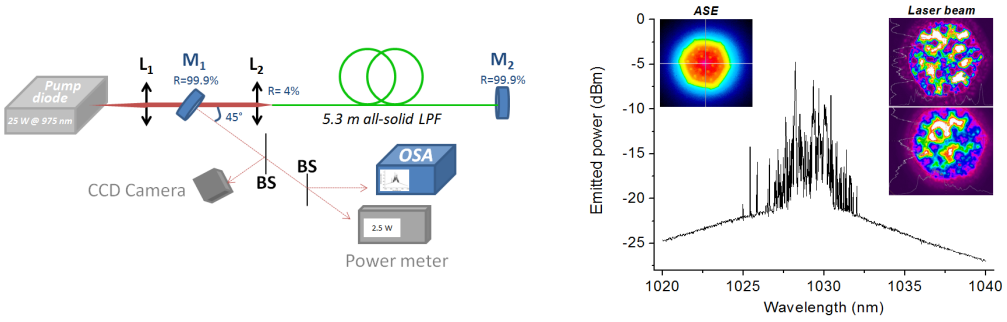


(a) (b)

**Figure 4.8:** (a) Schematic representation of the laser set-up with 0° cleaved fiber end facets. Beam splitters (BS) are used to collect the emitted spectrum with an OSA (Optical Spectrum Analyzer), to observe the mode intensity distribution on a CCD camera and to measure the emitted power. (b) Measured spectrum of the emitted laser beam. Insets: images of the intensity distributions for the Amplified Spontaneous Emission (left) and laser beam (rights).

depicted in the bottom inset of Fig. 4.8(b). Here, one can attribute intuitively the low quality of the emitted beam to two phenomena: i/ curvatures occurring along the fiber length and contributing to drift modes out of the gain region and/or ii/ a potential index depression of the Yb-doped rods compared to the passively doped material that acts as an anti-waveguide. Thus, a shorter piece of fiber was placed into a capillary to hold it straight and to limit the macro-bendings. No significant improvement of the beam quality was noticed.

Going further, complementary works were done within the company Eolite systems on a 1.4 m-long piece of fiber maintained straight by placing it on a holder. The laser cavity was this time composed of two dichroïc mirrors, one totally reflecting the laser radiation (high reflectivity: 99.9%) whereas the second allows a partial extraction of the power (reflectivity: 90%) to provide a strong feedback and act on the gain (Fig. 4.9(a)). The fiber end facets were locally melted, inducing the collapsing of the bubbles, and then angle-cleaved (AC) at 5° to avoid parasitic lasing effect on the fiber facets which were then imaged on the two dichroïc mirrors using the additional lenses $L_3$ and $L_4$.

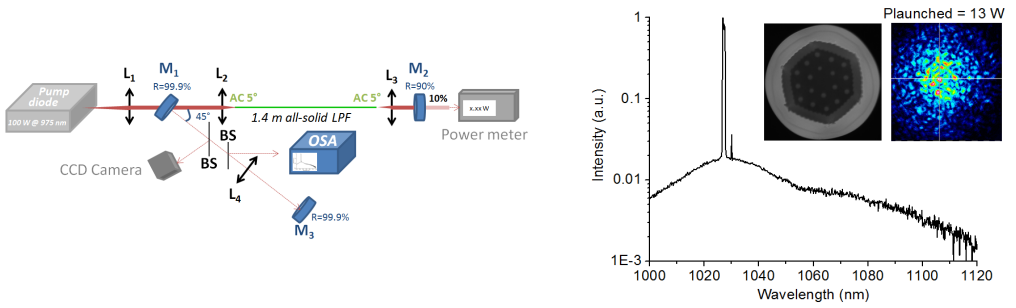


(a) (b)

**Figure 4.9:** (a) Schematic representation of the laser set-up: $M_1$ and $M_2$ are dichroïc mirrors allowing respectively a partial extraction (10%) and a total reflection of the laser radiation. (b) Measured spectrum of the emitted laser beam. Insets: microscope image of a fiber end face after fusion-cleaving (left) and intensity distribution of the emitted beam (right).

A laser effect was obtained in this configuration on a relatively narrow spectral band centered around 1027 nm (Fig. 4.9(b)). However, a multimode behaviour was clearly evidenced at low pump power by seeing the intensity repartition of the emitted beam (inset of Fig. 4.9(b)). The emitted beam exhibits a speckle pattern. Hence, the influence of the pump power rise on it has been observed. In Fig. 4.10, the intensity repartitions for three levels of launched power are reported. One can note that the laser beam distribution appears to be more and more confined into the gain region when the launched power increases.

Following this study, another all-solid microstructured fiber has been recently

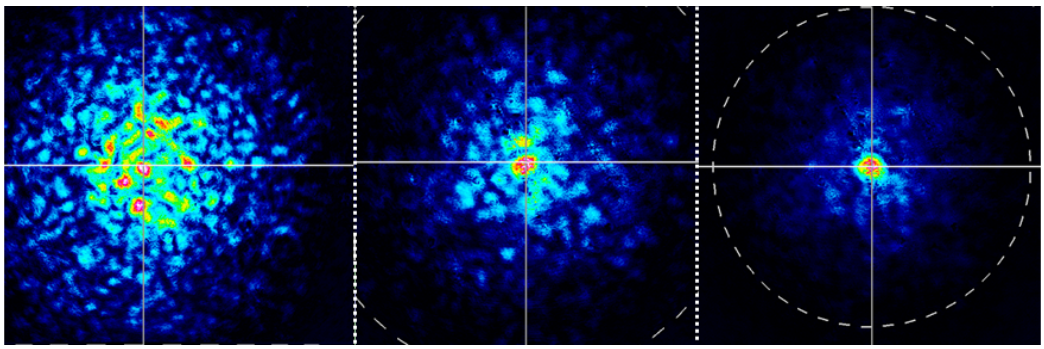

**Figure 4.10:** Intensity distributions of the emitted laser beam for three levels of launched power: 13 W (on the left side), 25 W (in the middle) and 31 W (on the right side).

manufactured. First, an air-clad structure was developed to replace the fluorine layer as pump cladding and avoiding thus the deformation of the inner cladding region during the drawing of a rod-type fiber.

## 4.4 Preparation of an air-clad jacket

In order to devise an air-clad structure providing a significant NA for the pump radiation, our approach was based on the theoretical investigation led by Issa *et al.* [Issa04]. In this article, the dependency of the NA to the fiber length L, the silica bridges width '$\delta$' and their length 'w' was described. Referring to this work, a NA larger than 0.5 should be achievable if the silica bridges are thinner than 0.6*$\lambda$ whereas their length should exceed 2*$\lambda$ at least ($\lambda$ being the operating wavelength). Up to now, the highest NA was reported by Wadsworth *et al.* : 0.8 [Wadsworth03]. In this Yb-doped PCF, the silica bridges measure 350 nm in thickness and 13 $\mu$m in length.

From these results, we initiated the realization of air-clad canes in which the microstructured preform may be inserted. Their development was led in several steps using three thin wall tubes:

1. The first was used to constitute the outer layer of the air-clad canes (inner/outer diameter: 26/28 mm).

2. A second was drawn into 1 mm capillaries to compose the air-clad structuration.

3. The last one was adjusted by our colleague Claudia Aichele (IPHT, Jena) on a MCVD lathe to fit the inner dimensions of the air-clad preform.

4. Finally, tubes and capillaries were stacked together and drawn into canes by applying vacuum into interstitial air holes, enabling their collapsing (see Fig. 4.11(a)).

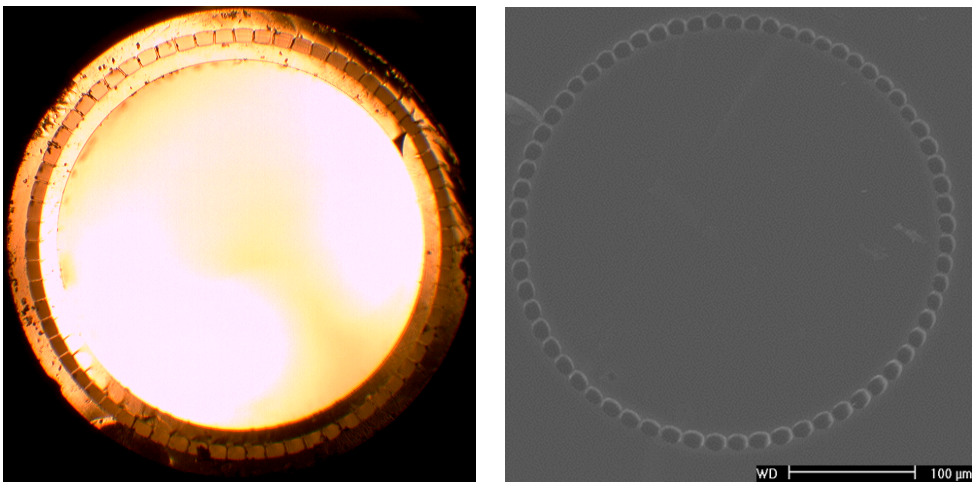


(a) (b)

**Figure 4.11:** (a) Image of the air-clad cane cross-section and (b) scanning electron microscope image of the passive rod-type fiber made in our laboratory.

Hence, an air-clad cane was filled with a pure silica rod and surrounds with a thick silica tube (inner/outer diameter: 3/15 mm) in order to get a rod-type fiber for the measurement of the NA. Fig. 4.11(b) depicts the cross-section of the manufactured passive fiber. During the fiber drawing, different levels of pressure were applied in the air holes to control their dimensions and the thickness of the silica bridges. Thus, we obtained silica bridges as thin as 390 nm for a pressure of 15 mbar, providing a NA reaching 0.55. The success of this fabrication demonstrates our ability to manufacture subsequently rod-type structures in which the pump radiation will be efficiently coupled. The 250 $\mu$m inner diameter of the air-clad perfectly matches our expectations as it allows an efficient coupling of our 400 W pump diode which is pigtailed on a 400 $\mu$m (NA = 0.22) multimodal fiber: the etendue of the beam is constant.

## 4.5 Hexagonal symmetry free fiber: $HSF_5$

Recently, a second all-solid microstructured fiber has been fabricated. At the beginning of this fabrication run, the numerical study on the inner cladding microstructuration defined the "$HSF_5$" (Hexagonal Symmetry Free fiber 5) as the most relevant solution to get a robust singlemode emission, explaining by the way the chosen design. Indeed, this fiber exhibits a large modal discrimination (56.2% for a 50 $\mu$m core at 1 $\mu$m) and a relatively good tolerance to an index mismatch ($7.5 \cdot 10^{-5}$). Unlike the all-solid LPF presented earlier, the fiber core was fully doped with ytterbium ions to benefit from the outstanding modal discrimination of this fiber structure. The cross-sections of the preform stack, the cane and the fiber are reported in Fig. 4.12. One can observe that the inner clad structuration and the pump cladding have not been deformed here. The fiber was drawn for two different core dimensions in order to evidence the impact on the intensity distribution. Up to now, the characterizations of this fiber were led in collaboration with Aurélien Benoit on fiber samples whose the transverse dimensions are: 44.2 $\mu$m for the core across inclusions, 133 $\mu$m across flat for the leaky region, and 238 $\mu$m for the air-clad. Tests on the 50.4 $\mu$m core fiber are now under progress. The fiber core exhibits a composition close to that

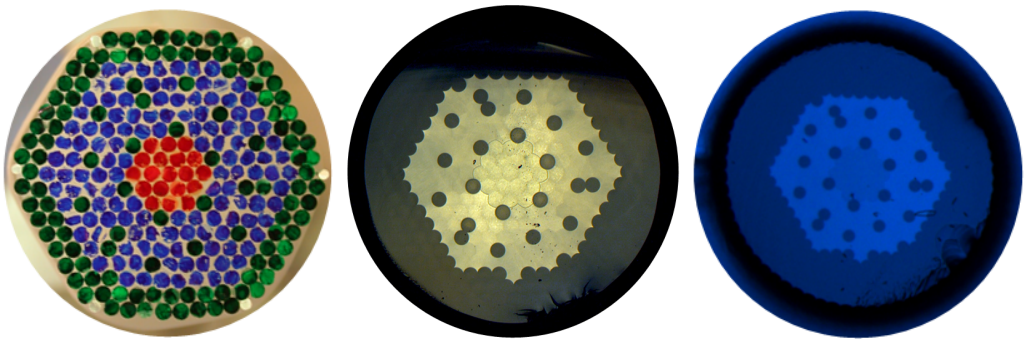

(a) (b) (c)

**Figure 4.12:** (a) Cross section of the preform stack w(Yb-doped rods in red, the passive ones in blue and the pure silica in green). (b-c) Microscope images of the cane and fiber cross-sections.

of the step-index fiber studied earlier: 0.15 mol% of $Yb_2O_3$, 0.11 mol% of $Ce_2O_3$ and 1.5 mol% of $Al_2O_3$. So the fiber absorption is expected to be in the vicinity of 20 dB/m, as for conventional PCFs or LPFs.

In order to characterize this fiber in a laser and amplifier schemes, we have prepared different lengths of rod-type $HSF_5$ fiber (60, 75 and 90 cms). It means that fiber end facets were first briefly heated using a $CO_2$ laser to collapse locally the air holes composing the air-clad. Then, the end facets were perpendicularly or angle-polished depending on their final use. This fiber preparation is a critical point on rod-type fiber laser/amplifier systems and we benefited from the experience of the company Eolite system to produce clean polished facets. Indeed, the quality of the fiber cleaves influences the optical properties of the emitted beam and can led to inaccurate observations.

Initially, a 60 cm-long piece of rod-type $HSF_5$ fiber was implemented within a laser cavity whose the resonator was composed of one mirror (noted $M_3$ in Fig. 4.13(a)) and a perpendicularly polished (PP) fiber end facet (see Fig. 4.13(a)). Two dichroïc mirrors were added: $M_1$ deviated the laser radiation at 45° towards the mirror $M_3$ whereas $M_2$ filtered the residual pump power (dichroïc mirror oper-

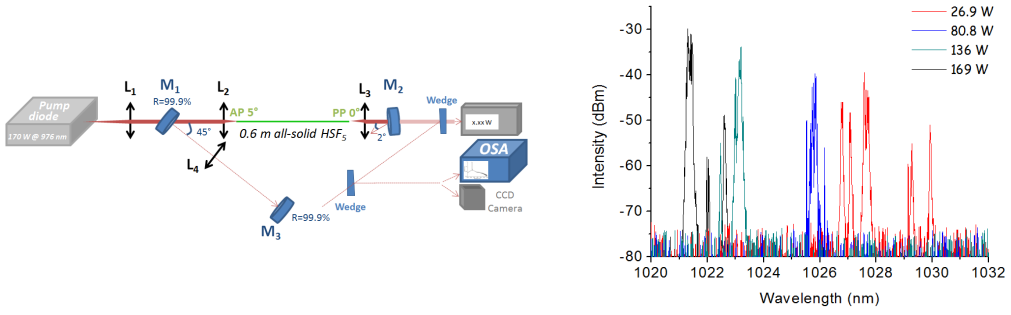


(a) (b)

**Figure 4.13:** (a) Scheme representation of the laser set-up. The laser cavity is composed of a highly reflecting $M_3$ mirror and the perpendicularly polished (PP) fiber end facet. The input end face was angle-polished (AP) at 5° to avoid a parasitic lasing effect. $M_2$ allows to extract the residual pump power and then measure the emitted signal power, spectrum and intensity pattern. (b) Evolution of the emission spectrum for different levels of pump power measured at the output of the pump source.

ating at 0° which is positioned around 2°). Moreover, the lens $L_4$ was employed to ensure the stability of the resonator. The pump source provided up to 170 W at 976 nm and the maximum laser power extracted from the fiber laser was around 53 W. In Fig. 4.13(b), one can note that the central emission wavelength was blue-shifted from 1028 to 1020 nm when the pump power was increased. This can be explained by the relative flatness of the emission cross-section from 1000 to 1030 nm (observed through the ASE spectrum) and by the population rise in the high energy/short wavelength Stark sub-level when the pump power is increased. Hence, the central operating wavelength is drifted to shorter wavelengths. However, the emission cross-section should be measured to confirm this assumption.

Furthermore, the intensity profile of the emitted beam was collected for different levels of pump power in order to check whether a robust singlemode operation is obtained. It was also intended to observe the influence of the pump power increase on the intensity profile through a thermal induced refractive index change for instance. In Fig. 4.14, one can unfortunately notice that the laser beam appears multimode. Although the major part of the intensity is localized into the fiber core, demonstrating the good confinement of the emitted radiation, the intensity distribution is not purely Gaussian. Moreover, the position of the intensity maxima is moving during the power rise due to the multimode behaviour of the emitted beam. Here, the spot size is stable. Additional experiments have been done with longer pieces of fiber but no noticeable improvements have been highlighted.

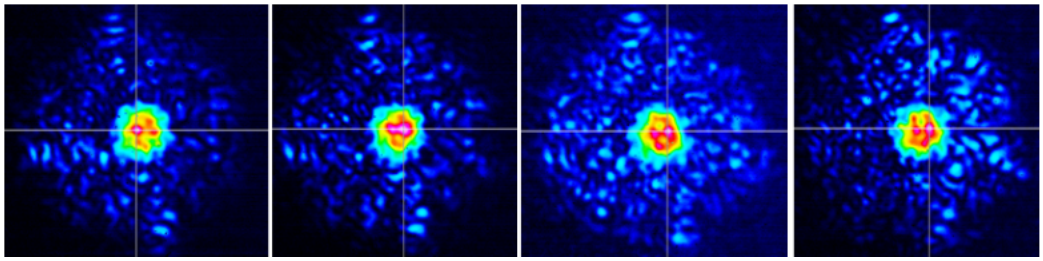

**Figure 4.14:** Intensity distribution of the emitted laser beam for four levels of emitted power: 4.2 W, 21.4 W, 40 W and 52.2 W (from left to right).

To go further and demonstrate an efficient light confinement into the fiber core,

it was decided to launch a beam with a pure Gaussian intensity distribution into the core and observe whether the transmitted beam undergoes spatial distortions. Thus, we achieved few measurements using a 75 cm-long piece of rod-type fiber in an amplification configuration (see Fig. 4.15). A contra-propagative seed beam generated by a mode-locked source emitting 27 ps pulses at 1031 nm was coupled into the fiber core. This beam was adjusted by acting on the lens $L_3$ to fit the core size. Moreover, the co-propagative pump source was the same as previously and the fiber end facets were angle-cleaved at 5° to avoid parasitic lasing.

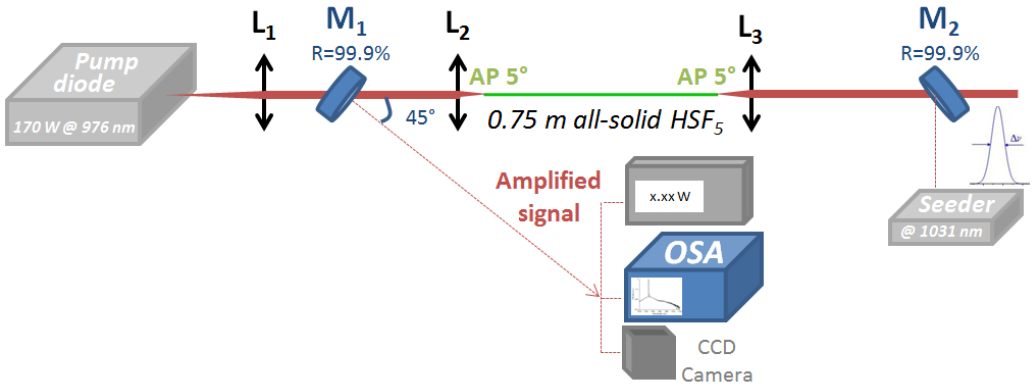


**Figure 4.15:** Schematic representation of the amplifier set-up: the beam generated by the pulsed mode-locked seeder is launched into the fiber core. The co-propagative pump source can provide up to 170 W at 976 nm and fiber end facets are angle-cleaved to avoid parasitic lasing effect.

In this configuration, the fiber characterization was achieved in two steps. First, the pump source was kept off, allowing thus to observe only the influence of the waveguide on the intensity distribution and spectrum (no selective amplification by the gain). These measurements are depicted in Fig. 4.16(a). It is worth noting that the spectrum is not significantly influenced by the propagation through the 0.75 m $HSF_5$ fiber whereas the intensity pattern appears disturbed (see of Fig. 4.16). Indeed, the transmitted intensity is no longer strictly singlemode.

Then, the pump source at 976 nm was used and results are reported in Fig. 4.16(b). One can observe that the amplification of the shorter wavelength is favoured with the increase of the pump power thanks to a good population inver-

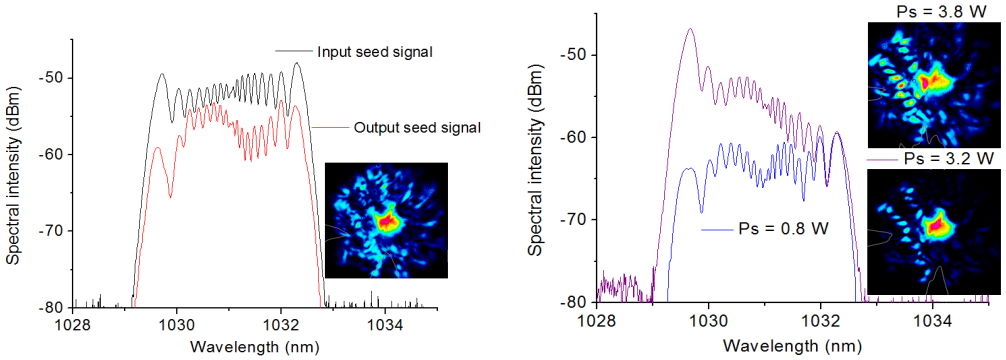


(a) (b)

**Figure 4.16:** (a) Seed signal spectrum before and after propagation through the fiber core without pumping (no amplification). Inset, intensity distribution of the output beam. (b) Evolution of the emission spectrum from 0.8 W (blue curve) to 3.2 W of emitted signal power (purple curve). Insets: Intensity distribution of the amplified seed signal for two levels of emitted signal power: 3.2 W (bottom) and 3.8 W (top).

sion. Unfortunately, we clearly noticed a poor beam quality. The intensity located into the core appears really disturbed and a chain of lobes spread through the leaky region. This should be a consequence of a multimodal confinement induced by an index mismatch between the refractive indices of the active and passive materials. At high level of pump powers, intensity is increased but no noticeable change has been observed on the intensity distribution. For this reason, we plan to realize additional tests on rod-type $HSF_5$ fibers to observe the behaviour of the transmitted beam in the amplifier configuration for different fiber lengths and transverse dimensions (core size in particular).

## 4.6 Discussion

The current status of our experimentations is yet not sufficient to clearly evidence the reasons of the poor beam quality obtained with these all-solid fibers. Nevertheless, one key hurdle remains still under unresolved and must be measured with accuracy: the RI profile. Indeed, it was demonstrated in Chapter 3 that leaky structures exhibit a relatively low tolerance to an index mismatch between the Yb-doped region

and the surrounding passively doped material ($10^{-4}$ to the best). However, the accuracy of the RI measurement methods achieved on fiber structures is commonly in the vicinity of 2-3 $\cdot 10^{-4}$, so larger than what is required in our all-solid fibers to ensure an accurate control of the index matching. Thus, the characterization of material (RI profile and homogeneity) will be a major issue in the pursuit of this work. In this context, it would be useful to devise a set-up enabling a precise measurement of the RI profile. Moreover, from a material point of view, it would provide a deeper understanding of the contribution of each co-dopant, as well as the impact of the manufacturing and drawing conditions, on the refractive index change. This could significantly increase the RI predictability for the Repusil process.

Several works have been done during the last decades to get accurate measurements of the RI profile. Different techniques have been employed, in transmission or in reflection: the minimum deviation method on prismatic sample (accuracy currently in the range of few $10^{-4}$), the critical angle method ($10^{-4} \approx 10^{-5}$) ... To date, an index precision as low as $10^{-5}$ has also been reached using an interferometric approach. Nevertheless, these methods have mainly demonstrated their interest on large sample (preform and prism for instance). For optical fibers, the accuracy seems to be limited around $1 \cdot 10^{-4}$.

Thus, in order to strengthen the reliability of our fabrication procedure, we would like to enhance the accuracy of the RI control on the two preforms which must be index-matched. For this, we intend to take benefit from a recent work done by Choi *et al.* [Choi10] on which a relative RI uncertainty of $10^{-5}$ was reported. This approach is based on an interferometric process. A collimated and monochromatic incident beam stemming from a He-Ne laser for instance is propagated through a preform slice whose the two end facets must be strictly plane and parallel (see Fig. 4.17). As a Fabry-Pérot cavity, the reflections occurring on the two faces of the sample are delayed compared to the directly transmitted beam. Thus, the transmitted intensity $I_{tot}(\theta)$ is influenced by the angle between the incident beam

direction and the normal to the sample surface as follows:

$$I_{tot}(\theta) = I_0 \frac{[1 - R(\theta)]^2}{R^2(\theta) + 1 - 2R(\theta)sin\phi(\theta)} \tag{4.1}$$

where $I_0$ is the intensity of the incident beam, $R(\theta)$ is the reflection coefficient on each face for an angle of incidence $\theta$, and $\phi(\theta)$ is the phase difference between the directly transmitted wave and reflected ones:

$$\phi(\theta) = \frac{4\pi d}{\lambda}\sqrt{n^2 - n_0^2\ sin^2(\theta)} \tag{4.2}$$

Here, d stands for the thickness of the sample, $\lambda$ for the operating wavelength, n is the material RI and $n_0$ that of the air, which has to be defined rigorously with the atmospheric pressure, the temperature and the humidity. Hence, a set of fringe is measured. The position and the number of maxima allow to determine the RI of the sample under test with a precision in the range of $10^{-5}$. In addition, a second laser source, for instance a Distributed FeedBack (DFB) laser diode at 1550 nm, can be implemented to measure finely the sample thickness and increase the precision of

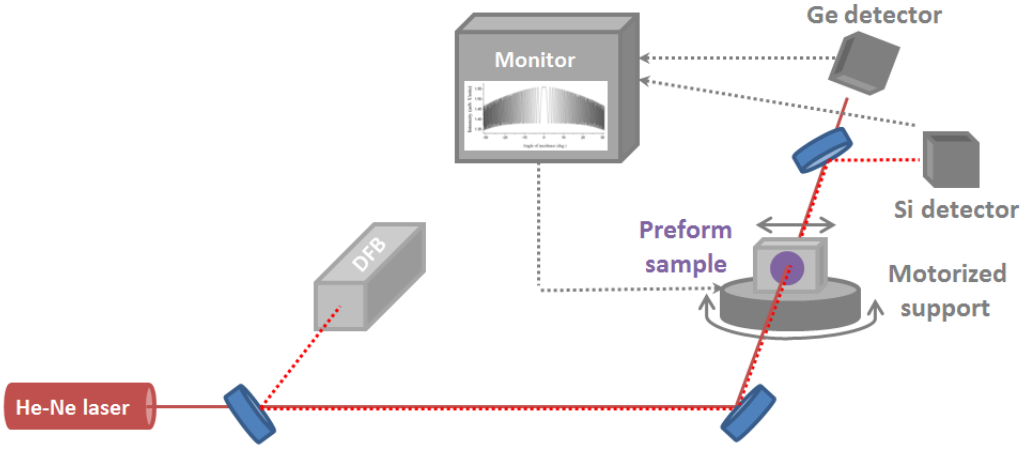


**Figure 4.17:** Schematic representation of a set-up aiming to measure accurately the refractive index of a preform sample: two lasers sources, a He-Ne and a Distributed FeedBack (DFB) laser, are collimated together and propagate through the sample under test. Then, the support is rotated, varying the transmitted intensity at the two wavelengths, which are collected by appropriate photodetectors. Finally, the support can be step-by-step translated to get the RI profile of the sample.

this technique. Furthermore, it will be useful in our case to translate horizontally the sample to get the RI profile and not only the local index.

Through this proposal, we demonstrate that we strive to improve further the accuracy of controls achieved along the manufacturing procedure, pushing them closer and closer to a successful realization of an all-solid LPF fulfilling our expectations.

## 4.7 Conclusion

In this last chapter relative to the fabrication of our microstructured optical fibers, we have demonstrated first on a simple step-index fiber the relevance of the Repusil process to manufacture efficient active material whose the background losses are low ($\approx$ 20 dB/km). Then, we reported the fabrication of an all-solid LPF. The use of a fluorine layer as pump cladding was detrimental due to the generation of air bubbles. Unfortunately, the intensity was not clearly confined into the fiber. The emitted radiation was multimode and spreads across the inner cladding. Two assumptions have been established as origin of these unexpected results: fiber macro-bendings or an index mismatching between the gain region and the surrounding passive material. To go further and relieve the constraint due to bending, we opted to the fabrication of an air-clad, which provide a high NA and thus a strong coupling of the pump power. Hence, we have recently drawn another all-solid fiber whose the inner cladding was unconventional but straightly induced for the Chap. 3. Although the experimental investigation of this fiber is not complete, first results have been discussed. In particular, it was observed that an incident gaussian beam is distorted during the propagation through a 75 cm-long rod-type fiber. Nevertheless, the intensity is this time efficiently confine into the fiber core. Additional tests are under progress in order to understand in details the reason why the transmitted beam is multimode. Finally, we propose a interferometric technique allowing to measure accurately the RI profile. Thus, we intend to increase the RI predictability of our fabrication procedure.

The pursuit of this work will be now focused on new fabrication of all-solid fibers, notably the Spiral LPF. A special care will be carried all along the manufacturing process on the perfect matching of the active and passive material RI, which is the essential point to get a robust singlemode operation.

# General conclusion

During the last two decades, the development of new microstructured optical fibers has known a strong infatuation. In particular, periodically arranged air/silica microstructured fibers (PCFs, LPFs, 2D PBG ...) were used to maintain a singlemode emission in Large-Mode Area fiber. Their core size can exceed 40 $\mu$m while mitigating spectral and temporal distortions commonly induced by non-linear processes for high propagated power. In these fibers, an efficient confinement of the fundamental Gaussian mode into the fiber core is achieved whereas high-order modes undergo higher propagation losses due to their larger tendency to leak out this region. More recently, fibers combining two guidance principles (TIR and PBG) were devised. These structures called Distributed Mode Filtering fibers enable a good modal discrimination as well as a spectral filtering. However, disturbing phenomena called modal instabilities occur in these fibers at high power levels, degrading the beam quality. In this context, my work was dedicated to the improvement of the singlemode robustness in Large Mode Area fibers to push away the appearance threshold of these unwanted processes.

In this purpose, I proposed a novel concept of optical all-solid microstructured fibers in which the core Refractive Index (RI) has no longer to match the silica index. Thus, the constraints on the core RI are partially relieved, offering the potential to heavily doped the fiber core. Furthermore, we resort to an alternative manufacturing process based on the sintering and vitrification of doped powders , providing a precise control of the RI profile and reducing the manufacturing cost. Hence, a theoretical investigation was first led on conventional air/silica LPF structures to demonstrate the relevance of our numerical approach. The behaviour of guided modes into such kind of fiber structures was observed thoroughly, evidencing statements useful for the improvement of the state-of-the-art high power fiber lasers performances. All along the Chapter 3, the development of 50 $\mu$m core all-solid fibers whose the modal

discrimination reaches up to 62% at 1 $\mu$m has been demonstrated through a symmetry reduction and the suppression of the inner cladding periodicity. By this way, an efficient delocalization of competitive high-order modes was numerically highlighted and the strong sensitivity of leaky fibers to an index mismatch between the gain region and the surrounding high-index material was theoretically demonstrated. An optimum Spirally shaped inner cladding microstructuration was presented as the outcome of this numerical investigation as it exhibits a modal discrimination larger than 50% for core diameters ranging from 50 to 100 $\mu$m at least. Moreover, these performances were confirmed over the whole spectral range of investigation. This represents the major outcome of my work.

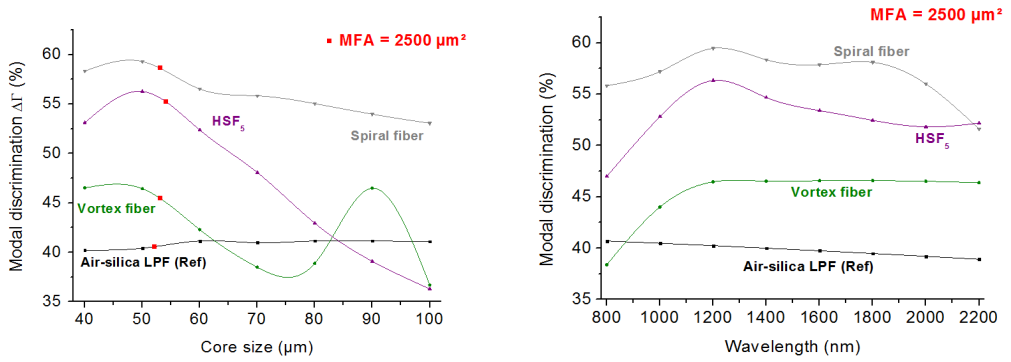


(a) (b)

**Figure 4.18:** Investigated fiber: (a) scalability, for a core size ranging from 40 to 100 $\mu$m and (b) wavelength tunability over the near IR range (800-2200nm) .

Finally, a practical work has been initiated and two all-solid microstructured fibers have been manufactured and characterized. The very first results do not fulfil our expectations in term of beam quality. This was attributed to an index mismatch between the RE-doped region and the passively doped high-index material. Thus, it will be absolutely required to develop a tailored methods to measure accurately the refractive index profile of i/ the high index passive and active rods, making possible a better adaptation of their refractive index, and ii/ the microstructured fiber, to evidence potential stress induced refractive index change. Moreover, the

demonstration of the guidance principle and effectiveness of mode selection using passive structures made of homogeneous materials (pure silica or high-index rods) should be of great interest. Thus, this work will be pursued by new fabrication of all-solid fiber during the next year.

# Bibliography


[Abate81] J. A. Abate, L. Lund, D. Brown, S. Jacobs, S. Refermat, J. Kelly, M. Gavin, J. Waldbillig, and O. Lewis, *"Active mirror: a large-aperture medium-repetition rate Nd:glass amplifier"*, Applied Optics, vol. 20, no. 2, 1981. 12

[Agruzov09] Peter M Agruzov, Konstantin V Dukelskii, and Victor S Shevandin, *"Three types of microstructured large core fibers : development and investigation"*, In *Conference on Lasers and Electro-Optics (CLEO)*, 2009. 118

[Aleshkina11] S. Aleshkina, M. Likhachev, A. Pryamikov, D. Gaponov, A. Denisov, M. Bubnov, M. Salganskii, A. Laptev, A. Guryanov, Y. Uspenskii, N. Popov, and S. Février, *"Very-large-mode-area photonic bandgap Bragg fiber polarizing in a wide spectral range"*, Optics letters, vol. 36, no. 18, 2011. 54

[Alkeskjold11] T. Alkeskjold, M. Laurila, L. Scolari, and J. Broeng, *"Single mode ytterbium doped large-mode-area photonic bandgap rod fiber amplifier"*, Optics Express, vol. 19, no. 8, 2011. 56

[Argyros02] A. Argyros, *"Guided modes and loss in Bragg fibres"*, Optics express, vol. 10, no. 24, 2002. 53

[Atkins06] G. R. Atkins and A. L. G. Carter, *"Photodarkening in Tb3+ -doped phosphosilicate and germanosilicate optical fibers"*, Optics Letters, vol. 19, no. 12, 2006. 33

[Baumgartl11] M. Baumgartl, F. Jansen, F. Stutzki, C. Jauregui, B. Ortaç, J. Limpert, and A. Tünnermann, *"High average and peak power femtosecond large-pitch photonic-crystal-fiber laser"*, Optics letters, vol. 36, no. 2, 2011. 51, 81, 83, 143

[Beaudou12] B. Beaudou, F. Gerôme, Y. Y. Wang, M. Alharbi, T. D. Bradley, G. Humbert, J. Auguste, J. M. Blondy, and F. Benabid, *"Millijoule laser pulse delivery for spark ignition through kagome hollow-core fiber"*, Optics letters, vol. 37, no. 9, 2012. 54

[Behrens90] E. Behrens, R. Powell, and D. Blackburn, *"Characteristics of laser-induced gratings in Pr3+ and Eu 3+ -doped silicate glasses"*, JOSA B, vol. 7, no. 8, 1990. 33

[Belforte13] D. Belforte, *"Annual market review and forecast"*, 2013. ix, iv

[Benabid06] F. Benabid, *"Hollow-core photonic bandgap fibre: new light guidance for new science and technology"*, Philosophical transactions of the royal society A, vol. 364, no. 1849, 2006. 54

[Birks97] T. A. Birks, J. C. Knight, and P. S. Russell, *"Endlessly single-mode photonic crystal fiber"*, Optics letters, vol. 22, no. 13, 1997. 48

[Bouwmans05] G. Bouwmans, L. Bigot, Y. Quiquempois, F. Lopez, L. Provino, and M. Douay, *"Fabrication and characterization of an all-solid 2D photonic bandgap fiber with a low-loss region (< 20 dB/km) around 1550 nm"*, Optics Express, vol. 13, no. 21, 2005. 55

[Bouwmans07] G. Bouwmans, V. Pureur, A. Betourne, Y. Quiquempois, M. Perrin, L. Bigot, and M. Douay, *"Progress in solid core photonic bandgap fibers"*, Optical and Quantum Electronics, vol. 39, no. 12-13, 2007. x, 43

[Brechet00] F. Brechet, J. Marcou, D. Pagnoux, and P. Roy, *"Complete Analysis of the Characteristics of Propagation into Photonic Crystal Fibers, by the Finite Element Method"*, Optical Fiber Technology, vol. 6, no. 2, 2000. 67

[Bridges64] W. Bridges, *"Laser Oscillation in Singly Ionized Argon in the Visible Spectrum"*, Applied Physics Letters, vol. 4, no. 7, 1964. ii

[Broer91] M. M. Broer, R. L. Cone, and J. R. Simpson, *"Ultraviolet-induced distributed-feedback gratings in Ce3+ -doped silica optical fibers"*, Optics letters, vol. 16, no. 18, 1991. 33

[Broer93] M. M. Broer, D. M. Krol, and D. J. Digiovanni, *"Highly nonlinear near-resonant photodarkening in a thulium-doped aluminosilicate glass fiber"*, Optics Letters, vol. 18, no. 10, 1993. 33

[Brooks06] C. Brooks and F. Di Teodoro, *"Multimegawatt peak-power, single-transverse-mode operation of a 100 μm core diameter, Yb-doped rod like photonic crystal fiber amplifier"*, Applied Physics Letters, vol. 89, no. 11, 2006. 49

[Brown01] D. Brown and H. Hoffman, *"Thermal, stress, and thermo-optic effects in high average power double-clad silica fiber lasers"*, IEEE Journal of Quantum Electronics, vol. 37, no. 2, 2001. 29, 30

[Chen10] H. Chen, T. Sosnowski, C. Liu, L. Chen, J. Birge, A. Galvanauskas, F. Kärtner, and G. Chang, *"Chirally-coupled-core Yb-fiber laser delivering 80-fs pulses with diffraction-limited beam quality warranted by a high-dispersion mirror based compressor"*, Optics express, vol. 18, no. 24, 2010. 46

[Chen06] M Chen, *"All-solid silica-based photonic crystal fibers"*, Optics Communications, vol. 266, no. 1, 2006. 48

[Chen04] X. Chen, M. Li, N. Venkataraman, M. Gallagher, W. Wood, A. Crowley, J. Carberry, L. Zenteno, and K. Koch, *"Highly birefringent hollow-core photonic bandgap fiber"*, Optics express, vol. 12, no. 16, 2004. 54

[Choi10] Hee Joo Choi, Hwan Hong Lim, Han Seb Moon, Tae Bong Eom, Jung Jin Ju, and Myoungsik Cha, *"Measurement of refractive index and thickness of transparent plate by dual-wavelength interference"*, Optics express, vol. 18, no. 9, 2010. 156

[Colladon42] D. Colladon, *"On the reflections of a ray of light inside a parabolic liquid stream"*, Comptes Rendus, vol. 15, 1842. 40

[Cregan99] R. F. Cregan, *"Single-Mode Photonic Band Gap Guidance of Light in Air"*, Science, vol. 285, no. 5433, 1999. x, 48, 54

[Dawson08] J. W. Dawson, M.J. Messerly, R. J. Beach, M. Y. Shverdin, A. Stappaerts, A. K. Sridharan, P. H. Pax, J. E. Heebner, C. W. Siders, and C. P. .J. Barty, *"Analysis of the scalability of diffraction-limited fiber lasers and amplifiers to high average power"*, Optics Express, vol. 16, 2008. 26

[Deschamps13] T. Deschamps, H. Vezin, C. Gonnet, and N. Ollier, *"Evidence of AlOHC responsible for the radiation-induced darkening in Yb doped fiber"*, Optics Express, vol. 21, no. 7, 2013. 33

[Desurvire87] E. Desurvire, J. R. Simpson, and P. C. Becker, *"High-gain erbium-doped traveling-wave fiber amplifier"*, Optics letters, vol. 12, no. 11, 1987. iii, 13

[Devautour09a] M. Devautour (2009a). *Etude de fibres actives combinant large coeurs et fort niveau de dopage pour l'émission unimodale.* PhD thesis. 68

[Devautour09b] Mathieu Devautour, Philippe Roy, Sébastien Février, Carlos Pedrido, Frédéric Sandoz, and Valerio Romano, *"Nonchemical-vapor-deposition process for fabrication of highly efficient Yb"*, Applied optics, vol. 48, no. 31, 2009. 21

[Dong09a] L Dong, *"All glass micro-structured optical fibres"*, Optical fibers new development, 2009. x, 52, 53

[Dong09b] L. Dong, J. Li, H. A. McKay, L. Fu, and B. K. Thomas, *"Large effective mode area optical fibers for high-power lasers"*, Proceedings of SPIE, vol. 7195, 2009. 82

[Dong06] L. Dong, J. Li, and X. Peng, *"Bend-resistant fundamental mode operation in ytterbium-doped leakage channel fibers with effective areas up to 3160 μm2"*, Optics express, vol. 14, no. 24, 2006. 52

[Dong08] L. Dong, H. A. McKay, and L. Fu, *"All-glass endless single-mode photonic crystal fibers"*, Optics letters, vol. 33, no. 21, 2008. 48

[Dong09c] L. Dong, H. A. Mckay, L. Fu, M. Ohta, A. Marcinkevicius, S. Suzuki, and M. E. Fermann, *"Ytterbium-doped all glass leakage channel fibers with highly fluorine-doped silica pump cladding"*, Optics Express, vol. 17, no. 11, 2009. 53

[Dong09d] L. Dong, H. A. Mckay, A. Marcinkevicius, L. Fu, J. Li, B. K. Thomas, and M. E. Fermann, *"Extended effective are of fundamental mode in optical fibers"*, Journal of Lightwave Technology, vol. 27, no. 11, 2009. 52, 82

[Duguay86] M. A. Duguay, Y. Kokubun, T. L. Koch, and L. Pfeiffer, *"Antiresonant reflecting optical waveguides in SiO2-Si multilayer structures"*, Applied Physics Letters, vol. 49, no. 1, 1986. 54

[Eidam10] T. Eidam, S. Hanf, E. Seise, T. V. Andersen, T. Gabler, C. Wirth, T. Schreiber, J. Limpert, and A. Tünnermann, *"Femtosecond fiber CPA system emitting 830 W average output power"*, Optics letters, vol. 35, no. 2, 2010. 31

[Eidam11a] T. Eidam, J. Rothhardt, F. Stutzki, F. Jansen, S. Hädrich, H. Carstens, C. Jauregui, J. Limpert, and A. Tünnermann, *"Fiber chirped-pulse amplification system emitting 3.8 GW peak power"*, Optics express, vol. 19, no. 1, 2011. 26, 28, 51

[Eidam11b] T. Eidam, C. Wirth, C. Jauregui, F. Stutzki, F. Jansen, H.-J. Otto, O. Schmidt, T. Schreiber, J. Limpert, and A. Tünnermann, *"Experimental observations of the threshold-like onset of mode instabilities in high power fiber amplifiers"*, Optics express, vol. 19, no. 14, 2011. ix, 32, 33

[Einstein17] A. Einstein, *"Zur Quantentheorie der Strahlung"*, Physikalische Zeitschrift, vol. 18, 1917. i, 4

[Engholm09] M. Engholm, P. Jelger, F. Laurell, and L. Norin, *"Improved photodarkening resistivity in ytterbium-doped fiber lasers by cerium codoping"*, Optics letters, vol. 34, no. 8, 2009. 35

[Engholm08] M. Engholm and L. Norin, *"Preventing photodarkening in ytterbium-doped high power fiber lasers; correlation to the UV-transparency of the core glass"*, Optics express, vol. 16, no. 2, 2008. 35

[Engholm07] M. Engholm, L. Norin, and D. Aberg, *"Strong UV absorption and visible luminescence in ytterbium-doped aluminosilicate glass under UV excitation"*, Optics letters, vol. 32, no. 22, 2007. 33

[Feng03] X. Feng, T. Monro, P. Petropoulos, V. Finazzi, and D. Hewak, *"Solid microstructured optical fiber"*, Optics express, vol. 11, no. 18, 2003. 48

[Février08] S. Février, D. A. Gaponov, P. Roy, M. E. Likhachev, S. L. Semjonov, M. M. Bubnov, E. M. Dianov, M. Y. Yashkov, V. F. Khopin, M. Y. Salganskii, and A. N. Guryanov, *"High-power photonic-bandgap fiber laser"*, Optics letters, vol. 33, no. 9, 2008. 54

[Fini05] J. M. Fini, *"Design of solid and microstructure fibers for suppression of higher-order modes"*, Optics Express, vol. 13, no. 9, 2005. 47

[Fini06a] J. M. Fini, *"Bend-resistant design of conventional and microstructure fibers with very large mode area"*, Optics express, vol. 14, no. 1, 2006. x, 44, 45

[Fini06b] J. M. Fini, M. D. Mermelstein, M. F. Yan, R. T. Bise, A. D. Yablon, P. W. Wisk, and M. J. Andrejco, *"Distributed suppression of stimulated Raman scattering in an Yb-doped filter-fiber amplifier"*, Optics letters, vol. 31, no. 17, 2006. 28

[Frith07] G Frith, B Samson, A Carter, J Farroni, and K Tankala (2007). *"High-efficiency 100W level monolithic fibre devices operating at 2 microns"*. 16

[Furuse13] H. Furuse, H. Chosrowjan, J. Kawanaka, N. Miyanaga, M. Fujita, and Y. Izawa, *"ASE and parasitic lasing in thin disk laser with anti-ASE cap"*, Optics Express, vol. 21, no. 11, 2013. 13

[Gaponov10] D. A. Gaponov, S. Février, M. Devautour, P. Roy, M. E. Likhachev, S. S. Aleshkina, M. Y. Salganskii, M. V. Yashkov, and A. N. Guryanov, *"Management of the high-order mode content in large (40 μm) core photonic bandgap Bragg fiber laser"*, Optics letters, vol. 35, no. 13, 2010. 54, 84

[Gapontsev08] D. Gapontsev, *"6kW CW single mode ytterbium fiber laser in all-fiber format"*, 1st Annual Solid State and Diode Laser Technology review, vol. 258, 2008. 26

[Gebavi13] H. Gebavi, S. Taccheo, L. Lablonde, B. Cadier, T. Robin, D. Méchin, and D. Tregoat, *"Mitigation of photodarkening phenomenon in fiber lasers by 633 nm light exposure"*, Optics letters, vol. 38, no. 2, 2013. 35

[Gebavi12] H. Gebavi, S. Taccheo, D. Tregoat, A. Monteville, and T. Robin, *"Photobleaching of photodarkening in ytterbium doped aluminosilicate fibers with 633 nm irradiation"*, Optical Materials Express, vol. 2, no. 9, 2012. 35

[Geusic64] J. E. Geusic, H. M. Marcos, and L. G. Van Uitert, *"Laser oscillations in Nd-doped Yttrium Aluminum, Yttrium Gallium and Gadolinium Garnets"*, Applied Physics Letters, vol. 4, no. 10, 1964. ii, 9

[Giesen94] A. Giesen, H. Hiigep, A. Voss, K. Wittig, U. Brauch, and H. Opower, *"Scalable Concept for Diode-Pumped High-Power Solid-State Lasers"*, Applied Physics B: Lasers and Optics, vol. 372, no. 58, 1994. 12

[Gordon54] J. Gordon, H. Zeiger, and C. Townes, *"Molecular Microwave Oscillator and New Hyperfine Structure in the Microwave Spectrum of NH3"*, Physical Review, vol. 95, 1954. i

[Gordon55] J. Gordon, H. Zeiger, and C. Townes, *"The Maser - New type of microwave amplifier, frequency standard, and spectrometer"*, Physical Review, vol. 99, no. 4, 1955. i

[Guzman-Chavez07] A.D. Guzman-Chavez, A. V. Kir'yanov, Y. O. Barmenkov, and N.N. Il'ichev, *"Reversible photo-darkening and resonant photo- bleaching of Ytterbium-doped silica fiber at in-core 977-nm and 543-nm irradiation"*, Laser Physics LettersPhysics, vol. 10, no. 4, 2007. 35

[Hädrich06] S Hädrich, T Schreiber, T Pertsch, and J Limpert, *"Thermo-optical behavior of rare-earth-doped low-NA fibers in high power operation"*, Optics Express, vol. 14, no. 13, 2006. 30

[Hall62] R. N. Hall, G. E. Fenner, J. D. Kingsley, and T. J. Soltys, *"Coherent light emission from GaAs junctions"*, Physical review Letters, vol. 9, 1962. ii

[Hansen13] K. R. Hansen, T. T. Alkeskjold, J. Broeng, and J. Læ gsgaard, *"Theoretical analysis of mode instability in high-power fiber amplifiers"*, Optics Express, vol. 21, no. 2, 2013. 31

[Issa04] N. A. Issa, *"High numerical aperture in multimode microstructured optical fibers"*, Applied optics, vol. 43, no. 33, 2004. 38, 149

[Jackson03] S. D. Jackson and S. Mossman, *"Efficiency dependence on the Tm3+ and Al3+ concentrations for Tm3+-doped silica double-clad fiber lasers."*, Applied optics, vol. 42, no. 15, 2003. 16

[Jackson07] Stuart D. Jackson, Alexander Sabella, and David G. Lancaster, *"Application and Development of High-Power and Highly Efficient Silica-Based Fiber Lasers Operating at 2 μm"*, IEEE Journal of Selected Topics in Quantum Electronics, vol. 13, no. 3, 2007. 16

[Jansen11] F. Jansen, F. Stutzki, C. Jauregui, Je. Limpert, and A. Tünnermann, *"Avoided crossings in photonic crystal fibers"*, Optics express, vol. 19, no. 14, 2011. xi, 51, 71, 74, 77, 78, 81, 83

[Jansen10] F. Jansen, F. Stutzki, H.-J. Otto, M. Baumgartl, C. Jauregui, J. Limpert, and A. Tünnermann, *"The influence of index-depressions in core-pumped Yb-doped large pitch fibers"*, Optics express, vol. 18, no. 26, 2010. 50, 51, 71, 72, 83, 89

[Jasapara06] J. Jasapara, M. Andrejco, D. Digiovanni, and R. Windeler, *"Effect of heat and H2 gas on the photo-darkening of Yb + 3 fibers"*, Conference on Lasers and Electro-Optics (CLEO), 2006. 35

[Jauregui12] C. Jauregui, T. Eidam, H.-J. Otto, F. Stutzki, F. Jansen, J. Limpert, and A. Tünnermann, *"Physical origin of mode instabilities in high-power fiber laser systems"*, Optics express, vol. 20, no. 12, 2012. 31

[Javan61] A. Javan, *"Population inversion and continuous optical maser oscillation in a gas discharge containing a He-Ne mixture"*, Physical review Letters, vol. 6, no. 3, 1961. ii, 7

[Jelger10] P. Jelger, M. Engholm, L. Norin, and F. Laurell, *"Degradation-resistant lasing at 980 nm in a Yb/Ce/Al-doped silica fiber"*, Journal of the Optical Society of America B, vol. 27, no. 2, 2010. 35

[Jeong04] Y Jeong, J Sahu, D Payne, and J Nilsson, *"Ytterbium-doped large-core fiber laser with 1.36 kW continuous-wave output power"*, Optics express, vol. 12, no. 25, 2004. 45

[Jetschke09] S. Jetschke and U. Röpke, *"Power-law dependence of the photodarkening rate constant on the inversion in Yb doped fibers"*, Optics letters, vol. 34, no. 1, 2009. 33

[Jetschke13] S. Jetschke, A. Schwuchow, S. Unger, M. Leich, M. Jäger, and J. Kirchhof, *"Deactivation of Yb3+ ions due to photodarkening"*, Optical Materials Express, vol. 3, no. 4, 2013. 34

[Jetschke12] Sylvia Jetschke, Sonja Unger, Martin Leich, and Johannes Kirchhof, *"Photodarkening kinetics as a function of Yb concentration and the role of Al codoping"*, Applied Optics, vol. 51, no. 32, 2012. 96

[Jetschke07] S. Jetschke, S. Unger, U. Röpke, and J. Kirchhof, *"Photodarkening in Yb doped fibers: experimental evidence of equilibrium states depending on the pump power"*, Optics express, vol. 15, no. 22, 2007. 33

[Jetschke08] S. Jetschke, S. Unger, A. Schwuchow, M. Leich, and J. Kirchhof, *"Efficient Yb laser fibers with low photodarkening by optimization of the core composition"*, Optics Express, vol. 16, no. 20, 2008. 35

[Jiang08] Z. Jiang and J. R. Marciante, *"Impact of transverse spatial hole burning on beam quality in large-mode-area Yb-doped fibers"*, America, vol. 25, no. 2, 2008. 70

[Jø rgensen12] M. M. Jø rgensen, S. R. Petersen, M. Laurila, J. Læ gsgaard, and T. T. Alkeskjold, *"Optimizing single mode robustness of the distributed modal filtering rod fiber amplifier"*, Optics express, vol. 20, no. 7, 2012. 68, 82

[Johansen13] M.M. Johansen, K. R. Hansen, M. Laurila, T. T. Alkeskjold, and J. Læ gsgaard, *"Estimating modal instability threshold for photonic crystal rod fiber amplifiers"*, Optics express, vol. 21, no. 13, 2013. 57

[Kao86] K.C. Kao and G.A. Hockham, *"Dielectric-fibre surface waveguides for optical frequencies"*, IEEE Proceedings J Optoelectronics, vol. 113, 1986. iii, 13, 18

[Kashiwagi12] M. Kashiwagi, K. Saitoh, K. Takenaga, S. Tanigawa, S. Matsuo, and M. Fujimaki, *"Effectively single-mode all-solid photonic bandgap fiber with large effective area and low bending loss for compact high-power all-fiber lasers"*, Optics express, vol. 20, no. 14, 2012. 55

[Kastler50] A. Kastler, *"Quelques suggestions concernant la production optique et la détection optique d'une inégalité de population des niveaux de quantification spatiale des atomes"*, Journal de Physique et le radium, vol. 11, no. 1, 1950. i

[Kirchhof03] Johannes Kirchhof, Sonja Unger, Anka Schwuchow, Physikalische Hochtechnologie, and V Jena, *"Fiber lasers: materials, structures and technologies"*, Proc. SPIE, vol. 4957, 2003. 141

[Knight96] J. C. Knight, T. A. Birks, P. S. Russell, and D. M. Atkin, *"All-silica single-mode optical fiber with photonic crystal cladding"*, Optics letters, vol. 21, no. 19, 1996. x, 48

[Koester64] C. J. Koester and E. Snitzer, *"Amplification in a Fiber Laser"*, Applied Optics, vol. 3, no. 10, 1964. ii, 13

[Koplow00] J. P. Koplow, D. A. Kliner, and L. Goldberg, *"Single-mode operation of a coiled multimode fiber amplifier"*, Optics letters, vol. 25, no. 7, 2000. 45

[Koponen08] J. Koponen, M. Söderlund, H. J. Hoffman, D. V. Kliner, J. P. Koplow, and M. Hotoleanu, *"Photodarkening rate in Yb-doped silica fibers"*, Applied optics, vol. 47, no. 9, 2008. 34

[Koponen06] J. J. Koponen, M. J. Söderlund, and H. J. Hoffman, *"Measuring photodarkening from single-mode ytterbium doped silica fibers"*, Optics Express, vol. 14, no. 24, 2006. 33

[Koponen05] J .J. Koponen, M. J. Söderlund, S. K. T. Tammela, and H. Po, *"Photodarkening in ytterbium-doped silica fibers"*, 2005. 26, 33, 35

[Kotov13] L V Kotov, M E Likhachev, M M Bubnov, O I Medvedkov, M V Yashkov, and A N Guryanov, *"75W 40% efficiency single-mode all-fiber erbium-doped laser cladding pumped at 976 nm"*, Optics letters, vol. 38, no. 13, 2013. 15

[Kuhlmey02] B. T. Kuhlmey, R. C. McPhedran, and C. Martijn de Sterke, *"Modal cutoff in microstructured optical fibers"*, Optics letters, vol. 27, no. 19, 2002. 48, 102

[Langner08] Andreas Langner, Gerhard Schötz, Mario Such, Volker Reichel, Stephan Grimm, and Johannes Kirchhof, *"A new material for high power laser fibers"*, Proc. SPIE, vol. 6873, 2008. 21, 138

[Langner12] Andreas Langner, Mario Such, Gerhard Schötz, Florian Just, Martin Leich, Anka Schwuchow, Stephan Grimm, Hagen Zimer, Marcin Kozak, and Björn Wedel, *"Multi-kW single fiber laser based on an extra large mode area design"*, 2012. xv, 22, 138, 139, 140, 143

[Laperle06] P. Laperle, C. Paré, H. Zheng, A. Croteau, and Y. Taillon, *"Yb-doped LMA triple-clad fiber laser"*, In *Photonics North*, 2006. 46

[Laurila13a] Marko Laurila, Roman Barankov, Mette M. Jø rgensen, Thomas T. Alkeskjold, Jes Broeng, Jesper Læ gsgaard, and Siddharth Ramachandran, *"Cross-correlated imaging of single-mode photonic crystal rod fiber with distributed mode filtering"*, Optics Express, vol. 21, no. 8, 2013. 57

[Laurila12] M. Laurila, M. M. Jø rgensen, K. R. Hansen, T. T. Alkeskjold, J. Broeng, and J. Læ gsgaard, *"Distributed mode filtering rod fiber amplifier delivering 292W with improved mode stability"*, Optics Express, vol. 20, no. 5, 2012. 57

[Laurila13b] M. Laurila, M. M. Jø rgensen, J. Læ gsgaard, and T. T. Alkeskjold, *"Highly efficient 90$\mu$m core rod fiber amplifier delivering $>$ 300W without beam instabilities"*, In *Conference on Lasers and Electro-Optics Europe*, volume 10833, 2013. 57

[Laurila11] M. Laurila, J. Saby, T. T. Alkeskjold, L. Scolari, B. Cocquelin, F. Salin, J. Broeng, and J. Læ gsgaard, *"Q-switching and efficient harmonic generation*

*from a single-mode LMA photonic bandgap rod fiber laser"*, Optics express, vol. 19, no. 11, 2011. x, 56, 57

[Lavoute06] L Lavoute, P Roy, A Desfarges-Berthelemot, V Kermène, and S Février, *"Design of microstructured single-mode fiber combining large mode area and high rare earth ion concentration."*, Optics express, vol. 14, no. 7, 2006. 47

[Lee08] Y. W. Lee, S. Sinha, M. J. F. Digonnet, R. L. Byer, and S. Jiang, *"Measurement of high photodarkening resistance in heavily Yb3+ -doped phosphate fibres"*, Electronics Letters, vol. 44, no. 1, 2008. 35

[Lefrancois13] S. Lefrancois, C.H. Liu, M. L. Stock, T. S. Sosnowski, A. Galvanauskas, and F. W. Wise, *"High-energy similariton fiber laser using chirally coupled core fiber"*, Optics letters, vol. 38, no. 1, 2013. 46

[Leich11] M. Leich, F. Just, A. Langner, M. Such, G. Schötz, T. Eschrich, and S. Grimm, *"Highly efficient Yb-doped silica fibers prepared by powder sinter technology"*, Optics letters, vol. 36, no. 9, 2011. xv, 22, 138, 139, 143

[Leich09] M. Leich, U. Röpke, S. Jetschke, S. Unger, V. Reichel, and J. Kirchhof, *"Non-isothermal bleaching of photodarkened Yb- doped fibers"*, Optics Express, vol. 17, no. 15, 2009. 35

[Leproux01] P. Leproux, S. Février, V. Doya, P. Roy, and D. Pagnoux, *"Modeling and optimization of double-clad fiber amplifiers using chaotic propagation of the pump"*, Optical Fiber Technology, vol. 7, no. 4, 2001. 15, 37

[Limpert12a] Jens Limpert, *"Large-pitch fibers: Pushing very large mode areas to highest powers"*, In *International Conference on Fibre Optics and Photonics*, 2012. Optical Society of America. 118

[Limpert06] J. Limpert, O. Schmidt, J. Rothhardt, F. Röser, T. Schreiber, A. Tünnermann, S. Ermeneux, P. Yvernault, and F. Salin, *"Extended single-mode photonic crystal fiber lasers"*, Optics express, vol. 14, no. 7, 2006. x, 48, 49

[Limpert12b] J. Limpert, F. Stutzki, F. Jansen, H.-J. Otto, T. Eidam, C. Jauregui, and A. Tünnermann, *"Yb-doped large-pitch fibres: effective single-mode operation based on higher-order mode delocalisation"*, Light: Science & Applications, vol. 1, 2012. x, xi, 42, 50, 71, 72, 73, 74, 83, 87, 90

[Litchinitser04] N. Litchinitser, S. Dunn, P. Steinvurzel, B. J. Eggleton, T. White, R. McPhedran, and C. Martijn de Sterke, *"Application of an ARROW model for designing tunable photonic devices"*, Optics Express, vol. 12, no. 8, 2004. 55

[Litchinitser02] N. M. Litchinitser, A. K. Abeeluck, C. Headley, and B. J. Eggleton, *"Antiresonant reflecting photonic crystal optical waveguides"*, Optics letters, vol. 27, no. 18, 2002. 53

[Liu07] C.-H. Liu, Gu. Chang, N. Litchinitser, D. Guertin, N. Jacobsen, K. Tankala, and A. Galvanauskas, *"Chirally coupled core fibers at 1550-nm and 1064-nm for*

*effectively single-mode core size scaling"*, Conference on Lasers and Electro-Optics (CLEO), vol. 1, no. 2, 2007. x, 46, 47

[Luan04] F. Luan, A. K. George, T. D. Hedley, G. J. Pearce, D. M. Bird, J. C. Knight, and P. St J. Russell, *"All-solid photonic bandgap fiber"*, Optics letters, vol. 29, no. 20, 2004. 55

[Lureau12] François Lureau, Sébastien Laux, Olivier Casagrande, Christophe Radier, Olivier Chalus, Frédéric Caradec, and Christophe Simon-Boisson, *"High repetition rate PetaWatt level Titanium Sapphire laser system for laser wakefield acceleration"*, Conference on Lasers and Electro-Optics 2012, 2012. 10

[Mady10] F. Mady, M. Benabdesselam, Y. Mebrouk, and B. Dussardier, *"Radiation effects in ytterbium-doped silica optical fibers : traps and color centers related to the radiation-induced optical losses"*, In *Radecs 2010*, 2010. 33

[Maiman60a] T. Maiman, *"Optical and microwave optical experiments in Ruby"*, Physical review Letters, vol. 4, no. 11, 1960. ii, 2

[Maiman60b] T. Maiman, *"Stimulated optical radiation in Ruby"*, Nature, vol. 187, 1960. ii, 9

[Manek - Hönninger07] I. Manek - Hönninger, J. Boullet, T. Cardinal, F. Guillen, S. Ermeneux, M. Podgorski, R. Bello Doua, and F. Salin, *"Photodarkening and photobleaching of an ytterbium-doped silica double-clad LMA fiber"*, Optics Express, vol. 15, no. 4, 2007. ix, 34, 35

[Marciante07] J. R. Marciante, *"Gain Filtering for Single-Spatial-Mode Operation of Large-Mode-Area Fiber Amplifiers"*, In *Conference on Lasers and Electro-Optics*, number 1, 2007. 43

[Marciante09] John R. Marciante, *"Gain Filtering for Single-Spatial-Mode Operation of Large-Mode-Area Fiber Amplifiers"*, IEEE Journal of Selected Topics in Quantum Electronics, vol. 15, no. 1, 2009. 44, 84

[Marciante10] J. R. Marciante, R. G. Roides, V. V. Shkunov, and D. A. Rockwell, *"Near-diffraction-limited operation of step-index large-mode-area fiber lasers via gain filtering"*, Optics letters, vol. 35, no. 11, 2010. 44

[Markos12] Christos Markos, Spyros N. Yannopoulos, and Kyriakos Vlachos, *"Chalcogenide glass layers in silica photonic crystal fibers"*, Optics Express, vol. 20, no. 14, 2012. 23

[Morasse07] B. Morasse, S. Chatigny, E. Gagnon, C. Hovington, J.-P. Martin, and J.-P. De Sandro, *"Low photodarkening single cladding ytterbium fibre amplifier"*, In *SPIE Photonics West*, 2007. 35

[Mortensen03] N. A. Mortensen, J. R. Folkenberg, M. D. Nielsen, and K. P. Hansen, *"Modal cutoff and the V parameter in photonic crystal fibers"*, Optics letters, vol. 28, no. 20, 2003. 48

[Moulton10] Peter F Moulton, Thomas Ehrenreich, Ryan Leveille, Imtiaz Majid, Kanishka Tankala, and Glen Rines, *"1-kW , all-glass Tm : fiber laser"*, In *SPIE Photonics West*, 2010. 16

[Nagel82] S. R. Nagel and K. L. Walker, *"An overview of the Modified Chemical Vapor,Deposition (MCVD) process and performance"*, IEEE Transaction on microwave theory and techniques, vol. MTT-30, no. 4, 1982. 19

[Nicholson08] J. W. Nicholson, A. D. Yablon, S. Ramachandran, and S. Ghalmi, *"Spatially and spectrally resolved imaging of modal content in large-mode-area fibers"*, Optics Express, vol. 16, no. 10, 2008. 45

[Olausson08] C. B. Olausson, C. I. Falk, J. K. Lyngsø, B. B. Jensen, K. T. Therkildsen, J. W. Thomsen, K P Hansen, A Bjarklev, and J Broeng, *"Amplification and ASE suppression in a polarization-maintaining ytterbium-doped all-solid photonic bandgap fibre"*, Optics Express, vol. 16, no. 18, 2008. x, 54

[Olausson10] C. B. Olausson, A. Shirakawa, M. Chen, J. K. Lyngsø, J. Broeng, K. P. Hansen, A. Bjarklev, and K.-I. Ueda, *"167 W, 1178 nm Ytterbium-Doped Photonic Bandgap Fiber Amplifier with Power Scalability"*, Conference on Lasers and Electro-Optics, 2010. 55

[Ouzounov03] D. G. Ouzounov, F. R. Ahmad, D. Müller, N. Venkataraman, M. T. Gallagher, M. G. Thomas, J. Silcox, K. W. Koch, and A. L. Gaeta, *"Generation of megawatt optical solitons in hollow-core photonic band-gap fibers"*, Science, vol. 301, no. 5640, 2003. 42, 55

[Overton13] G. Overton, A. Nogee, D. A. Belforte, and C. Holton, *"Laser markets rise above global headwinds"*, 2013. iv, 7

[Pagnoux94] D. Pagnoux, J.-M. Blondy, P. Faugeras, and P. Facq, *"Cutoff wavelength measurement for singlemode fibre"*, Journal of Lightwave Technology, vol. 12, no. 3, 1994. xi, 70, 71, 87, 103, 106, 116

[Paschotta97] R. Paschotta, J. Nilsson, P. R. Barber, J. E. Caplen, A. C. Tropper, and D. C. Hanna, *"Lifetime Quenching in Yb Doped Fibres"*, Optics Communications, no. 136, 1997. 33

[Patel64] K. N. Patel, *"Continuous wave laser action on vibrational rotational transitions of CO2"*, Physical Review, vol. 136, no. 5A, 1964. ii

[Payne87] D. N. Payne, I. M. Jauncey, L Reekie, and R. J. Mears, *"High gain rare earth doped fiber amplifier at 1.54 μm"*, International Conference on Integrated Optics and Optical Fiber Communication, 1987. iii, 13

[Poole86] S. B. Poole, D. N. Payne, R. J. Mears, M. E. Fermann, and R. I. Laming, *"Fabrication and characterization of low loss optical fibers containing rare-earth ions"*, Journal of light, vol. LT-4, no. 7, 1986. 19

[Pureur08] V. Pureur, L. Bigot, G. Bouwmans, Y. Quiquempois, M. Douay, and Y. Jaouen, *"Ytterbium doped solid core photonic bandgap fiber for laser operation around 980nm"*, Applied Physics Letters, vol. 92, no. 061113, 2008. 55

[Rydberg13] S. Rydberg and M. Engholm, *"Experimental evidence for the formation of divalent ytterbium in the photodarkening process of Yb-doped fiber lasers"*, Optics Express, vol. 21, no. 6, 2013. 34

[Schawlow58] A. L. Schawlow and C. H. Townes, *"Infrared and Optical Masers"*, Physical Review, vol. 112, 1958. ii

[Schermer07] R.T. Schermer, *"Mode scalability in bent optical fibers"*, Optics Express, vol. 15, no. 24, 2007. 44, 86

[Schimpf11] D. N. Schimpf, R. A. Barankov, and S. Ramachandran, *"Cross-correlated (C2) imaging of fiber and waveguide modes"*, Optics Express, vol. 19, no. 14, 2011. 45

[Smith11] A. V. Smith and J. J. Smith, *"Mode competition in high power fiber amplifiers"*, Optics Express, vol. 19, no. 12, 2011. 31

[Snitzer61] E. Snitzer, *"Proposed Fiber Cavities for Optical Masers"*, Journal of Applied Physics, vol. 32, no. 1, 1961. iii

[Snitzer88] E. Snitzer, H. Po, F. Hakimi, R. Tumminelli, and B.C. McCollum, *"Double clad, offset core Nd fiber laser"*, In *Optical Fiber Sensors*, volume 2, 1988. Optical Society of America. 37

[Söderlund09] M. J. Söderlund, J. J. Montiel i Ponsoda, J. P. Koplow, and S. Honkanen, *"Thermal bleaching of photodarkening-induced loss in ytterbium-doped fibers"*, Optics letters, vol. 34, no. 17, 2009. 35

[Sorokin60] P. Sorokin and M. Stevenson, *"Stimulated Infrared Emission from Trivalent Uranium"*, Physical Review Letters, vol. 5, no. 12, 1960. ii, 9

[Stutzki11] Fabian Stutzki, Florian Jansen, Cesar Jauregui, Jens Limpert, and Andreas Tünnermann, *"Non-hexagonal Large-Pitch Fibers for enhanced mode discrimination"*, Optics express, vol. 19, no. 13, 2011. 118

[Stutzki12] F. Stutzki, F. Jansen, A. Liem, C. Jauregui, J. Limpert, and A. Tünnermann, *"26mJ, 130W Q-switched fiber laser system with near-diffraction-limited beam quality"*, Optics letters, vol. 37, no. 6, 2012. 51

[Tammela06] Simo Tammela, Mikko Söderlund, Joona Koponen, Valery Philippov, Per Stenius, and Liekki Corporation, *"The potential of direct nanoparticle deposition for the next generation of optical fibers"*, Philosophical transactions of the royal society A, 2006. 21

[Tang03] C Tang, C L Yang, and J Chen, *"Design of Diode Pumped 10 kW High Power Nd: YAG Disc Laser"*, In *Proceedings of SPIE*, volume 5120, 2003. 13

[Tolman24] R. C. Tolman, *"Duration of molecules in upper quantum states"*, Proceeding of the National academy of sciences, vol. 10, no. 3, 1924. i

[Townsend87] J.E. Townsend, S.B. Poole, and D.N. Payne, *"Solution doping technique for fabrication of rare earth doped optical fibres"*, Electronics Letters, vol. 23, no. 7, 1987. 20

[Tünnermann10] A. Tünnermann, T. Schreiber, and J. Limpert, *"Fiber lasers and amplifiers: an ultrafast performance evolution"*, Applied optics, vol. 49, no. 25, 2010. 37

[Vivona12] Marilena Vivona, Sylvain Girard, Senior Member, Thierry Robin, Benoit Cadier, Lavinia Vaccaro, Marco Cannas, Aziz Boukenter, and Youcef Ouerdane, *"Influence of Ce3+ codoping on the photoluminescence excitation channels of phosphosilicate Yb / Er-doped glasses"*, IEEE Photonics Technology Letters, vol. 24, no. 6, 2012. 96

[Wadsworth03] W. Wadsworth, R. Percival, G. Bouwmans, J. Knight, and P. St J. Russell, *"High power air-clad photonic crystal fibre laser"*, Optics express, vol. 11, no. 1, 2003. 38, 149

[Wang12] Y. Y. Wang, X. Peng, M. Alharbi, C. Fourcade Dutin, T. D. Bradley, F. Gérôme, M. Mielke, T. Booth, and F. Benabid, *"Design and fabrication of hollow-core photonic crystal fibers for high-power ultrashort pulse transportation and pulse compression"*, Optics letters, vol. 37, no. 15, 2012. 54

[Ward12] B. Ward, C. Robin, and I. Dajani, *"Origin of thermal modal instabilities in large mode area fiber amplifiers"*, Optics express, vol. 20, no. 10, 2012. 31

[Wielandy07] S. Wielandy, *"Implications of higher-order mode content in large mode area fibers with good beam quality"*, Optics Express, vol. 15, no. 23, 2007. 45

[Wong05] W. S. Wong, X. Peng, J. M. McLaughlin, and L. Dong, *"Breaking the limit of maximum effective area for robust single-mode propagation in optical fibers"*, Optics letters, vol. 30, no. 21, 2005. 52

[Yablonovitch93] E. Yablonovitch, *"Photonic band-gap structures"*, Journal of the Optical Society of America B, vol. 10, no. 2, 1993. 42

[Yan05] M. Yan, *"Introduction to microstructured optical fibers"*, 2005. 47

[Yeh76] P. Yeh and A. Yariv, *"Bragg reflection waveguides"*, Optics Communications, vol. 19, no. December, 1976. 53

[Yeh78] P. Yeh, A. Yariv, and E. Marom, *"Theory of Bragg fiber"*, JOSA, vol. 68, no. 9, 1978. 53

[Yoo07] S. Yoo, J. Nilsson, and D Payne, *"Photodarkening in Yb-doped aluminosilicate fibers induced by 488 nm irradiation"*, Optics letters, vol. 32, no. 12, 2007. 35

[Zhang12] G. Zhang, Q. Zhou, C. Yu, L. Hu, and D. Chen, *"Neodymium-doped phosphate fiber lasers with an all-solid microstructured inner cladding"*, Optics letters, vol. 37, no. 12, 2012. 48

# Scientific contributions

## Articles in listed international peer-reviewed journals

Romain Dauliat, Dmitry Gaponov, Aurélien Benoit, François Salin, Kay Schuster, Raphaël Jamier and Philippe Roy, "*Inner cladding microstructuration based on symmetry reduction for improvement of singlemode robustness in VLMA fiber*", Optics Express vol. 21 , Issue 16, pages 18927-18936, 2013.

## Communications with proceedings in an international peer-reviewed congress

Romain Dauliat, Dmitry Gaponov, Aurélien Benoit, François Salin, Kay Schuster, Sylvia Jetschke, Stephan Grimm, and Philippe Roy, "*Ytterbium doped all solid Large Pitch Fiber made from powder sintering and vitrification*" in International Conference on Fibre Optics and Photonics, p. TPo.7, 2012.

Dmitry Gaponov, Romain Dauliat, Stephan Grimm, Kay Schuster, and Philippe Roy, "*Cladding-pumped high-power mode-locked thulium laser based on fiber prepared by powder sinter technology*", European Conference on Lasers and Electro-Optics and XIIIth International Quantum Electronics Conference, CF/IE-8.2, 2013.

## Invited speakers at international congress

Philippe Roy, Romain Dauliat, Dmitry Gaponov, Raphaël Jamier, Kay Schuster, Stephan Grimm, Stéphane Valette, Aurélien Benoit and François Salin, "*Powder technology and innovative fiber design enable a new generation of high-power single-mode-fiber laser sources*", Advanced Laser Technology 12, 2012.

## Communications with proceedings in a national peer-reviewed congress

Romain Dauliat, Dmitry Gaponov, Philippe Roy, Kay Schuster, Stephan Grimm, and Sébastien Février, "*Conception d'une fibre microstructurée entièrement solide à très grande surface modale pour les sources lasers monomodes de puissance*", Journées Nationales d'Optique Guidée, 2011.

Ali Hreibi, Romain Dauliat, Asha Bhardwaj, Philippe Roy, Jean-Marc Blondy et Frédéric Gérôme, "*Conception de fibres optiques dopées aux quantum dots PbSe pour des applications laser*", Journées Nationales d'Optique Guidée, 2012.

Romain Dauliat, Dmitry Gaponov, Raphael Jamier, Stephan Grimm, Kay Schuster et Philippe Roy, "*Laser efficace à fibre dopée Thulium synthétisée par frit-*

*tage et vitrification de poudres dopées*", Journées Nationales d'Optique Guidée, 2012.

## Oral communications in an international workshop

Philippe Roy, Romain Dauliat, Raphaël Jamier, Dmitry Gaponov, Mathieu Devautour and Sébastien Février, "*Recent advances in Fiber design*", LIFT Project, Session3-7, 2011.

The development of tailored micro-structured optical fibers has known a real infatuation during the last two decades allowing an outstanding management of optical properties. In particular, this approach was beneficial to the emission of a robust singlemode beam from large mode area fibers whose the core size exceeds 40 $\mu$m. This ability has made fiber lasers serious and competitive candidates for widespread applications such as micro-machining or surgery. In this purpose, several fiber structures have been devised (Large Pitch Fibers and Distributed Mode Filtering fibers for instance), pushing further the performances of high-power fiber lasers and amplifiers. However, new detrimental phenomena impact their operation at high-power regime. Indeed, a degradation of the beam quality is noticed when the emitted power overcomes a certain threshold, because of the inherent capability of state-of-the-art fibers to sustain several guided modes into their core. In this context, I first investigated thoroughly the behavior of guided modes in state-of-the-art ultra large-mode-area fibers and highlighted several milestones allowing to get an efficient selective amplification. Hence, I benefited from these statements to propose novel kinds of all-solid micro-structured fibers exhibiting an enhancement of the singlemode robustness. I demonstrated a record modal discrimination in a so-called Spiral LPF whose the inner cladding pattern is totally asymmetry. The first fabrications of these all-solid fibers are also reported, contributing to clearly define the prospect of this work as well as the fabrication hurdles.

Le développement de fibres optiques micro-structurées spécifiques a connu un réel engouement au cours des 20 dernières années permettant un contrôle remarquable des propriétés optiques. En particulier, cette approche a été bénéfique à l'émission d'un faisceau monomode robuste à partir de fibres à large aire modale dont le diamètre de cœur excède 40 $\mu$m. Cette capacité a promu les lasers à fibres au rang de sérieux et compétitifs candidats pour des applications répandues telles que le micro-usinage ou la chirurgie. Dans ce but, de multiples structures de fibres ont été mise au point (Large Pitch Fibers et les "Distributed Mode Filtering fibers" par exemple), accroissant les performances des lasers et amplificateurs fibrés de fortes puissances. Cependant, de nouveaux phénomènes néfastes impactent leur fonctionnement dans ce régime. En effet, une dégradation de la qualité du faisceau est notable lorsque la puissance émise surpasse un certain seuil, en raison de la capacité inhérente des fibres de l'état de l'art à supporter plusieurs modes guidés dans leur cœur. Dans ce contexte, j'ai premièrement étudié attentivement le comportement des modes guidés dans les fibres à très large aire modale de l'état de l'art et mis en lumière plusieurs principes fondamentaux utiles à l'obtention d'une amplification sélective efficace. Ensuite, j'ai tiré bénéfice de ces constats pour proposer de nouveaux types de fibres microtructurées exhibant une amélioration de la robustesse de leur unimodalité. J'ai ainsi démontré une discrimination modale record dans une fibre appelé LPF Spirale dont le motif de la gaine interne est totalement asymétrique. Les premières fabrications de ces fibres toute solides sont également rapportées, contribuant à clairement définir les perspectives de ces travaux ainsi que les contraintes de fabrication.